Alma Mater Studiorum – Università di Bologna

DOTTORATO DI RICERCA IN

Ingegneria Energetica, Nucleare e del Controllo Ambientale

Ciclo XXII

Settore scientifico-disciplinare di afferenza: ING-IND/10 FISICA TECNICA INDUSTRIALE

SECOND LAW ANALYSIS AND SIMULATION TECHNIQUES FOR THE ENERGY OPTIMIZATION OF BUILDINGS

Presentata da: Tiziano Terlizzese

Coordinatore Dottorato
Prof. Antonio Barletta

_____

Relatore
Prof. Enzo Zanchini

_____

Esame finale anno 2010

SECOND LAW ANALYSIS AND SIMULATION TECHNIQUES FOR THE ENERGY OPTIMIZATION OF BUILDINGS

Tiziano Terlizzese

Alma Mater Studiorum – Università di Bologna
Dipartimento di Ingegneria Energetica, Nucleare e del Controllo Ambientale

For Alessia and Matteo

CONTENTS

PREFACE

The research activity described in this thesis is focused mainly on the study of finite-element techniques applied to thermo-fluid dynamic problems of plant components and on the study of dynamic simulation techniques applied to integrated building design in order to enhance the energy performance of the building. The first part of this doctorate thesis is a broad dissertation on second law analysis of thermodynamic processes with the purpose of including the issue of the energy efficiency of buildings within a wider cultural context which is usually not considered by professionals in the energy sector.

In particular, the first chapter includes a rigorous deduction of the expressions for molar exergy and molar flow exergy of pure chemical fuels. The study shows that molar exergy and molar flow exergy coincide when the temperature and pressure of the fuel are equal to those of the environment in which the combustion reaction takes place. A simple method to determine the Gibbs free energy of reaction for non-standard values of the temperature and pressure of the environment is then presented. For hydrogen, carbon dioxide, and several hydrocarbons, the dependence of the molar exergy on the temperature and relative humidity of the environment is reported, together with an evaluation of molar exergy and molar flow exergy when the temperature and pressure of the fuel are different from those of the environment (E. Zanchini, T. Terlizzese, Molar exergy and flow exergy of pure chemical fuels, Energy, Vol. 34, pp. 1246-1259, 2009). As an application of second law analysis, a comparison of the thermodynamic efficiency of a condensing boiler and of a heat pump is also reported.

The second chapter presents a study of borehole heat exchangers, that is, a polyethylene piping network buried in the soil which allows a ground-coupled heat pump to exchange heat with the ground. After a brief overview of low-enthalpy geothermal plants, an apparatus designed and assembled by the author to carry out thermal response tests is presented. Data obtained by means of *in situ* thermal response tests are reported and evaluated by means of a finite-element simulation method, implemented through the software package COMSOL Multyphysics. The simulation method allows the determination of the precise value of the effective thermal properties of the ground and of the grout, which are essential for the design of borehole heat exchangers (E. Zanchini, T. Terlizzese, Finite-element evaluation of thermal response tests performed on U-tube borehole heat exchangers, Proceedings of the COMSOL Conference Hannover 2008, Hannover, Germany, November 4–6, 2008).

In addition to the study of a single plant component, namely the borehole heat exchanger, in the third chapter a thorough process is presented for the plant design of a zero carbon building complex.

The plant is composed of: 1) a ground-coupled heat pump system for space heating and cooling, with electricity supplied by photovoltaic solar collectors; 2) air dehumidifiers; 3) thermal solar collectors to match 70% of domestic hot water energy use, and a wood pellet boiler for the remaining domestic hot water energy use and for exceptional winter peaks. This chapter includes the description of the design methodology adopted: 1) dynamic simulation of the building complex with the software package TRNSYS for evaluating the energy requirements of the building complex; 2) ground-coupled heat pumps modelling by means of TRNSYS; 3) evaluation of the total length of the borehole heat exchanger by an iterative method developed by the author. An economic feasibility and an exergy analysis of the proposed plant, compared with two other plants, are reported. The exergy analysis was performed by considering the embodied energy of the components of each plant and the exergy loss during the functioning of the plants. A first version of this work was presented at the International Congress SET 2009 (E. Zanchini, G.L. Morini, and T. Terlizzese, Design of a ground-coupled heat pump and solar collector system for a zero carbon residential building complex, SET 2009 – 8th International Conference on Sustainable Energy Technologies, Aachen, Germany, August 31–September 3, 2009), and an extended version was submitted to the international journal Energy and Buildings.

Chapter 1

EXERGY OF CHEMICAL FUELS

Nomenclature

c_p	molar heat capacity at constant pressure, [J/(mol K)]	ΔH	enthalpy of reaction [J]
E	energy, [J]	ΔS	entropy of reaction [J/K]
e	molar energy, [J/mol]	$\Delta\xi$	$\xi(T_B,p_v) - \xi(T_B,p_B)$ [J/mol]
G	Gibbs free energy, [J]	$\Delta\psi$	$\psi(T_B,p_v) - \psi(T_B,p_B)$ [J/mol]
g	molar Gibbs free energy, [J/mol]	ε	degree of reaction
H	enthalpy, [J]	μ	chemical potential [J/mol]
h	molar enthalpy, [J/mol]	ζ	speed, axial velocity [m/s]
m	mass, [kg]	υ	stoichiometric coefficient
n	number of moles, [mol]	Ξ	exergy [J]
$\dot{n}$	molar flow rate, [mol/s]	ξ	molar exergy [J/mol]
p	pressure, [Pa]	φ	relative humidity
R	universal gas constant, [J/(mol K)]	Φ	Keenan's availability function per mole [J/mol]
S	entropy, [J/K]	χ	Keenan's flow availability per mole [J/mol]
s	molar entropy, [J/(mol K)]	ψ	molar flow exergy [J/mol]
$\dot{S}_{irr}$	entropy production rate, [W/K]	Subscripts	
T	temperature [K]	B	system B
U	internal energy [J]	F	fuel
u	molar internal energy [J/mol]	gas	gas state
v	specific volume [m^3/mol]	i	i-th component
W	work [J]	liquid	liquid state
$\dot{W}$	power [W]	u	useful (shaft)
Greek symbols		v	vapour-liquid equilibrium
ΔG	Gibbs free energy of reaction [J]	0	reference condition

1.1 INTRODUCTION

Second law analysis is widely recognized as a necessary tool to determine the thermodynamic efficiency of a whole process or parts thereof. Recent research papers deal with the evaluation and the optimization of the thermodynamic efficiency of systems that employ chemical fuels, such as cogeneration plants [1], fuel cells [2] and power plants [3]. A basic datum, necessary to evaluate the thermodynamic efficiency of any system that employs a chemical fuel is the maximum work obtainable by one mole of the fuel. Indeed, two different cases must be considered: the fuel may be available in a container or in steady duct flow. Following the terminology proposed by Brzustowski and Golem [4], we will call the molar exergy of a fuel the maximum work obtainable by one mole of the fuel in the first case and the molar flow exergy of a fuel the maximum shaft work obtainable by one mole of fuel in the second case

Several papers dealing with the molar exergy (or flow exergy) of chemical fuels are available in the literature. Most of them refer to the standard molar exergy (or flow exergy), that is, the maximum work (or shaft work) obtainable by one mole of the fuel if the system *B,* which represents the environment, is in a reference stable-equilibrium state. For the evaluation of the exergy of hydrogen and hydrocarbons, the environment considered is (almost always) the atmosphere, but a general agreement on the choice of the reference state of system *B,* which represents the atmosphere, has not been reached.

In Refs. [4,5], the evaluation method is presented and values of the standard molar exergy of some fuels are reported, with the following choice of the reference state of *B*: pressure $p_B = p_0 = 1.01325$ bar, temperature $T_B = T_0 = 298.15$ K, relative humidity $\varphi_B = 0.65$. Morris and Szargut [6] evaluated the exergy of several substances, with reference to different environments. For nine elements, the reference environment is the atmosphere and the representative system *B* is in the reference state $p_B = p_0$, $T_B = T_0$ and $\varphi_B = 0.7$.

The choice $p_B = p_0$ and $T_B = T_0$ is made by most authors to simplify the calculations, because the tables of the standard Gibbs free energy and of the standard enthalpy of formation of chemical species are available in these conditions. Note, however, that T_0 is higher than the mean temperature of the air close to the surface of the Earth, which is about 15 °C.

A logical scheme for the evaluation of the molar exergy (or flow exergy) of pure substances for $T_B \neq T_0$and/or $p_B \neq p_0$ is presented by Szargut [7] and by Kotas [8]; however, a complete expression of the result is not reported in these references. In Ref. [8], three terms are considered as negligible and not evaluated. In the same reference, the difference between the molar flow exergy ψ and the molar exergy ξ of a pure substance with temperature *T*, pressure *p* and specific volume *v* is shown to be

$$\psi(T,p) - \xi(T,p) = (p - p_B)\,v(T,p)\,; \tag{1.1.1}$$

where p_B is the pressure of the environment. Therefore, if $p = p_B$, the molar exergy and the molar flow exergy coincide. Indeed, Eq.(1.1.1) is correct, but the argument employed by the author in the deduction is not rigorous.

A complete expression of the molar flow exergy (and, on account of Eq. (1.1.1), also of the molar exergy) of a pure substance with the same pressure and temperature as the environment, for $T_B \neq T_0$and/or $p_B \neq p_0$, is reported in a recent paper by Ertesvag [9], without a detailed discussion of the evaluation method. The author first reports in a table the values of the standard molar exergy of some gaseous fuels and atmospheric gases, with the choice, $T_B = T_0$, $p_B = p_0$ and $\varphi_B = 0.7$; then he illustrates, in graphical form, the effects of the changes of T_B, φ_B, and p_B on the values of the molar exergy. The analysis of the literature reported above suggests the following remarks. The method

for the evaluation of the molar exergy and of the molar flow exergy of a pure substance, including the proof that these quantities are equal if $p_B = p_0$, is not yet completely sharpened, at least for the case $T_B \neq T_0$ and $p_B \neq p_0$. The effect of the changes in the conditions of the environment on the value of the molar exergy is not negligible [9]. It is difficult to find a general agreement on the conditions of the environment that define the standard molar exergy; moreover, the temperature commonly chosen at present as standard is higher than the mean temperature of atmospheric air close to the surface of the Earth.

The aim of this first chapter is to propose a rigorous method for second law analysis with particular reference to the evaluation of molar exergy and molar flow exergy of a pure substance. In order to achieve this, Section 1.2 gives the basic definitions and the theorems that will be then adopted. Section 1.3 presents a rigorous scheme for the deduction of the expression of the molar exergy and the molar flow exergy with the same temperature T_B and pressure p_B as the environment. The evaluation of molar exergy and molar flow exergy in the case $T_B \neq T_0$ and $p_B \neq p_0$ is shown in Section 1.4. Section 1.5 includes tables that allow a simple calculation of the molar exergy (for $T_B = T_0$ and $p_B = p_0$) of hydrogen, carbon dioxide and several hydrocarbons, with p_B =1.01325 bar, for any value of T_B and φ_B in the range 268.15 K $\leq T_B \leq$ 313.15 K and $0.1 \leq \varphi_B \leq 1$. Additional tables allow the evaluation of the so-called thermophysical exergy or thermophysical flow exergy [9], that is, the difference between the exergy or the flow exergy of the fuel in its given initial state and the exergy (or flow exergy) at $T = T_B$ and $p = p_B$. In these tables, it is assumed that the temperature of the fuel is equal to the ambient temperature T_B and that the pressure of the fuel is in the range $1.01325 \leq p \leq 200$ bar; the fuel may be gas or liquid.

Finally, as an example of the application of the improved second law analysis (Sections 1.2 – 1.5), Section 1.6 shows the evaluation of the thermodynamic efficiency of an air to air heat pump and of a condensing gas boiler under different environmental conditions.

1.2 BASIC PRINCIPLES OF THERMODYNAMICS

In this Section a rigorous logical scheme for the definition of temperature, entropy, and internal energy for both closed and open systems, is presented. Elements of chemical thermodynamics are also reported: the fundamental relation, the Gibbs free energy and the Euler equation are defined for an arbitrary set of stable equilibrium states of a simple open system. The equivalence between the Gibbs free energy and the chemical potential of a generic constituent is also presented. All the concepts employed have been thoroughly defined, except for the following basic definitions given in Ref. [11]: constituent, force field, system, closed and open systems, isolated system, process, reversible process, weight process, and energy for a closed system.

1.2.1 Theorems and Definitions

Assumption 1 – Normal Systems

We define *normal system* a system A that, regardless of its initial state, can be changed to a non-equilibrium state with higher energy by means of a weight process for A in which the regions of space occupied by the constituents of A have no net change. From now on, we consider only normal systems.

Theorem 1 – Impossibility of a Perpetual Motion Machine of the Second Kind (PMM2)

If a normal system A is in a stable equilibrium state, it is impossible to lower its energy by means of a weight process for A in which the regions of space occupied by the constituents of A have no net change.

Proof

Suppose that, starting from a stable equilibrium state A_{se} of A, by means of a weight process Π_1 with positive work $W^{A\rightarrow}$, the energy of A is lowered and the regions of space R^A occupied by the constituents of A have no net change. On account of Assumption 1, it would be possible to perform a weight process Π_2 for A in which the regions of space R^A occupied by the constituents of A have no net change, the weight M is restored to its initial state so that the positive amount of energy $W^{A\leftarrow}$, is supplied back to A, and the final state of A is a non-equilibrium state, namely, a state clearly different from A_{se}. Thus, the zero-work sequence of weight processes (Π_1, Π_2) would violate the definition of a stable equilibrium state.

Systems in Mutual Stable Equilibrium

Systems A and B are in mutual stable equilibrium if the composite system AB is in a stable equilibrium state.

Thermal Reservoir

A thermal reservoir is defined as a system R contained in a fixed region of space, with energy values restricted to a finite range in which any pair of identical copies of the reservoir, R and R^d, is in mutual stable equilibrium when R and R^d are in stable equilibrium states. For example, water at the triple point is a good approximation of a thermal reservoir.

Reference Thermal Reservoir

A thermal reservoir chosen as a reference is called a reference thermal reservoir.

Second Law (for closed separable systems without internal partitions).

Among all the states of a system A with a given value E of energy and such that A is contained in a prescribed region of space R^A, there exists a unique stable equilibrium state.

Standard Weight Process

Let (A_1, A_2) be a given pair of states of system A and let R be a thermal reservoir, we define a standard weight process of AR from A_1 to A_2 as a weight process of the composite system AR in which the initial and final states of R are stable equilibrium states.

Assumption 2

For a system A, any pair of states (A_1, A_2) can be interconnected by means of a standard reversible weight process of AR, where R is an arbitrary chosen thermal reservoir.

Theorem 2

Let us consider a system A and a thermal reservoir R. Among all standard weight processes for AR between a given pair of states (A_1, A_2) of system A, the energy change of the thermal reservoir R has a lower bound which is reached whenever the process is reversible.

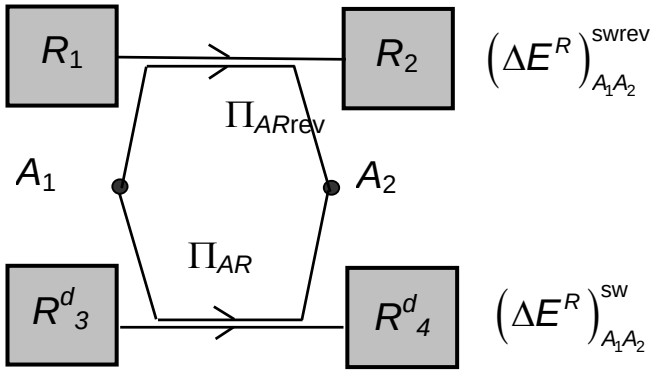

Figure 1.2.1 – Sketch of a standard reversible weight process of AR from A_1 to A_2 nd of a standard weight process of AR^d from A_1 to A_2

Proof

Let Π_{AR} be a standard weight process of AR from A_1 to A_2, and Π_{ARev} a reversible one; let $(\Delta E^R)_{A1A2}{}^{sw}$ e $(\Delta E^R)_{A1A2}{}^{swrev}$ be the energy change of R in the processes Π_{AR} and Π_{ARev} respectively. We will show, whatever is the initial state of R, that:

a) $(\Delta E^R)_{A1A2}{}^{swrev} \le (\Delta E^R)_{A1A2}{}^{sw}$;

b) if also Π_{AR} is reversible, then $(\Delta E^R)_{\mathrm{A1A2}}{}^{\mathrm{swrev}} = (\Delta E^R)_{\mathrm{A1A2}}{}^{\mathrm{sw}}$;

c) if $(\Delta E^R)_{\mathrm{A1A2}}{}^{\mathrm{swrev}} = (\Delta E^R)_{\mathrm{A1A2}}{}^{\mathrm{sw}}$, then also Π_{AR} is reversible.

Proof a)

Let R_1 and R_2 be the initial and final state of R in the process Π_{ARev}. Let R^d be a duplicate of R employed in the process Π_{AR}, and let $R^d{}_3$ and $R^d{}_4$ be the initial and final states of R^d in this process. Let us assume, by contradiction, that $(\Delta E^R)_{\mathrm{A1A2}}{}^{\mathrm{swrev}} > (\Delta E^R)_{\mathrm{A1A2}}{}^{\mathrm{sw}}$. Then, the sequence of the processes $(-\Pi_{AR\mathrm{rev}}, \Pi_{AR})$ would be a weight process of RR^d which, starting from the stable equilibrium state $R_2R^d{}_3$, the energy of RR^d decreases and the regions of space, occupied by the constituents of RR_d, do not change, in opposition to theorem 1.

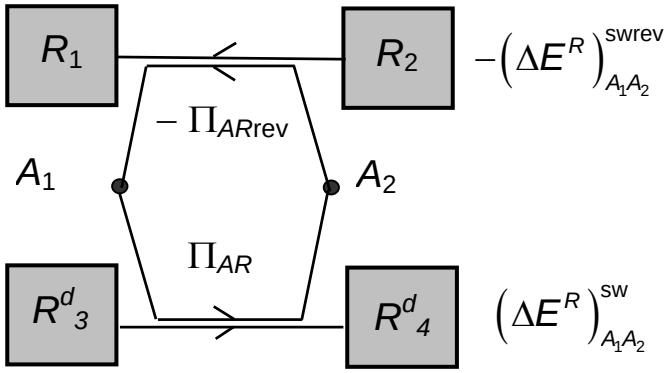

Figure 1.2.2 – Sketch of a standard reversible weight process of AR from A_2 to A_1 and of a standard weight process of AR^d from A_1 to A_2

Proof b)

Assume that also Π_{AR} is reversible, then $(\Delta E^R)_{\mathrm{A1A2}}{}^{\mathrm{swrev}} \le (\Delta E^R)_{\mathrm{A1A2}}{}^{\mathrm{sw}}$ is valid, but also $(\Delta E^R)_{\mathrm{A1A2}}{}^{\mathrm{sw}} \le (\Delta E^R)_{\mathrm{A1A2}}{}^{\mathrm{swrev}}$ is valid; then: $(\Delta E^R)_{\mathrm{A1A2}}{}^{\mathrm{swrev}} = (\Delta E^R)_{\mathrm{A1A2}}{}^{\mathrm{sw}}$.

Proof c)

Let Π_{AR} be a standard weight process of AR, from A_1 to A_2, for which $(\Delta E^R)_{\mathrm{A1A2}}{}^{\mathrm{sw}} = (\Delta E^R)_{\mathrm{A1A2}}{}^{\mathrm{swrev}}$, and let R_1 be the initial state of R for this process. Let Π_{ARrev} be a standard reversible weight process of AR, from A_1 to A_2, with the same initial state R_1 of R.

The sequence of the processes $(\Pi_{AR}, -\Pi_{AR\mathrm{rev}})$ is a cycle of the isolated system ARB, where B is the environment of AR. Hence, Π_{AR} is reversible.

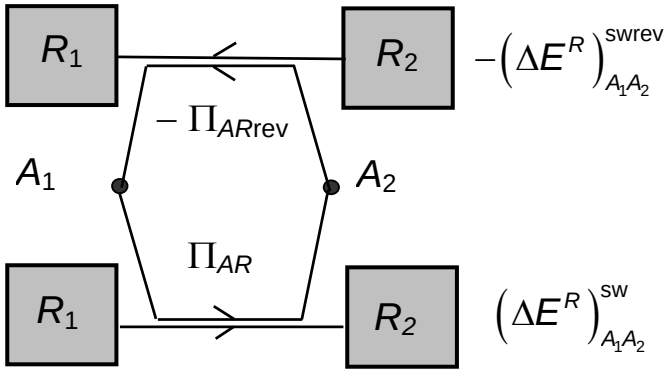

Figure 1.2.3 – Sketch of a standard reversible weight process of AR from A_2 to A_1 and of a standard weight process of AR from A_1 to A_2

Theorem 3

Let R' and R" be any two thermal reservoirs and consider the energy changes, $(\Delta E^{R'})_{\text{A1A2}}{}^{\text{swrev}}$ and $(\Delta E^{R''})_{\text{A1A2}}{}^{\text{swrev}}$ respectively, in standard reversible weight processes of AR' and AR" from A_1 to A_2, where (A_1, A_2) is an arbitrary pair of states of an arbitrary system A. Then the ratio $(\Delta E^{R'})_{\text{A1A2}}{}^{\text{swrev}}/(\Delta E^{R''})_{\text{A1A2}}{}^{\text{swrev}}$ is positive and depends only on R' and R", i.e., it is independent of

(a) the initial stable equilibrium states of R' and R";

(b) the choice of system A;

(c) the choice of states A_1 and A_2

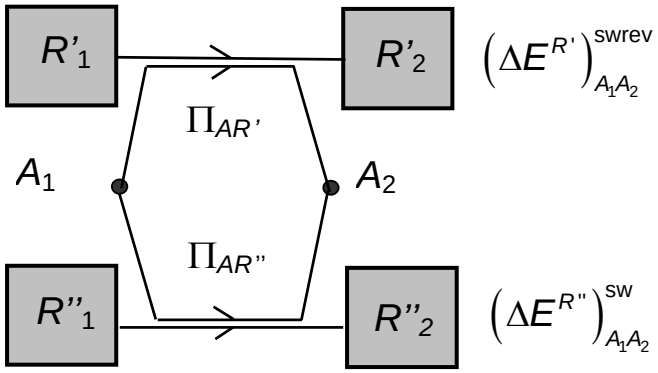

Figure 1.2.4– Sketch of a standard reversible weight process of AR' from A_1 to A_2 and of a standard weight process of AR'' from A_1 to A_2

Definition of temperature of a thermal reservoir

Let R be a given thermal reservoir and R_o a reference thermal reservoir. Select an arbitrary pair of states (A_1, A_2) of an arbitrary system A, and consider the energy changes $(\Delta E^{R})_{\text{A1A2}}{}^{\text{swrev}}$ and $(\Delta E^{Ro})_{\text{A1A2}}{}^{\text{swrev}}$ respectively, in standard reversible weight processes from A_1 to A_2 of AR and of AR^o. We call temperature of R the positive quantity

$$T_R = T_{R_0} \frac{\left(\Delta E^{R}\right)^{swrev}_{A_1A_2}}{\left(\Delta E^{R_0}\right)^{swrev}_{A_1A_2}} \tag{1.2.1}$$

where T_{Ro} is a positive constant associated arbitrarily with the reference thermal reservoir R^o. If for R^o we select water at the triple point and we set T_{Ro} =273.16 K, we obtain the Kelvin temperature scale. Clearly, the temperature T_R of R is defined only up to an arbitrary multiplicative constant.

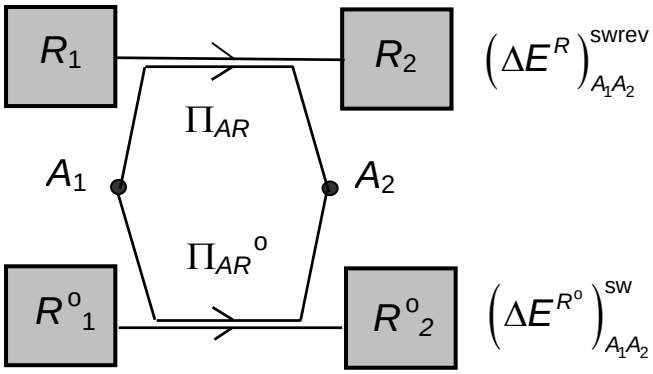

Figure 1.2.5– Sketch of a standard reversible weight process of AR from A_1 to A_2 and of a standard weight process of AR^0 from A_1 to A_2

Corollary 1

The ratio between the temperatures of two thermal reservoirs, R' and R", is independent from the choice of the reference thermal reservoir and can be directly measured as follows:

$$\frac{T_{R'}}{T_{R''}} = \frac{\left(\Delta E^{R'}\right)_{A_1A_2}^{swrev}}{\left(\Delta E^{R''}\right)_{A_1A_2}^{swrev}} \tag{1.2.2}$$

where $(\Delta E^{R'})_{\mathrm{A1A2}}{}^{\mathrm{swrev}}$ and $(\Delta E^{R''})_{\mathrm{A1A2}}{}^{\mathrm{swrev}}$ are the energy changes of R' and R" in standard reversible weight processes from A_1 to A_2 of AR' and AR" respectively.

Proof

Let $(\Delta E^{Ro})_{\mathrm{A1A2}}{}^{\mathrm{swrev}}$ be the energy change in the reference thermal reservoir R^o for any standard reversible weight process from A_1 to A_2 of AR^0. Then:

$$T_{R'} = T_{R_0} \frac{\left(\Delta E^{R'}\right)_{A_1A_2}^{swrev}}{\left(\Delta E^{R_0}\right)_{A_1A_2}^{swrev}} \tag{1.2.3}$$

and

$$T_{R''} = T_{R_0} \frac{\left(\Delta E^{R''}\right)_{A_1A_2}^{swrev}}{\left(\Delta E^{R_0}\right)_{A_1A_2}^{swrev}} \quad . \tag{1.2.4}$$

Thus, dividing Eq. (1.2.3) by Eq. (1.2.4), one gets Eq. (1.2.2).

Corollary 2

Let (A_1, A_2) be any pair of states of system A, and let $(\Delta E^R)_{A1A2}{}^{swrev}$ be the energy change of a thermal reservoir R, with temperature T_R, in any reversible standard weight process from A_1 to A_2 of AR. Then, for the given system A, the ratio $(\Delta E^R)_{A1A2}{}^{swrev}/\ T_R$ depends only on the pair of states (A_1, A_2), *i.e.*, the ratio is independent of the choice of the thermal reservoir R and of its initial stable equilibrium state R_1.

Proof

Let us consider two reversible standard weight processes from A_1 to A_2, one of AR' and the other of AR", where R' is a thermal reservoir with temperature $T_{R'}$ and $R"$ is a thermal reservoir with temperature $T_{R"}$. From corollary 1, one gets:

$$\frac{T_{R'}}{T_{R"}} = \frac{\left(\Delta E^{R'}\right)_{A_1A_2}^{swrev}}{\left(\Delta E^{R"}\right)_{A_1A_2}^{swrev}} \tag{1.2.5}$$

hence,

$$\frac{\left(\Delta E^{R'}\right)_{A_1A_2}^{swrev}}{T_{R'}} = \frac{\left(\Delta E^{R"}\right)_{A_1A_2}^{swrev}}{T_{R"}} \tag{1.2.6}$$

Definition of Property Entropy

Let (A_1, A_2) be any pair of states of system A and let R be an arbitrarily chosen thermal reservoir.

We call entropy difference between A_2 and A1 the quantity

$$S_2^A - S_1^A = -\frac{\left(\Delta E^R\right)_{A_1A_2}^{swrev}}{T_R} \tag{1.2.7}$$

where $(\Delta E^R)_{A1A2}{}^{swrev}$ is the energy change of R in any reversible standard weight process of AR from A_1 to A_2 and T_R is the temperature of R. On account of corollary 2, the second member of Eq. (1.2.7) is uniquely determined by states A_1 and A_2.

Let A_0 be a reference state of system A to which we assign an arbitrary value of entropy $S_0{}^A$. Then, the value of entropy of A, in any other state A_1 is uniquely determined by the equation

$$S_1^A - S_0^A = -\frac{\left(\Delta E^R\right)_{A_0A_1}^{swrev}}{T_R} \quad . \tag{1.2.8}$$

Therefore entropy is a property of A.

Theorem 4 – Additive Property of Entropy

If $C_1 = A_1B_1$ and $C_2=A_2B_2$ are arbitrary chosen states of a composite system C=AB, then

$$S_2^C - S_1^C = S_2^A - S_1^A + S_2^B - S_1^B \tag{1.2.9}$$

Proof.

Let R be a thermal reservoir, with temperature T_R, and let (Π_{AR} , Π_{BR}) be a sequence of processes where Π_{AR} is a reversible standard weight process of AR from A_1 to A_2, and Π_{BR} is a reversible standard weight process of BR from B_1 to B_2. The sequence of processes (Π_{AR} , Π_{BR}) is a reversible standard weight process of CR from C_1 toC_2, in which the energy change of R is given by the sum of the energy change of the constituent processes. Hence:

$$\frac{\left(\Delta E^R\right)_{C_1C_2}^{swrev}}{T_R} = \frac{\left(\Delta E^R\right)_{A_1A_2}^{swrev}}{T_R} + \frac{\left(\Delta E^R\right)_{B_1B_2}^{swrev}}{T_R} \tag{1.2.10}$$

From Eq. (10), by employing the definition of entropy, one obtains Eq. (9).

Theorem 5

Let (A_1, A_2) be any pair of states of system A and let R be a thermal reservoir with temperature T_R. Let Π_{ARirr} an irreversible standard weight process of AR from A_1 to A_2 and let $(\Delta E^R)_{A1A2}{}^{swirr}$ be the energy change of R in this process. Then

$$-\frac{\left(\Delta E^R\right)_{A_1A_2}^{swirr}}{T_R} < S_2^A - S_1^A \tag{1.2.11}$$

Proof

Let Π_{ARrev} be a reversible standard weight process of AR from A_1 to A_2 and let $(\Delta E^R)_{A1A2}{}^{swrev}$ be the energy change of R in this process. On account of Theorem 2, one obtains:

$$\left(\Delta E^R\right)_{A_1A_2}^{swrev} < \left(\Delta E^R\right)_{A_1A_2}^{swirr} \tag{1.2.12}$$

from which,

$$-\left(\Delta E^R\right)_{A_1A_2}^{swrev} > -\left(\Delta E^R\right)_{A_1A_2}^{swirr} \quad . \tag{1.2.13}$$

Dividing both members of Eq. (1.2.13) by T_R, and on account of the definition of property entropy, one gets Eq. (1.2.11).

Theorem 6 – Principle of Nondecrease of Entropy

Let (A_1, A_2) be any pair of states of system A and let $(A_1 \rightarrow A_2)_W$ be a weight process of A from A_1 to A_2. Then, the entropy difference $S_2{}^A$-$S_1{}^A$ equals zero if and only if the weight process is reversible; it is strictly positive if and only if the process is irreversible.

Proof

If $(A_1 \rightarrow A_2)_W$ is reversible, then it is a special case of reversible standard weight process of AR in which the initial stable equilibrium state of R does not change. Hence, $(\Delta E^R)_{A1A2}{}^{swrev}=0$ and, on account of the definition of entropy, one gets $S_2{}^A - S_1{}^A = 0$.

If $(A_1 \rightarrow A_2)_W$ is irreversible, then it is a special of irreversible standard weight process of AR in which the initial stable equilibrium state does not change. Hence, $(\Delta E^R)_{A1A2}{}^{swirr}=0$ and, on account of Eq. (11), one gets $S_2{}^A - S_1{}^A > 0$.

On the other hand, if a weight process of A from A_1 to A_2 is such that $S_2{}^A - S_1{}^A = 0$ then it is reversible, otherwise one would get $S_2{}^A - S_1{}^A > 0$. If a weight process of A from A_1 to A_2 is such that $S_2{}^A - S_1{}^A > 0$ then it is irreversible, otherwise one would get $S_2{}^A - S_1{}^A = 0$.

Theorem 7 – Highest Entropy Principle

Among all the states of a closed system A, in which the constituents of A are in a prescribed region of space R^A, and the value E^A of the energy of A is fixed, the entropy of A reaches the maximum value only in the unique state A_{se} of stable equilibrium determined by R^A and by E^A.

Proof.

Let A_g be any other state in the region of space R^A considered. On account of the first law of thermodynamic and on account of the definition of energy [11], A_g and A_{se} can be interconnected by means of a zero-work weight process of A, either $(A_g \rightarrow A_{se})_w$ or $(A_{se} \rightarrow A_g)_w$. Yet, the existence of a zero-work weight process $(A_{se} \rightarrow A_g)_w$ would contradict the definition of stable equilibrium state. Therefore, a zero-work weight process $(A_g \rightarrow A_{se})_w$ exists and it is irreversible, hence on account of theorem 6 one gets $S_{se}{}^A > S_g{}^A$.

Set of equivalent stable equilibrium states

We call set of equivalent stable equilibrium states of a closed system A, in symbol ESE^A, a subset of the stable equilibrium states of A such as:

- any two states of the subset have different geometrical features;
- any two states of the subset have the same composition;
- any two states of the subset can be interconnected through a zero-work reversible weight process of A. Hence, they have the same energy and the same entropy.

Parameters of a Closed System

We call parameters of a closed system A, a minimum set of real parameters β_1, … βs, such as for any set of parameter values corresponds only one set of equivalent stable equilibrium states of A. We hereby consider systems with a finite number *s* of parameters.

Simple System

We define simple system a system that:

- it has only one parameter which is volume;
- if the system is in a stable equilibrium state and it is divided in an arbitrary number of parts then the effects of the partitions are negligible.

Internal energy

We call internal energy, *U*, the energy of a simple system in a stable equilibrium state.

Fundamental Relation

Two equivalent stable equilibrium states have the same values of *U, V, S*. For all the stable equilibrium states of a simple system we can define the following equation:

$$S = S(U,V) \tag{1.2.14}$$

Assumption 3

The fundamental relation, Eq. (1.2.14), is continuous and differentiable.

Theorem 8

For any fixed value of the volume *V*, the function $S(U)_V$ is strictly increasing.

Proof

Let A_{se1} and A_{se2} be two stable equilibrium states of a simple system A, with energy E_1^A and E_2^A, entropy S_{se1}^A and S_{se2}^A and with the same region of space of system A (*i.e.* with the same volume). Let us assume that $E_1^A > E_2^A$. On account of assumption 1, let us consider a weight process of system A, in which the region of space of the system has no net change, from A_{se1} to a non-equilibrium state A_2 with energy E_2^A. On account of Theorem 6, one gets $S_2^A > S_{se2}^A$. Now, it is always possible to consider an irreversible zero-work weight process of system A from A_2 to A_{se2}. In this process the entropy of system A grows. Therefore one gets:

$$S_{se2}^A > S_2^A \geq S_{se1}^A \tag{1.2.15}$$

Inversion of the fundamental relation

The fundamental relation $S = S(U,V)$ can be written as

$$U = U\left(S, V\right) \quad . \tag{1.2.16}$$

Indeed, on account of theorem 8, for any fixed value of V, the function $S(U)_V$ is strictly increasing and therefore invertible.

Temperature of a System

We call temperature of a simple system A, in a stable equilibrium state, the value

$$T = \left(\frac{\partial U}{\partial S}\right)_V \tag{1.2.17}$$

On account of theorem 8 the temperature of a system is non-negative.

Gibbs equation for a simple system

We call *pressure* of a system A in a stable equilibrium state A_s, the property

$$p = -\left(\frac{\partial U}{\partial V}\right)_S \tag{1.2.18}$$

and let us consider the differential of Eq. (16)

$$\mathrm{d}U = \left(\frac{\partial U}{\partial S}\right)_V \mathrm{d}S + \left(\frac{\partial U}{\partial V}\right)_S \mathrm{d}V \quad , \tag{1.2.19}$$

then, substituting Eq. (18) and Eq. (17) in Eq. (19), one gets

$$\mathrm{d}U = T\,\mathrm{d}S - p\,\mathrm{d}V \quad . \tag{1.2.20}$$

Eq. (1.2.20) is called Gibbs equation and holds for any pair of stable equilibrium states infinitely close of a simple closed system *A*.

Theorem 9. Necessary Condition for Mutual Stability of a Stable Equilibrium State.

Let A and B be closed system and let C=AB be a composite system. The necessary condition so that *C* is in a stable equilibrium state is that A and B are in stable equilibrium states and $T^A = T^B$.

Proof

Let *I* be the set of all the states of C such as: A and B are in stable equilibrium states; R^A and R^B are the regions of space occupied by the constituents of A and B; the energy value of C is E. Let C_1 be any state of *I*. The necessary condition so that C_1 is in a stable equilibrium state is that C_1 is the state with maximum entropy among the set of states of *I*. For the addictivety property of entropy, one gets

$$S^C = S^A + S^B \tag{1.2.21}$$

Within I, S^A and S^B are differentiable function of E^A and E^B respectively; since $E^B = E^C - E^A$ and E^C is fixed, S^C is a differentiable function of E^A, then:

$$S^C\left(E^A\right) = S^A\left(E^A\right) + S^B\left(E^C - E^A\right) \tag{1.2.22}$$

$$\frac{\mathrm{d}S_C}{\mathrm{d}E_A} = \frac{\mathrm{d}S^A}{\mathrm{d}E^A} - \frac{\mathrm{d}S^B}{\mathrm{d}\left(E^C - E^A\right)} = \frac{\mathrm{d}S^A}{\mathrm{d}E^A} - \frac{\mathrm{d}S^B}{\mathrm{d}E^B} \quad . \tag{1.2.23}$$

R^A and R^B are fixed then also the volumes V^A and V^B are fixed. Considering A and B as simple systems and on account of the definitions of T^A and T^B, Eq. (1.2.23) can be written as:

$$\frac{\mathrm{d}S_C}{\mathrm{d}E^A} = \frac{1}{T^A} - \frac{1}{T^B} \tag{1.2.24}$$

Finally, the state C_1 of I is the state of maximum entropy, if

$$\frac{\mathrm{d}S_C}{\mathrm{d}E^A} = 0 \tag{1.2.25}$$

from which one gets $T^A = T^B$.

Assumption 4

Let A be any closed system and let B be a duplicate of A. Let A and B be in the same state. Then A is in mutual stable equilibrium with B.

Theorem 10

Let us consider the set of stable equilibrium states of a simple closed system with fixed volume, then the fundamental relation, Eq. (1.2.14), is convex, *i.e.*:

$$\left(\frac{\partial^2 S}{\partial U^2}\right)_V < 0 \tag{1.2.26}$$

Proof

Let A be a simple closed system in a stable equilibrium state A_1. Let C = AB be a composite system, with B equal to A, in the state $C_1 = A_1B_1$, with B_1 equal to A_1. On account of assumption 4, C_1 is in a stable equilibrium state and it is the state of maximum entropy among the set of states I in which A and B are in stable equilibrium state, with prescribed region of space and prescribed energy of C. In the set I the entropy of C is a function of U^A and we can write as follows

$$S^C\left(U^A\right) = S^A\left(U^A\right) + S^B\left(U^C - U^A\right) \tag{1.2.27}$$

from which

$$\frac{\mathrm{d}S^C}{\mathrm{d}U^A} = \frac{\mathrm{d}S^A}{\mathrm{d}U^A} - \frac{\mathrm{d}S^B}{\mathrm{d}\left(U^C - U^A\right)} \quad . \tag{1.2.28}$$

Differentiating Eq. (1.2.28) with respect to U^A, one obtains

$$\frac{d^2S^C}{d\left(U^A\right)^2}=\frac{\mathrm{d}^2S^A}{\mathrm{d}\left(U^A\right)^2}+\frac{\mathrm{d}^2S^B}{\mathrm{d}\left(U^C-U^A\right)^2}=\frac{\mathrm{d}^2S^A}{\mathrm{d}\left(U^A\right)^2}+\frac{\mathrm{d}^2S^B}{\mathrm{d}\left(U^B\right)^2} \quad . \tag{1.2.29}$$

Since C_1 is the state of maximum entropy of C in the set *I*, we can write as follows

$$\frac{\mathrm{d}^2S^C}{\mathrm{d}\left(U^A\right)^2}<0 \tag{1.2.30}$$

Since B is equal to A and the state B_1 is equal to the state A_1, the two addendums and the second member of Eq. (1.2.29) are equal, and from Eq. (1.2.29) and Eq. (1.2.30) one obtains

$$\frac{\mathrm{d}^2S^A}{\mathrm{d}\left(U^A\right)^2}<0 \tag{1.2.31}$$

Corollary 3

For the set of stable equilibrium states of a simple closed system with fixed volume, the temperature is a strictly growing function of the internal energy.

Proof

On account of the definition of temperature, we can write as follows

$$T=\left(\frac{\partial U}{\partial S}\right)_V \quad . \tag{1.2.32}$$

On account of theorem 10, one obtains

$$\left(\frac{\partial^2 S}{\partial U^2}\right)_V=\frac{\partial}{\partial U}\left(\frac{\partial S}{\partial U}\right)_V<0 \quad . \tag{1.2.33}$$

Differentiating $1/T$ with respect to the internal energy *U*, one gets

$$\frac{\partial}{\partial U}\left(\frac{1}{T}\right)_V=-\frac{1}{T^2}\left(\frac{\partial T}{\partial U}\right)_V<0 \quad , \tag{1.2.34}$$

which implies that

$$\left(\frac{\partial T}{\partial U}\right)_V>0 \quad . \tag{1.2.35}$$

Theorem 11. Necessary and Sufficient Condition for the Mutual Stability of the Equilibrium.

Let C = AB be a composite system, with A and B closed systems. Necessary and sufficient condition so that C is in a stable equilibrium state is that A and B are in stable equilibrium states and that $T^A=T^B$.

Proof

It has already been proved that it is a necessary condition (see theorem 10). Now, let us consider a state C_1 of C, with A and B closed systems and $T^A = T^B$. On account of corollary 3, T^A and T^B determine U^A and U^B respectively and therefore $U^C = U^A + U^B$ is also determined. For any fixed U^C and for any fixed region of space occupied by A and B, there exists a unique stable equilibrium state of C. The necessary condition $T^A = T^B$ is satisfied by the state C_1. Hence, the state C_1 is the only stable equilibrium state of C with the energy determined by T^A and T^B.

Zeroth Law of Thermodynamics

If A is in mutual stable equilibrium with B and B is in mutual stable equilibrium with C, then A is in mutual stable equilibrium with C.

Proof.

The thesis is a direct consequence of theorem 11.

Corollary 4

A simple system C in a stable equilibrium state can be considered as the union of an arbitrary number of closed simple systems, in mutual stable equilibrium, with the same temperature T.

Proof

On account of its definition, C can be considered as union of an arbitrary number of closed simple systems without any effect on the state. The subsets are in mutual stable equilibrium, hence, on account of theorem 9, they have the same temperature T.

Theorem 12

A simple system C in a stable equilibrium state can be considered as the union of an arbitrary number of simple closed subsets, in mutual stable equilibrium, with the same pressure p.

Proof

Let us consider C divided into two simple closed subsets, A and B, by an internal movable wall without any effect on the state. Let us move the wall by means of an infinitesimal weight process Π of C, consisting of quasi-static reversible weight processes of A and B, in which the volume changes of A and B are dV^A and dV^B respectively, with $dV^B = - dV^A$. The external wall of C is kept

fixed. The work done by C in the process Π can not be positive. Indeed, it would be possible: changing C to a stable equilibrium state without external effects and without moving any wall, removing the internal movable wall, changing C to a non equilibrium state by means of a weight process, and this would contradict the definition of stable equilibrium state.

The work done in the process C is equal to the sum of the energy reductions of A and B. Hence, by employing Gibbs equation for A and B, one gets:

$$\delta W^C = -\left(\mathrm{d}U^A + \mathrm{d}U^B\right) = -\left(-p^A \mathrm{d}V^A - p^B \mathrm{d}V^B\right) \tag{1.2.36}$$

Since $\mathrm{d}V^B = -\mathrm{d}V^A$, Eq. (36) can be written as follows

$$\delta W^C = \left(p^A - p^B\right)\mathrm{d}V^A \tag{1.2.37}$$

Since δW^C can not be positive, either for $\mathrm{d}V^A > 0$ or for $\mathrm{d}V^A < 0$, then it must be $p^A = p^B$.

On account of corollary 4 and on account of theorem 12, for a simple closed system in a stable equilibrium state, the properties T and p are intensive, *i.e.* they have the same value for the system and for any system subsets.

Elements of Chemical Thermodynamics

Open separable system

Let O be an open system and let the open system Q be the environment of O. Let OQ be an isolated system. We say that O is separable from Q at time t, if the state $(OQ)_t$ can be reproduced in the state of an isolated system AB, with the same external field, such as A and B are closed and separable at time t.

Set of Elementary Chemical Species

We call set of elementary chemical species a set of constituents obtained by choosing, among all the chemical species composed of a single atomic nucleon, those with the most stable structure at the standard temperature and pressure condition.

Energy and Entropy of an Open System

Let O be an open system and let the open system Q be the environment of O. Let OQ be an isolated system. System O is composed of r constituents, r regions of space and an arbitrary number of admissible chemical reactions. Let O_1 be a state of O with composition $\boldsymbol{n}_1 = (n_1, n_2, n_3, \ldots, \mathrm{nr})$. Let $A^{\boldsymbol{n}1}B$ be an isolated system with the same external field of OQ. Let $A^{\boldsymbol{n}1}$ be a closed system, with the same admissible chemical reaction of system O and a composition compatible with $\boldsymbol{n}_1$. Let $A_1{}^{\boldsymbol{n}1}$ be

a state of $A^{\boldsymbol{n}1}$ that coincides with state O_1, that is, it gives the same results for any measurement procedure that can be applied. We define energy and entropy of O, in the state O_1, the energy value and entropy value of $A^{\boldsymbol{n}1}$ in the state $A_1{}^{\boldsymbol{n}1}$.

The energy and entropy values of $A^{\boldsymbol{n}1}$ in the state $A_1{}^{\boldsymbol{n}1}$ are determined by choosing a reference state $A_0{}^{\boldsymbol{n}1}$ and by applying the definitions of energy difference and entropy difference between two states of a closed system.

The reference state $A_0{}^{\boldsymbol{n}1}$ and the values of energy and entropy of such state are chosen as follows. Let $A^{\boldsymbol{n}1}$ be the union of s closed subsystems, A^1, A^2, …, A^S, which contains only one elementary chemical species respectively; subsystems are chosen such as the composition of $A^{\boldsymbol{n}1}$ is compatible with $\boldsymbol{n}_1$.

Any subsystem A^j is composed of n_j particles of the *j*-th elementary chemical species and it is included in a spherical box; any spherical box is far from the others and it is located in a region of space where the external force field is null. The reference state $A_0{}^{\boldsymbol{n}1}$ is chosen such as any subsystem A^j is in a stable equilibrium state $A^j{}_0$ with temperature T_0 and pressure p_0.

The values of energy and entropy of the reference state $A_0{}^{\boldsymbol{n}1}$ are chosen such as:

$$E\left(A_0^{n1}\right)=\sum_{i=1}^{s}E_0^{A^i} \qquad\qquad S\left(A_0^{n1}\right)=\sum_{i=1}^{s}S_0^{A^i} \tag{1.2.38}$$

Usually, $E_0{}^{\boldsymbol{n}1} = S_0{}^{\boldsymbol{n}1} = 0$.

Stable Equilibrium State of an Open System

We call stable equilibrium state of an open system the state of an open system O if it can be reproduced as stable equilibrium state of a closed system A with the same external field.

Fundamental Relation for an Open System

Let SE^0 be the set of stable equilibrium states of a simple open system O with r non-reactive constituents. Let SE^0-$\mathbf{n}_1$ the subset of SE^0 the composition of which is $\mathbf{n}_1$ and let A^{n1} be a closed system the composition of which is $\mathbf{n}_1$ such as its stable equilibrium states are equal to those of SE^0-$\mathbf{n}_1$. Any set of equivalent stable equilibrium states of O whose composition is $\mathbf{n}_1$, is equal to a set of equivalent stable equilibrium states of A^{n1} which is uniquely determined by the internal energy *U* and the volume *V* of A^{n1}. The same argumentation holds for any composition of O. Hence, the fundamental relation

$$S = S\left(U,V,n\right) \tag{1.2.39}$$

holds for the whole set SE^0.

The fundamental relation can be written also as follows:

$$U = U\left(S,V,n\right) \tag{1.2.40}$$

Gibbs equation for an open system.

By differentiating the fundamental relation, Eq. (1.2.40), one obtains

$$\mathrm{d}U = T\,\mathrm{d}S - p\,\mathrm{d}V + \sum_{i=1}^{r} \mu_i\, dn_i \tag{1.2.41}$$

where

$$\mu_i = \left(\frac{\partial U}{\partial n_i}\right)_{S,V,n'} \tag{1.2.42}$$

is called chemical potential of the *i*-th constituents. We call Eq. (1.2.41), the Gibbs equation for a simple open system O.

Differential of Enthalpy and of the Gibbs Free Energy for an Open System

Let H be the enthalpy of an open system and G the Gibbs free energy of an open system.

Since $H = U + pV$, one obtains

$$\mathrm{d}H = T\,\mathrm{d}S + V\,\mathrm{d}p + \sum_{i=1}^{r} \mu_i\, dn_i \tag{1.2.43}$$

Since $G = H - TS$, from Eq. (1.2.28) one gets

$$\mathrm{d}G = -S\,\mathrm{d}T + V\,\mathrm{d}p + \sum_{i=1}^{r} \mu_i\, dn_i \tag{1.2.44}$$

Theorem 13

A simple open system C in a stable equilibrium state can be considered as the union of an arbitrary number of simple subsystems, in mutual stable equilibrium state, with the same chemical potential of C for each constituents.

Proof

Let us consider C divided in two simple open subsystems, A and B, by means of a fix membrane, which is permeable at the k-th constituent, without any effect on the state of C. Let us consider an infinitesimal weight process Π of C, in which the number of particles $\mathrm{d}n_\mathrm{k}$ of the *k*-th constituents is transferred from B to A; systems A and B maintain a stable equilibrium state with volume unchanged and entropy unchanged. On account of the first law and of the principle of non-decreasing entropy, the process exists and, since the entropy is unchanged, it is reversible. The work done by C in the process Π can not be positive. Indeed, it would be possible: changing C to a stable

equilibrium state without external effects and without moving any wall, removing the permeable membrane, changing C to a non equilibrium state by means of a weight process, and this would contradict the definition of stable equilibrium state.

The work done by C in the process Π is equal to the sum of the internal energy decrease of system A and B. Therefore, by employing Gibbs equation for A and B, one obtains:

$$\delta W^C = -\left(\mathrm{d}U^A + \mathrm{d}U^B\right) = -\left(\mu_k^A \mathrm{d}n_k - \mu_k^B \mathrm{d}n_k\right) = \left(\mu_k^B - \mu_k^A\right)\mathrm{d}n_k \tag{1.2.45}$$

Since δW^C can not be positive either for dn_k>0 or for dn_k<0, then it must be $\mu_k^A = \mu_k^B$.

On account of theorem 13, for a simple system in a stable equilibrium state, the chemical potential of constituents are intensive properties, *i.e.* they have the same value for the system and for any system subsets.

Euler Equation

Let us consider a portion of a simple system in stable equilibrium state. Let us employ the fundamental equation to evaluate the energy difference between the portion considered and a bigger one. Since T, p and μ are uniform, one obtains

$$\Delta U = T\,\Delta S - p\,\Delta V + \sum_{i=1}^{r} \mu_i \Delta n_i \tag{1.2.46}$$

Let us assume that the second portion is k times the first one. Then, the internal energy of the second portion will be k times the first one, *i.e.*, the internal energy difference ΔU between the second portion and the first one will be k-1 times the value of the internal energy U of the first one. The same consideration can be applied to ΔS, ΔV and Δn_i. Therefore, one obtains:

$$(k-1)U = (k-1)TS - (k-1)pV + (k-1)\sum_{i=1}^{r} \mu_i n_i \quad . \tag{1.2.47}$$

Then, dividing for k-1, one gets

$$U = TS - pV + \sum_{j=1}^{r} \mu_j n_j \quad . \tag{1.2.48}$$

Eq. (1.2.48) is called Euler equation.

Since $H = U + pV$, from the Euler equation one gets

$$H = TS + \sum_{j=1}^{r} \mu_j n_j \tag{1.2.49}$$

Since $G = H - TS$, from Eq. (1.2.49), one gets

$$G = \sum_{j=1}^{r} \mu_j n_j \tag{1.2.50}$$

In case of only one constituent, with reference to a mole of matter, one obtains

$$g = \mu \tag{1.2.51}$$

Chemical Potential of an Ideal Gas

Let us consider a set of states of an ideal gas with the same temperature T, and let μ^0 be the chemical potential of the gas at the reference pressure p_0. Then

$$\mu = \mu^0 + RT\, ln\frac{p}{p_0} \quad . \tag{1.2.52}$$

Indeed, for any two states of an ideal gas, with the same temperature T, one has

$$g_2 - g_1 = h_2 - h_1 - T\left(s_2 - s_1\right) = -T\left(s_2 - s_1\right) \tag{1.2.53}$$

and for an ideal gas

$$s_2 - s_1 = -R\, ln\frac{p_2}{p_1} \quad , \tag{1.2.54}$$

Finally, by substituting Eq. (1.2.54) in Eq. (1.2.53) and by employing Eq. (1.2.51), one gets Eq. (1.2.52).

Chemical Potential of the i-th Constituent of an Ideal Gas Mixture

In a Gibbs separation process of an ideal gas mixture, the values of U, H, S and T remain constant, hence $G = H - TS$ remain also constant. Therefore one has

$$G' = G \tag{1.2.55}$$

where G' is the Gibbs free energy of the mixture and G the sum of the Gibbs free energy of the single constituents, at temperature T and partial pressure p_i. By employing the additivity property of G for the single constituents, Eq. (1.2.50) for the mixture and Eq. (1.2.55), one gets:

$$G' = \sum_{j=1}^{r} \mu_j' n_j = \sum_{j=1}^{r} \mu_j\left(T, p_j\right) n_j \quad , \tag{1.2.56}$$

where μ_j' is the chemical potential of the j-th constituent of the mixture.

Since Eq. (1.2.56) must hold for any values of moles number n_j, one has

$$\mu_j' = \mu_j\left(T, p_j\right) = \mu_j^0 + RT\, ln\frac{p_j}{p_0} \quad . \tag{1.2.57}$$

Sign Convention for Stoichiometric Coefficients

The convention is to assign negative coefficients to *reactants* and positive ones to *products*.

Let us consider a generic chemical reaction among the constituents C_A, C_B, C_M,C_N:

$$\nu_A C_A + \nu_B C_B = \nu_M C_M + \nu_N C_N \quad . \tag{1.2.58}$$

By employing the sign convention for stoichiometric coefficient, Eq. (1.2.58) can be written as

$$0 = \sum_j \nu_j C_j \quad . \tag{1.2.59}$$

1.3 MOLAR EXERGY AND MOLAR FLOW EXERGY OF A PURE CHEMICAL FUEL

In the first part of the present Section, by employing the definitions and theorems reported in Section 1.2, the general expression of the exergy of a simple system is determined, and the expression of the molar exergy of a pure chemical fuel is presented as a special case. Then, since a fuel is often supplied by a steady flux in a duct, the expression of the shaft work obtainable by each mole of the fuel, namely the molar flow exergy, is also evaluated. The effects of the gravity field and of the kinetic energy of the fuel delivered in a duct are neglected.

Let us consider a simple system *A*, which is contained within a simple system *B*. The latter, which is an idealization of a part of Earth's atmosphere, crosses only stable equilibrium states with fixed values of the temperature T_B, of the pressure p_B and of the chemical potentials μ_{iB}. The composite system *AB* can exchange only work with its environment; the final volume of AB must be equal to the initial volume; matter exchange between *A* and *B* is allowed. The composite system *AB* is sketched in Fig. 1.3.1. We will assume that all the constituents of *A* are present also in *B*. The initial state A_1 of *A* is chosen arbitrarily. We wish to determine the maximum work which can be performed by *AB* in an adiabatic process at the end of which all the matter initially contained in *A* is contained in *B*.

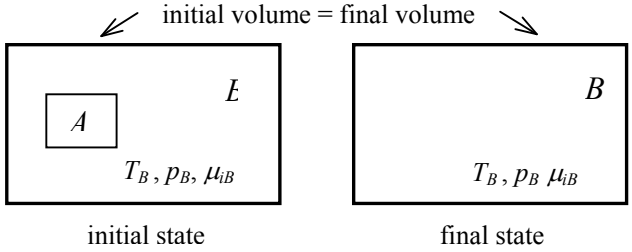

Figure 1.3.1 – Initial state and final state of AB

Let A_2 be another arbitrarily chosen state of *A*. The work performed by *AB* in any adiabatic process in which the initial state of *A* is A_1 and the final state of *A* is A_2 is given by

$$W_{1\to 2} = \left(E_1 - E_2\right)_A + \left(U_1 - U_2\right)_B \quad , \tag{1.3.1}$$

where E denotes the energy and U denotes the internal energy, *i.e.*, the energy of a simple system in a stable equilibrium state [10]. For instance, if a state of system A differs from a stable equilibrium state only on account of the motion of the centre of mass of A, with a (non-relativistic) speed ζ, one has for that state

$$E = U + \frac{1}{2} m \zeta^2 \quad , \tag{1.3.2}$$

where m is the mass of A. Since the intensive parameters T_B, p_B and μ_{iB} are constants, the Gibbs equation yields, for every pair of states of B,

$$\left(U_1 - U_2\right)_B = T_B \left(S_1 - S_2\right)_B - p_B \left(V_1 - V_2\right)_B + \sum_{i=1}^{r} \mu_{iB} \left(n_{i1} - n_{i2}\right)_B \quad , \tag{1.3.3}$$

where r is the number of constituents present in B. By substituting Eq. (1.3.3) in Eq. (1.3.1), one obtains

$$W_{1\to 2} = \left(E_1 - E_2\right)_A + T_B \left(S_1 - S_2\right)_B - p_B \left(V_1 - V_2\right)_B + \sum_{i=1}^{r} \mu_{iB} \left(n_{i1} - n_{i2}\right)_B \quad . \tag{1.3.4}$$

Since the final volume of AB is equal to the initial volume,

$$-\left(V_1 - V_2\right)_B = \left(V_1 - V_2\right)_A \quad . \tag{1.3.5}$$

Let us assume that the constituents of AB are involved in a chemical reaction, where ν_i is the stoichiometric coefficient of the *i-th* constituent. Let us consider the sign convention for stoichiometric coefficient (see Section 1.2), namely the convention is to assign negative coefficients to *reactants* and positive ones to *products*. The stoichiometric coefficient ν_I equals zero if the *i-th* constituent is not involved in the reaction. Then, the changes in the mole numbers of the constituents of AB are given by

$$\left(n_{i2} - n_{i1}\right)_{A+B} = \nu_i \, \varepsilon \quad , \tag{1.3.6}$$

where ε is a positive real number. Equation (1.3.6) yields

$$\nu_i = \frac{\left(n_{i2} - n_{i1}\right)_{A+B}}{\varepsilon} \quad . \tag{1.3.7}$$

Moreover, the condition of chemical equilibrium for B yields

$$\sum_{i=1}^{r} \nu_i \, \mu_{iB} = 0 \quad . \tag{1.3.8}$$

From Eqs. (1.3.7) and (1.3.8) one gets

$$\sum_{i=1}^{r} \mu_{iB} \left(n_{i1} - n_{i2}\right)_{A+B} = 0 \quad , \tag{1.3.9}$$

i.e.,

$$\sum_{i=1}^{r} \mu_{iB} \left(n_{i1} - n_{i2} \right)_B = -\sum_{i=1}^{r} \mu_{iB} \left(n_{i1} - n_{i2} \right)_A \quad . \tag{1.3.10}$$

By substituting Eqs. (1.3.5) and (1.3.10) in Eq. (1.3.4) one obtains

$$W_{1\to 2} = \left(E_1 - E_2 \right)_A + T_B \left(S_1 - S_2 \right)_B + p_B \left(V_1 - V_2 \right)_A - \sum_{i=1}^{r} \mu_{iB} \left(n_{i1} - n_{i2} \right)_A \quad . \tag{1.3.11}$$

Since the process of *AB* is adiabatic, the principle of entropy nondecrese for *AB* yields

$$\left(S_2 - S_1 \right)_A + \left(S_2 - S_1 \right)_B \geq 0 \Rightarrow \left(S_1 - S_2 \right)_B \leq \left(S_2 - S_1 \right)_A \quad , \tag{1.3.12}$$

where the equal sign holds for reversible processes. Equations (1.3.12) and (1.3.11) yield the expression of the maximum work

$$\left(W_{1\to 2} \right)_{\max} = \left(E_1 - E_2 \right)_A - T_B \left(S_1 - S_2 \right)_A + p_B \left(V_1 - V_2 \right)_A - \sum_{i=1}^{r} \mu_{iB} \left(n_{i1} - n_{i2} \right)_A \quad . \tag{1.3.13}$$

Equation (1.3.13) can be written in the form

$$\left(W_{1\to 2} \right)_{\max} = \Xi_1 - \Xi_2 \quad , \tag{1.3.14}$$

where

$$\Xi = E - T_B S + p_B V - \sum_{i=1}^{r} \mu_{iB} n_i \tag{1.3.15}$$

is called the exergy of *A*. Equations (1.3.14) and (1.3.15) yield the maximum work obtainable from *AB* for every initial state A_1 and final state A_2 of *A*. Let us assume that, in the final state, system *A* is in mutual stable equilibrium with *B*. Then, we can choose the boundary between *A* and *B* so that *A* has zero volume and zero mole numbers, and therefore also zero energy and zero entropy; thus, in the final state and one has $\Xi_2 = 0$ .The statement that $\Xi = 0$ when *A* and *B* are in mutual stable equilibrium can also be proved by means of the Euler equation (see Section 1.2, Eq. (1.2.48)). With this choice of the final state of *A*, the maximum work obtainable from *AB* is given by Eq. (1.3.15), with the properties of *A* evaluated in the initial state.

If system *A* is a pure chemical fuel, we will refer to one mole of *A* and will denote the molar properties of *A* with the subscript *F* (fuel). Clearly, the molar exergy of *A* is given by

$$\xi_F = e_F - T_B s_F + p_B v_F - \mu_F \left(T_B, p_{FB} \right) \quad , \tag{1.3.16}$$

where p_{FB} is the partial pressure of the fuel in the atmosphere. Since reliable values of p_{FB} are not available, let us consider the reaction of the fuel with oxygen. Let us denote by ν_i the stoichiometric coefficients (with positive values for reaction products) and by p_{iB} the partial pressures in the atmosphere. The condition of chemical equilibrium for *B* yields

$$\sum_i \nu_i \, \mu_i \left(T_B, p_{iB} \right) = 0 \quad , \tag{1.3.17}$$

i.e.

$$\nu_F \mu_F \left(T_B, p_{FB}\right) = -\sum_{i \neq F} \nu_i \, \mu_i \left(T_B, p_{iB}\right) \quad . \tag{1.3.18}$$

Equations (1.3.16) and (1.3.19) yield

$$\xi_F = e_F - T_B \, s_F + p_B \, v_F + \sum_{i \neq F} \frac{\nu_i}{\nu_F} \mu_i \left(T_B, p_{iB}\right) \quad . \tag{1.3.19}$$

Let us suppose that the initial state of the fuel is the stable equilibrium state with $T = T_B$ and $p = p_B$. In this case, $e_F = u_F \left(T_B, p_{iB}\right)$ and the molar exergy of A is given by

$$\xi_F \left(T_B, p_B\right) = g_F \left(T_B, p_B\right) + \sum_{i \neq F} \frac{\nu_i}{\nu_F} \mu_i \left(T_B, p_{iB}\right) \quad , \tag{1.3.20}$$

where g_F is the molar Gibbs free energy of the fuel. Equation (1.3.20), multiplied by ν_F, gives

$$\nu_F \, \xi_F \left(T_B, p_B\right) = \nu_F g_F \left(T_B, p_B\right) + \sum_{i \neq F} \nu_i \, \mu_i \left(T_B, p_{iB}\right) \quad . \tag{1.3.21}$$

Since oxygen and the combustion products are ideal gases in the atmosphere, for $i \neq F$ one can write

$$\mu_i \left(T_B, p_{iB}\right) = \mu_i \left(T_B, p_B\right) + RT_B \ln \frac{p_{iB}}{p_B} \quad , \tag{1.3.22}$$

where R is the universal gas costant. Equations (1.3.21) and (1.3.22) yield

$$\nu_F \, \xi_F \left(T_B, p_B\right) = \nu_F \, g_F \left(T_B, p_B\right) + \sum_{i \neq F} \nu_i \, \mu_i \left(T_B, p_B\right) + RT_B \sum_{i \neq F} \nu_i \ln \frac{p_{iB}}{p_B} \quad , \tag{1.3.23}$$

i.e. [12]

$$\nu_F \, \xi_F \left(T_B, p_B\right) = \Delta G \left(T_B, p_B\right) + RT_B \sum_{i \neq F} \nu_i \ln \frac{p_{iB}}{p_B} \quad , \tag{1.3.24}$$

where $\Delta G\left(T_B, p_B\right)$ is the standard Gibbs free energy of reaction at temperature T_B and pressure p_B. From Eq. (1.3.24) one obtains

$$\xi_F \left(T_B, p_B\right) = \frac{\Delta G\left(T_B, p_B\right)}{\nu_F} + \frac{RT_B}{\nu_F} \sum_{i \neq F} \nu_i \ln \frac{p_{iB}}{p_B} \quad , \tag{1.3.25}$$

which is the expression of the molar exergy of the fuel suitable for calculations.

In the special case $T_B = T_0 = 298.15$ K , $p_B = p_0 = 1.01325$ bar , one has

$$\xi_F \left(T_0, p_0\right) = \frac{\Delta G\left(T_0, p_0\right)}{\nu_F} + \frac{RT_0}{\nu_F} \sum_{i \neq F} \nu_i \ln \frac{p_{i0}}{p_0} \quad , \tag{1.3.26}$$

and $\xi_F \left(T_0, p_0\right)$ is called the *standard molar exergy*. The standard Gibbs free energy of reaction, $\Delta G\left(T_0, p_0\right)$, can be evaluated easily [12] by means of tables of the standard Gibbs free energy of formation [13].

A chemical fuel is often supplied to a building or to an industrial system by a steady flux in a tube, with constant values of temperature and pressure. The availability function to be considered in this case, to determine the maximum value of the *useful work* (or *shaft work*) obtainable by each mole of the fuel, will be called *flow exergy*. First, the expression of the molar flow exergy of a chemical fuel is deduced; then it is shown that if the initial state of the fuel is (T_B, p_B), the *molar flow exergy* coincides with the *molar exergy*.

Let us consider a control volume *V*, in steady state, in which *n* pure substances flow, mix and react; *V* has *n* inlet or outlet sections. Let us denote by $\dot{n}_i$ the number of moles of the *i-th* pure substance which flow through the *i-th* section, per unit time. Let us assume that $\dot{n}_i$ is positive if the *i-th* section is an inlet section and negative in the opposite case. The control volume delivers to its environment the useful power (or shaft power) $\dot{W}_u$ and receives from a thermal reservoir *B* with temperature T_B the thermal power $\dot{Q}$. A sketch of *V* is reported in Figure 1.3.2.

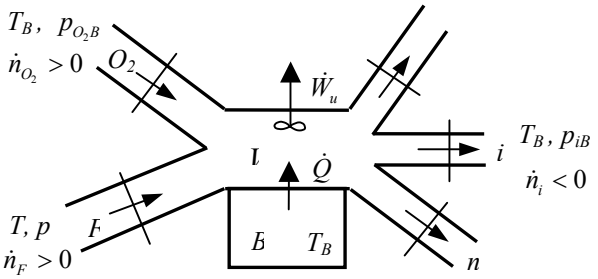

Figure 1.3.2 – Control volume in which n fluids mix and react.

The entering streams are a stream of a pure chemical fuel F (either gas or liquid), at temperature *T* and pressure *p*; a stream of oxygen O_2 at temperature T_B and at the partial pressure of O_2 in the atmosphere. The streams which leave V are composed of combustion gases in stable equilibrium with the surrounding atmosphere, *i.e.*, each at temperature T_B and at its partial pressure in the atmosphere, p_{iB}. The kinetic energy of the reaction products, in the outlet sections, and that of oxygen, in the inlet section, are vanishing. For simplicity, we will assume that the kinetic energy of the fuel, in the inlet section, is vanishing as well. If non negligible, the molar kinetic energy of the fuel must be added to the expressions here deduced in order to obtain the molar flow exergy of the fuel. Under the assumption of negligible kinetic energy of each stream, the energy balance equation for V can be written as [11]

$$\sum_i \dot{n}_i h_i + \dot{Q} - \dot{W}_u = 0 \quad . \tag{1.3.27}$$

Thus, one has

$$\dot{W}_u = \sum_i \dot{n}_i h_i + \dot{Q} \quad . \tag{1.3.28}$$

The entropy balance equation for V yields

$$\sum_i \dot{n}_i s_i + \frac{\dot{Q}}{T_B} + \dot{S}_{irr} = 0 \quad , \tag{1.3.29}$$

where $\dot{S}_{irr}$ is the entropy production in V, per unit time. From Eq. (1.3.29) one obtains

$$\dot{Q} = -T_B \sum_i \dot{n}_i s_i - T_B \dot{S}_{irr} \quad . \tag{1.3.30}$$

The substitution of Eq. (1.3.30) in Eq. (1.3.28) yields

$$\dot{W}_u = \sum_i \dot{n}_i \left(h_i - T_B s_i\right) - T_B \dot{S}_{irr} \quad . \tag{1.3.31}$$

Since $\dot{S}_{irr}$ is positive for irreversible processes and zero for reversible processes, the maximum useful power obtainable from V is given by

$$\dot{W}_{u,\max} = \sum_i \dot{n}_i \left(h_i - T_B s_i\right) \quad . \tag{1.3.32}$$

The maximum useful work obtainable by each mole of fuel, namely the *molar flow exergy* of the fuel, is

$$\psi_F = \frac{\dot{W}_{u,\max}}{\dot{n}_F} = \sum_i \frac{\dot{n}_i}{\dot{n}_F}\left(h_i - T_B s_i\right) = h_F - T_B s_F + \sum_{i\neq F} \frac{\dot{n}_i}{\dot{n}_F}\left(h_i - T_B s_i\right) \quad . \tag{1.3.33}$$

It is easily verified that

$$\frac{\dot{n}_i}{\dot{n}_F} = \frac{\nu_i}{\nu_F} \quad , \tag{1.3.34}$$

where ν_i is the *i-th* stoichiometric coefficient of the combustion reaction. Moreover, for $i \neq F$,

$$h_i - T_B s_i = g_i\left(T_B, p_{iB}\right) = \mu_i\left(T_B, p_{iB}\right) \quad . \tag{1.3.35}$$

From Eqs. (1.3.33), (1.3.34) and (1.3.35) one obtains

$$\psi_F = h_F - T_B s_F + \sum_{i\neq F} \frac{\nu_i}{\nu_F} \mu_i\left(T_B, p_{iB}\right) \quad . \tag{1.3.36}$$

Eq. (1.3.36) is the general expression of the molar flow exergy of a chemical fuel. If the fuel is delivered in the state (T_B , p_B), the molar flow exergy of the fuel is given by

$$\psi_F\left(T_B, p_B\right) = g_F\left(T_B, p_B\right) + \sum_{i\neq F} \frac{\nu_i}{\nu_F} \mu_i\left(T_B, p_{iB}\right) \quad . \tag{1.3.37}$$

A comparison of Eq. (1.3.37) with Eq. (1.3.20) shows that

$$\psi_F\left(T_B, p_B\right) = \xi_F\left(T_B, p_B\right) \quad . \tag{1.3.38}$$

Differences between ψ and ξ occur when the initial temperature and pressure of the fuel are not (T_B , p_B). Indeed, as is shown by Eqs. (1.3.16) and (1.3.36), for one mole of a fluid whose chemical composition remains constant, the change in molar exergy ξ coincides with the change in Keenan's

availability function $\phi = u + p_B v - T_B S$, while the change in molar flow exergy coincides with the change in Keenan's flow availability $\chi = h - T_B S$. Therefore, one has

$$\xi_F(T,p) - \xi_F(T_B,p_B) = u_F(T,p) - u_F(T_B,p_B) - T_0\left[s_F(T,p) - s_F(T_B,p_B)\right] + p_B\left[v_F(T,p) - v_F(T_B,p_B)\right] \quad , \tag{1.3.39}$$

$$\psi_F(T,p) - \psi_F(T_B,p_B) = h_F(T,p) - h_F(T_B,p_B) - T_0\left[s_F(T,p) - s_F(T_B,p_B)\right] \quad . \tag{1.3.40}$$

Eqs. (1.3.39) and (1.3.40) yield

$$\psi(T,p) - \xi(T,p) = (p - p_B)v(T,p) \quad . \tag{1.3.41}$$

1.4 EVALUATION OF THE MOLAR EXERGY FOR $T_B \neq T_O$ AND $p_B \neq p_0$

If $T_B \neq T_O$ and/or $p_B \neq p_0$, the evaluation of $\psi_F(T_B,p_B) = \xi_F(T_B,p_B)$ requires the calculation of the Gibbs free energy of reaction under non-standard conditions. The Gibbs free energy $G = H - TS$ can be considered as a special case of Keenan's flow availability $H - T_B S$,with $T = T_B$. Therefore, the decrease in Gibbs free energy which occurs in a chemical reaction such that the temperature T of the reaction products equals that of the reactants can be evaluated as the *shaft work* performed by a control volume V in steady state, in which the reaction occurs reversibly, such that V can exchange heat with a thermal reservoir with temperature $T = T_B$. Let us consider the process sketched in Fig. (1.4.1), which can be divided into three parts.

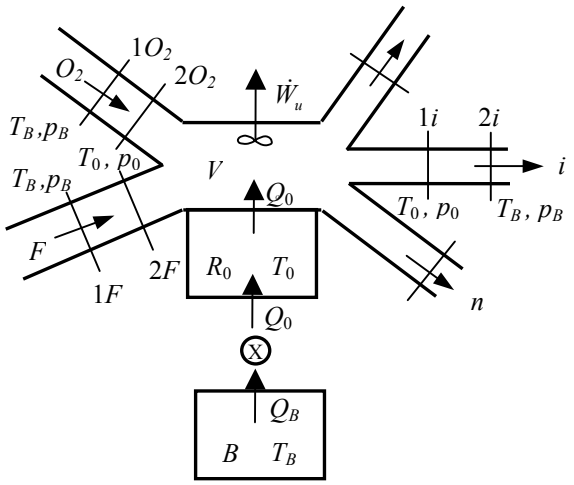

Figure 1.4.1 – Evaluation of $\Delta G(T_B,p_B)$ from $\Delta G(T_0,p_0)$

In the first part, oxygen and fuel, which enter the control volume V at (T_B, p_B) through sections $1O_2$ and $1F$, are brought to (T_0, p_0) (sections $2O_2$ and $2F$), while the *i-th* reaction product is brought from (T_0, p_0) (section $1i$) to (T_B, p_B) (section $2i$). In this process, heat is exchanged with the environment B, at temperature T_B. In agreement with the most common convention adopted in the tables of the standard molar Gibbs free energy of formation, and thus also in the evaluation of

$\Delta G(T_0,p_0)$, we will assume that fuel, oxygen and reaction products are ideal gases. Thus, if the initial and the final state are denoted by 1 and 2, one can write the shaft work obtained in this stage of the process, for one mole of each substance, in the form

$$w_u = \chi_1 - \chi_2 = h_1 - h_2 + T_B\left(s_2 - s_1\right) = c_p\left(T_1 - T_2\right) + T_B\left(c_p \ln\frac{T_2}{T_1} - R\ln\frac{p_2}{p_1}\right) \quad , \qquad (1.4.1)$$

where c_p is the mean specific heat capacity at constant pressure between the temperatures T_1 and T_2. Thus, by considering for each substance a number of moles equal to its stoichiometric coefficient, one obtains the following expression of the shaft work obtained in this part of the process

$$W_{u1} = \sum_i \nu_i \left[c_{pi}\left(T_0 - T_B\right) + T_B\left(c_{pi}\ln\frac{T_B}{T_0} - R\ln\frac{p_B}{p_0}\right)\right] \quad . \qquad (1.4.2)$$

In the second part of the process, the reaction takes place reversibly, at pressure p_0 and temperature T_0, while heat is exchanged with the heat reservoir R_0. In this part, the shaft work obtained is

$$W_{u2} = -\Delta G\left(T_0, p_0\right) \quad , \qquad (1.4.3)$$

while the heat taken from R_0 is

$$Q_0 = T_0\Delta S\left(T_0, p_0\right) = \Delta H\left(T_0, p_0\right) - \Delta G\left(T_0, p_0\right) \quad , \qquad (1.4.4)$$

where $\Delta S\left(T_0, p_0\right)$, $\Delta H\left(T_0, p_0\right)$ and $\Delta G\left(T_0, p_0\right)$ are the standard entropy, enthalpy and Gibbs free energy of reaction, respectively. Finally, R_0 is restored to its initial state by means of a reversible cyclic engine which operates between B and R_0. The shaft work obtained in this part of the process is

$$W_{u3} = Q_B - Q_0 = Q_0\left(\frac{T_B}{T_0} - 1\right) \quad . \qquad (1.4.5)$$

By substituting Eq. (1.4.4) in Eq. (1.4.5) one obtains

$$W_{u3} = \left[\Delta H\left(T_0, p_0\right) - \Delta G\left(T_0, p_0\right)\right]\left(\frac{T_B}{T_0} - 1\right) \quad . \qquad (1.4.6)$$

The sum of W_{u1}, W_{u2} and W_{u3} gives $-\Delta G\left(T_B, p_B\right)$. Thus, the sum of Eqs. (1.4.2), (1.4.3) and (1.4.6) yields

$$-\Delta G\left(T_B, p_B\right) = -\Delta G\left(T_0, p_0\right) + \left[\Delta H\left(T_0, p_0\right) - \Delta G\left(T_0, p_0\right)\right]\left(\frac{T_B}{T_0} - 1\right)$$

$$+\sum_i \nu_i \left[c_{pi}\left(T_0 - T_B\right) + T_B\left(c_{pi}\ln\frac{T_B}{T_0} - R\ln\frac{p_B}{p_0}\right)\right] \qquad (1.4.7)$$

Finally, from Eqs. (1.3.25), (1.3.36) and (1.4.7) one obtains

$$\xi\left(T_B, p_B\right)=\psi\left(T_B, p_B\right)=\frac{1}{v_f}\left\{\Delta G\left(T_0, p_0\right)-\begin{bmatrix}\Delta H\left(T_0, p_0\right)\\ -\Delta G\left(T_0, p_0\right)\end{bmatrix}\left(\frac{T_B}{T_0}-1\right)\right.$$

$$\left.-\sum_i \nu_i\left[c_{pi}\left(T_0-T_B\right)+T_B\left(c_{pi}\ln\frac{T_B}{T_0}-R\ln\frac{p_B}{p_0}\right)\right]+RT_B\sum_{i\neq F}\nu_i\ln\frac{p_{iB}}{p_B}\right\} \qquad (1.4.8)$$

Eq. (1.4.8) allows one to determine the values of the molar exergy (or flow exergy) of any pure chemical fuel, for any pair of values of (T_B, p_B), by employing tables of the standard enthalpy of formation and of the standard Gibbs free energy of formation [13]. In these tables, it is usually assumed that any substance is in a stable or metastable state of ideal gas at (T_0, p_0); the same assumption is employed here, both for (T_0, p_0) and for (T_B, p_B). Therefore, if a fuel is liquid at (T_B, p_B), the value of $\xi(T_B, p_B)$ determined here by Eq. (1.4.8) is the value of the molar exergy of the fuel in a metastable ideal gas state M of the fuel with $T = T_B$ and $p = p_B$. The molar exergy of the fuel in the stable equilibrium state S of liquid at (T_B, p_B) will be determined as follows.

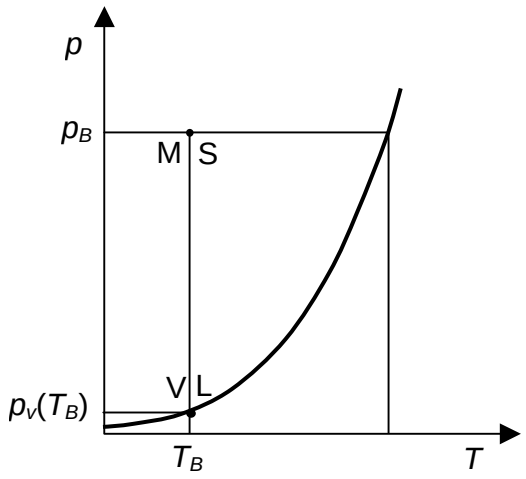

Figure 1.4.2 – Stable state (S), metastable state (M), vapour state (V), liquid state (L)

On account of Eqs. (1.3.16) and (1.3.33), the difference in molar exergy or flow exergy between two stable equilibrium states with $T = T_B$ and $p = p_B$ of a nonreactive closed system equals the difference in Gibbs free energy, which can be easily evaluated as follows (see Fig. 1.4.2):

$$g_S-g_M=\left(g_V-g_M\right)+\left(g_L-g_V\right)+\left(g_S-g_L\right)=\left(g_V-g_M\right)+\left(g_S-g_L\right) \quad , \qquad (1.4.9)$$

where $\left(g_L-g_V\right)$ equals zero since is the difference in Gibbs free energy in a phase change with constant values of T and p.

By employing Eqs. (1.2.53) and (1.2.54) for an ideal gas one obtains

$$g_V-g_M=RT\,ln\frac{p_v\left(T_B\right)}{p_B} \quad , \qquad (1.4.10)$$

where $p_v(T_B)$ is the liquid-vapour equilibrium pressure at $T = T_B$ and v_L is the specific volume of the liquid fuel at temperature T_B.

The second addendum of Eq. (1.4.9) can be evaluated by considering an isentropic compression of the liquid fuel from $p_v(T_B)$ to p_B. Since the specific volume v_L can be considered as constant in the pressure range $[p_v(T_B),p_B]$, one obtains

$$g_S - g_L = h_S - h_L = \int_{p_v(T_B)}^{p_B} v\mathrm{d}p \approx v_L\left[p_B - p_v\left(T_B\right)\right] \quad . \tag{1.4.11}$$

Therefore, one has

$$\xi_S - \xi_M = \psi_S - \psi_M = g_S - g_M = RT\,ln\frac{p_v\left(T_B\right)}{p_B} + v_L\left[p_B - p_v\left(T_B\right)\right] \quad . \tag{1.4.12}$$

1.5 VALUES OF THE MOLAR EXERGY AND MOLAR FLOW EXERGY AS A FUNCTION OF ENVIROMENTAL CONDITIONS AND INITIAL STATES OF CHEMICAL FUELS

By employing Eqs. (1.4.8) and (1.4.12) and the thermodynamic data reported in Refs. [13,14], the values of the molar exergy of several hydrocarbons, hydrogen and carbon monoxide have been evaluated, with reference to many different states of the environment. The pressure has been assumed constant and equal to the standard value $p_B = p_0 = 1.01325$ bar; the temperature has been assumed as variable between -5 °C and 40°C (268.15 K ≤ T_B ≤ 313.15 K); the relative humidity has been assumed as variable in the range $0.1 \le \varphi_B \le 1$. In agreement with [9], the U.S. Standard Atmosphere has been considered [15], with an updated value of the molar fraction of carbon dioxide [16]. Thus, the following molar composition of dry atmospheric air has been employed: nitrogen 0.78084, oxygen 0.209406, argon 0.00934, carbon dioxide 0.000384, and other gases 0.00003. The partial pressures of gases have been determined by evaluating the partial pressure of water vapour as a function of T_B [14] and φ_B, and keeping the total pressure constant.

The values of the standard molar exergy have been evaluated by assuming that the atmosphere is at the reference temperature $T_0 = 298.15$ K, either with a relative humidity $\varphi_0 = 0.65$ [5], or with a relative humidity $\varphi_0 = 0.70$ [9]. In Table 1.5.1, the values of the standard molar exergy of the fuels considered are reported and compared, for gas states, with those obtained by Brzustowski and Brena [5] and by Ertesvag [9]. The comparison with Refs. [5] and [9] reveals an excellent agreement. The small discrepancies are mainly due to the employment of different tables of enthalpy and Gibbs free energy of formation. For fuels which are liquid at $T = T_0$ and $p = p_0$, values of the molar exergy are reported in Table 1 both for the metastable gas state M and for the stable liquid state S of the fuel. The values of the standard molar exergy for the liquid state have been evidenced by a light gray background. The difference in molar exergy between the states S and M has been determined by Eq.

(1.4.12). For the fuels examined in Table 1.5.1, the values of the molar exergy for non-standard conditions of the environment are reported in Tables 1.5.2–5. The following temperatures of the atmosphere are considered: T_B = 268.15 K, T_B = 283.15 K, T_B = 298.15 K, T_B = 313.15 K. For each temperature, values of the molar exergy for φ_B = 0.1, 0.2, 0.3, 0.4, 0.5 are reported in Tables 1.5.2 and 1.5.3, while values of the molar exergy for φ_B = 0.6, 0.7, 0.8, 0.9, 1.0 are reported in Tables 1.5.4 and 1.5.5. The tables can be employed to determine accurately, through linear interpolation, the molar exergy of the fuels in the range 268.15 K ≤ T_B ≤ 313.15 K and 0.1 ≤ φ_B ≤ 1. If, at a given temperature, a fuel is liquid in the stable equilibrium state, the values of the molar exergy as a function of φ_B reported in Tables 2–5 refer to the metastable gas state M; the difference $\xi_S - \xi_M$ is reported in the third column of Tables 1.5.2 and 1.5.3.

Table 1.5.1 – Values of the standard molar exergy of some chemical fuels, in kJ/mol, and comparison with Refs. [5,9].

Fuel	Phase	φ_B=0.65	φ_B=0.70	[5]	[11]	Diff. % [5]	Diff. % [11]
Methane	gas	832.658	832.286	832.350	831.47	-0.037	-0.098
Ethane	gas	1497.94	1497.38	1497.108	1495.5	-0.055	-0.125
Propane	gas	2152.17	2151.43	2153.360	2151.1	+0.055	-0.015
n-Butane	gas	2806.57	2805.64	2806.549	2805	-0.001	-0.023
n-Pentane	gas	3461.17	3460.05	3462.190	3458.7	+0.030	-0.039
n-Pentane	liquid	3460.20	3459.08	–	–	–	–
n-Hexane	gas	4116.89	4115.59	4117.117	4113.3	+0.006	-0.056
n-Hexane	liquid	4112.90	4111.60	–	–		–
n-Heptane	gas	4771.56	4770.08	4772.383	–	+0.017	–
n-Heptane	liquid	4764.61	4763.12	–	–	–	–
n-Octane	gas	5426.11	5424.43	5427.641	–	-0.028	–
n-Octane	liquid	5416.21	5414.54	–	–	–	–
n-Nonane	gas	6081.79	6079.94	6082.902	–	+0.018	–
n-Nonane	liquid	6069.02	6067.16	–	–	–	–
n-Decane	gas	6736.70	6734.66	6738.16	–	+0.022	–
n-Decane	liquid	6721.05	6719.01	–	–	–	–
Acetylene	gas	1267.66	1267.47	1266.612	1265.4	-0.082	-0.163
Ethylene	gas	1361.86	1361.49	–	1360.4	–	-0.080
Propylene	gas	2002.27	2001.72	–	–	–	–
Benzene	gas	3300.53	3299.97	–	–	–	–
Benzene	liquid	3295.39	3294.83	–	–	–	–
Hydrogen	gas	236.439	236.254	–	236.098	–	-0.066
Carbon Monoxide	gas	274.872	274.874	–	274.87	–	-0.001

The dependence of the molar exergy on the relative humidity φ_B and on temperature T_B of the environment is illustrated in Figs. (1.5.1) and (1.5.2) for methane.

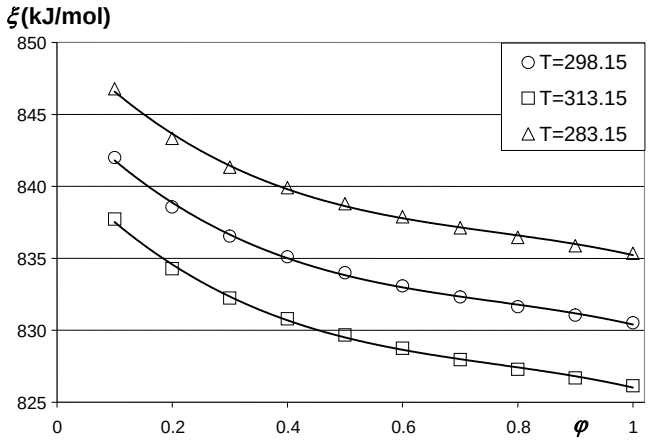

Figure 1.5.1 – Plots of ξ versus φ for methane, for three values of T_B

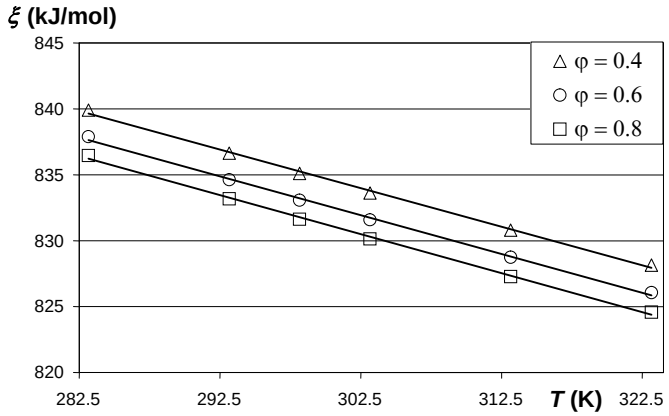

Figure 1.5.2 – Plots of ξ versus T_B for methane, for three values of φ.

In Fig. (1.5.1), plots of the molar exergy of methane versus φ_B are reported, for the temperatures considered in Tables 1.5.2–5. The figure shows that ξ is a decreasing function of φ_B and that a linear interpolation of the data reported in Tables 1.5.2–5 yields accurate values of ξ as a function of φ_B, at any given temperature, especially for $\varphi_B > 0.2$.

In Fig. (1.5.2), plots of the molar exergy of methane versus T_B are reported, for φ_B = 0.2, 0.4, 0.6 and 0.8, in the temperature range -5 °C to 40 °C. The figure shows that ξ is a decreasing function of T_B and that a linear interpolation of the data reported in Tables 1.5.2–5 yields accurate values of ξ as a function of T_B, for any value of φ_B. The dependence of ξ on φ_B is similar for all the fuels examined, except for carbon monoxide, for which this dependence is almost negligible, as evidenced in Tables 1.5.3 and 1.5.5. A wide graphical illustration of the effects of different environmental conditions on the molar exergy of some atmospheric gases and some chemical fuels (hydrogen, methane, n-butane, acetylene, carbon monoxide) is available in Ref. [9].

Table 1.5.2 – Values of the standard molar exergy of some chemical fuels, in kJ/mol, at $T = T_B$ and $p = p_B = 1.01325$ bar, as a function of relative humidity, for 0. 1≤ $\varphi_B \leq 0.5$.

Fuel	Temperature	$\xi_S - \xi_M$	φ_B=0.1	φ_B=0.2	φ_B=0.3	φ_B=0.4	φ_B=0.5
Methane	- 5 °C	–	852,404	848,967	846,955	845,528	844,421
	10 °C	–	846,770	843,331	841,317	839,888	838,779
	25 °C	–	841,981	838,537	836,519	835,085	833,970
	40 °C	–	837,702	834,247	832,218	830,773	829,648
Ethane	- 5 °C	–	1525,93	1520,77	1517,75	1515,61	1513,95
	10 °C	–	1518,29	1513,13	1510,11	1507,96	1506,30
	25 °C	–	1511,92	1506,75	1503,73	1501,58	1499,90
	40 °C	–	1506,32	1501,14	1498,10	1495,93	1494,24
Propane	- 5 °C	–	2188,34	2181,46	2177,44	2174,58	2172,37
	10 °C	–	2178,73	2171,85	2167,82	2164,97	2162,75
	25 °C	–	2170,82	2163,93	2159,90	2157,03	2154,80
	40 °C	–	2163,94	2157,03	2152,97	2150,08	2147,83
n-Butane	- 5 °C	-0.388	2850,90	2842,31	2837,28	2833,71	2830,94
	10 °C	–	2839,33	2830,73	2825,70	2822,12	2819,35
	25 °C	–	2829,88	2821,27	2816,23	2812,64	2809,85
	40 °C	–	2821,72	2813,09	2808,01	2804,40	2801,59
n-Pentane	- 5 °C	-3.680	3513,61	3503,30	3497,27	3492,98	3489,66
	10 °C	-2.312	3500,11	3489,79	3483,75	3479,46	3476,13
	25 °C	-0.972	3489,14	3478,81	3472,75	3468,45	3465,11
	40 °C	–	3479,70	3469,34	3463,25	3458,92	3455,54
n-Hexane	- 5 °C	-6.874	4177,44	4165,40	4158,36	4153,37	4149,49
	10 °C	-5.413	4162,00	4149,96	4142,91	4137,91	4134,03
	25 °C	-3.988	4149,52	4137,47	4130,40	4125,38	4121,48
	40 °C	-2.594	4138,83	4126,74	4119,64	4114,58	4110,64
n-Heptane	- 5 °C	-10.048	4840,26	4826,51	4818,47	4812,76	4808,33
	10 °C	-8.480	4822,87	4809,11	4801,06	4795,34	4790,90
	25 °C	-6.956	4808,86	4795,08	4787,01	4781,27	4776,81
	40 °C	-5.472	4796,89	4783,07	4774,95	4769,17	4764,67
n-Octane	- 5 °C	-13.205	5502,93	5487,46	5478,41	5471,99	5467,01
	10 °C	-11.525	5483,59	5468,11	5459,05	5452,62	5447,63
	25 °C	-9.898	5468,06	5452,56	5443,48	5437,03	5432,01
	40 °C	-8.318	5454,82	5439,28	5430,15	5423,65	5418,58

Table 1.5.3 – Values of the standard molar exergy of some chemical fuels, in kJ/mol, at $T = T_B$ and $p = p_B = 1.01325$ bar, as a function of relative humidity, for 0. 1≤ $\varphi_B \leq 0.5$.

Fuel	Temperature	$\xi_S - \xi_M$	φ_B=0.1	φ_B=0.2	φ_B=0.3	φ_B=0.4	φ_B=0.5
n-Nonane	- 5 °C	*-16.289*	6166.74	6149.55	6139.50	6132.36	6126.83
	10 °C	*-14.505*	6145.46	6128.26	6118.20	6111.05	6105.50
	25 °C	*-12.778*	6128.41	6111.19	6101.10	6093.93	6088.36
	40 °C	*-11.105*	6113.91	6096.64	6086.49	6079.27	6073.64
n-Decane	- 5 °C	*-19.368*	6829.78	6810.87	6799.81	6791.96	6785.87
	10 °C	*-17.477*	6806.55	6787.64	6776.56	6768.70	6762.60
	25 °C	*-15.649*	6787.98	6769.04	6757.94	6750.05	6743.92
	40 °C	*-13.879*	6772.21	6753.21	6742.05	6734.11	6727.92
Acethylene	- 5 °C	–	1280.35	1278.63	1277.62	1276.91	1276.36
	10 °C	–	1276.13	1274.41	1273.40	1272.69	1272.13
	25 °C	–	1272.32	1270.60	1269.59	1268.87	1268.31
	40 °C	–	1268.75	1267.03	1266.01	1265.29	1264.73
Ethylene	- 5 °C	–	1382.33	1378.89	1376.88	1375.46	1374.35
	10 °C	–	1376.33	1372.89	1370.88	1369.45	1368.34
	25 °C	–	1371.18	1367.74	1365.72	1364.28	1363.17
	40 °C	–	1366.54	1363.08	1361.05	1359.61	1358.48
Propylene	- 5 °C	–	2031.12	2025.97	2022.95	2020.81	2019.15
	10 °C	–	2023.06	2017.90	2014.88	2012.73	2011.07
	25 °C	–	2016.26	2011.09	2008.07	2005.92	2004.24
	40 °C	–	2010.23	2005.05	2002.00	1999.84	1998.15
Benzene	- 5 °C	*SOLID State*	3328.69	3323.54	3320.52	3318.38	3316.72
	10 °C	*-6.615*	3320.97	3315.81	3312.79	3310.65	3308.98
	25 °C	*-5.142*	3314.52	3309.35	3306.32	3304.17	3302.50
	40 °C	*-3.704*	3308.83	3303.65	3300.61	3298.44	3296.75
Hydrogen	- 5 °C	–	245.796	244.077	243.072	242.358	241.804
	10 °C	–	243.677	241.957	240.950	240.235	239.681
	25 °C	–	241.101	239.379	238.370	237.653	237.096
	40 °C	–	237.883	236.156	235.141	234.419	233.856
Carbon Monoxide	- 5 °C	–	277.447	277.448	277.448	277.449	277.449
	10 °C	–	276.151	276.153	276.154	276.156	276.157
	25 °C	–	274.850	274.854	274.858	274.862	274.866
	40 °C	–	273.547	273.556	273.565	273.575	273.584

Table 1.5.4 – Values of the standard molar exergy of some chemical fuels, in kJ/mol, at $T = T_B$ and $p = p_B = 1.01325$ bar, as a function of relative humidity, for $0.6 \leq \varphi_B \leq 1$.

Fuel	Temperature	φ_B=0.6	φ_B=0.7	φ_B=0.8	φ_B=0.9	φ_B=1.0
Methane	- 5 °C	843.516	842.751	842.088	841.503	840.979
	10 °C	837.872	837.104	836.439	835.852	835.327
	25 °C	833.059	832.286	831.616	831.024	830.494
	40 °C	828.726	827.942	827.261	826.658	826.116
Ethane	- 5 °C	1512.59	1511.45	1510.45	1509.57	1508.79
	10 °C	1504.94	1503.79	1502.79	1501.91	1501.12
	25 °C	1498.54	1497.38	1496.37	1495.49	1494.69
	40 °C	1492.86	1491.68	1490.66	1489.76	1488.95
Propane	- 5 °C	2170.56	2169.03	2167.70	2166.53	2165.49
	10 °C	2160.93	2159.40	2158.07	2156.89	2155.84
	25 °C	2152.98	2151.43	2150.09	2148.91	2147.85
	40 °C	2145.98	2144.42	2143.05	2141.85	2140.76
n-Butane	- 5 °C	2828.68	2826.77	2825.11	2823.65	2822.34
	10 °C	2817.08	2815.16	2813.50	2812.03	2810.72
	25 °C	2807.57	2805.64	2803.97	2802.49	2801.16
	40 °C	2799.28	2797.32	2795.62	2794.11	2792.76
n-Pentane	- 5 °C	3486.95	3484.65	3482.66	3480.91	3479.34
	10 °C	3473.41	3471.11	3469.11	3467.35	3465.78
	25 °C	3462.37	3460.05	3458.04	3456.27	3454.68
	40 °C	3452.77	3450.42	3448.38	3446.57	3444.95
n-Hexane	- 5 °C	4146.33	4143.65	4141.33	4139.28	4137.45
	10 °C	4130.85	4128.17	4125.84	4123.78	4121.95
	25 °C	4118.29	4115.59	4113.24	4111.17	4109.32
	40 °C	4107.41	4104.67	4102.29	4100.18	4098.28
n-Heptane	- 5 °C	4804.71	4801.65	4799.00	4796.66	4794.56
	10 °C	4787.27	4784.20	4781.54	4779.20	4777.09
	25 °C	4773.17	4770.08	4767.40	4765.03	4762.91
	40 °C	4760.98	4757.85	4755.12	4752.71	4750.54
n-Octane	- 5 °C	5462.93	5459.49	5456.51	5453.87	5451.52
	10 °C	5443.55	5440.10	5437.10	5434.46	5432.10
	25 °C	5427.91	5424.43	5421.42	5418.76	5416.37
	40 °C	5414.43	5410.91	5407.84	5405.13	5402.69

Table 1.5.5 – Values of the standard molar exergy of some chemical fuels, in kJ/mol, at $T = T_B$ and $p = p_B = 1.01325$ bar, as a function of relative humidity, for 0. 1≤ $\varphi_B \leq 0.5$.

Fuel	Temperature	φ_B=0.6	φ_B=0.7	φ_B=0.8	φ_B=0.9	φ_B=1.0
n-Nonane	- 5 °C	6122.30	6118.47	6115.16	6112.23	6109.62
	10 °C	6100.97	6097.13	6093.81	6090.87	6088.25
	25 °C	6083.80	6079.94	6076.59	6073.63	6070.98
	40 °C	6069.03	6065.11	6061.71	6058.69	6055.98
n-Decane	- 5 °C	6780.89	6776.68	6773.04	6769.82	6766.94
	10 °C	6757.61	6753.39	6749.73	6746.51	6743.62
	25 °C	6738.91	6734.66	6730.97	6727.72	6724.80
	40 °C	6722.84	6718.54	6714.79	6711.47	6708.49
Acethylene	- 5 °C	1275.90	1275.52	1275.19	1274.90	1274.64
	10 °C	1271.68	1271.30	1270.96	1270.67	1270.41
	25 °C	1267.86	1267.47	1267.14	1266.84	1266.58
	40 °C	1264.27	1263.87	1263.53	1263.23	1262.96
Ethylene	- 5 °C	1373.44	1372.68	1372.02	1371.43	1370.91
	10 °C	1367.43	1366.67	1366.00	1365.42	1364.89
	25 °C	1362.26	1361.49	1360.82	1360.22	1359.69
	40 °C	1357.56	1356.78	1356.10	1355.49	1354.95
Propylene	- 5 °C	2017.79	2016.64	2015.65	2014.77	2013.98
	10 °C	2009.71	2008.56	2007.56	2006.68	2005.89
	25 °C	2002.88	2001.72	2000.71	1999.82	1999.03
	40 °C	1996.76	1995.59	1994.57	1993.66	1992.85
Benzene	- 5 °C	3315.36	3314.21	3313.22	3312.34	3311.56
	10 °C	3307.62	3306.47	3305.47	3304.59	3303.80
	25 °C	3301.13	3299.97	3298.97	3298.08	3297.29
	40 °C	3295.37	3294.20	3293.17	3292.27	3291.46
Hydrogen	- 5 °C	241.352	240.969	240.638	240.345	240.084
	10 °C	239.227	238.844	238.511	238.218	237.955
	25 °C	236.640	236.254	235.919	235.623	235.358
	40 °C	233.395	233.003	232.663	232.361	232.090
Carbon Monoxide	- 5 °C	277.450	277.450	277.451	277.451	277.452
	10 °C	276.159	276.160	276.162	276.163	276.165
	25 °C	274.870	274.874	274.878	274.882	274.886
	40 °C	273.593	273.603	273.612	273.622	273.632

It has been assumed, so far, that both the temperature and the pressure of the fuel coincide with those of the environment. However, in many cases the fuel is available at a pressure much higher than that of the atmosphere; sometimes, also the fuel temperature can be different from the environment temperature. Therefore, it can be interesting to evaluate the corrections which must be applied to the molar exergy values reported in Tables 1.5.2 – 5 to take into account the difference between the fuel temperature and pressure, (T, p), and the environment temperature and pressure (T_B, p_B). The corrections are different for the molar exergy ξ and the molar flow exergy ψ. From Eqs. (1.3.16) and (1.3.33), one has, respectively:

$$\xi_F(T,p)-\xi_F(T_B,p_B)=u(T,p)-u(T_B,p_B)-T_0\left[s_F(T,p)-s(T_B,p_B)\right] +p_B\left[v(T,p)-v(T_B,p_B)\right] \quad , \tag{1.5.1}$$

$$\psi(T,p)-\psi(T_B,p_B)=h(T,p)-h(T_B,p_B)-T_0\left[s(T,p)-s(T_B,p_B)\right] \tag{1.5.2}$$

The environment pressure p_B has been considered equal to the standard atmospheric pressure p_0 = 1.01325 bar, while the fuel pressure p has been considered as variable in the range 1.01325 bar $\le p \le$ 200 bar. The fuel temperature T has been considered as equal to the environment temperature T_B; the latter has been considered as variable in the range - 5 °C ÷ 40 °C. For the fuels that do not change phase in the pressure range and in the temperature range considered, the values of $\xi(T_B, p)$ - $\xi(T_B, p_B)$ are reported in Table 1.5.6 for p = 2, 4, 6, 8, 10 MPa and in Table 1.5.7 for p = 12, 14, 16, 18, 20 MPa. The values of $\xi(T_B, p)$ - $\xi(T_B, p_B)$ for the fuels in the liquid state have been evidenced by a light gray background.

The tables show that, for liquid fuels, the values of $\xi(T_B, p)$ - $\xi(T_B, p_B)$ can be considered as negligible, so that no correction of the exergy values obtainable from Tables 1.5.2–5 is needed if $T = T_B$. For the fuels which change phase in the pressure and temperature ranges considered, the values of $\xi(T_B, p)$ - $\xi(T_B, p_B)$ are reported in Table 1.5.8 for p = 2, 4, 6, 8,10 MPa and in Table 1.5.9 for p = 12,14,16,18,20 MPa. The values of $\xi(T_B, p)$ - $\xi(T_B, p_B)$ for the fuels in the liquid state have been evidenced by a light gray background. In Table 1.5.10 are reported, for the same fuels, the values of the liquid–gas equilibrium pressure p_v, of the molar exergy difference $\Delta\xi_{gas}$ between the gas at (T_B, p_v) and the gas at (T_B, p_B), of the molar exergy difference $\Delta\xi_{liquid}$ between the liquid at (T_B, p_v) and the gas at (T_B, p_B). All the fuels which change phase in the pressure and temperature ranges considered, except ethane, become liquid at a pressure lower that 2 MPa, which is the pressure value reported in the first column of Table 1.5.8. For these fuels, the correction $\xi(T_B, p)$ - $\xi(T_B, p_B)$ can be evaluated as follows. First, one obtains p_v by means of Table 1.5.10. Then, if $p <$ p_v, the correction is determined through a linear interpolation between 0 (correction for $p = p_0$) and

$\Delta\xi_{\text{gas}}$, (correction for $p = p_v$). If $p > p_v$, the correction is determined through a linear interpolation between $\Delta\xi_{\text{liquid}}$ (correction for $p = p_v$) and the value reported in the first column of Table 1.5.8 (correction for p = 2 MPa).

For ethane, at the temperatures - 5 °C and 10 °C, if 2 MPa< p< 4 MPa, the value of $\xi(T_B, p)$ - $\xi(T_B, p_B)$ is obtained as follows. If $p < p_v$, the correction is determined through a linear interpolation between the value reported in Table 1.5.8 for 2 MPa and $\Delta\xi_{\text{gas}}$ (correction for $p = p_v$). If $p > p_v$, the correction is determined through a linear interpolation between $\Delta\xi_{\text{liquid}}$ (correction for $p = p_v$) and the value reported in Table 1.5.8 for 4 MPa. For ethane at 25 °C, one proceeds in a similar way if 4 MPa < p< 6 MPa.

In order to allow precise evaluations of the molar flow exergy for $p \neq p_B$, the values $\psi(T_B, p)$ - $\psi(T_B, p_B)$ are reported in Tables 1.5.11 and 1.5.12 for the fuels that do not change phase in the pressure range and in the temperature range considered. The tables show that, even for liquid fuels, the values of $\psi(T_B, p)$ - $\psi(T_B, p_B)$ may be non-negligible. The corrections for the molar flow exergy of fuels which change phase are reported in Tables 1.5.13 and 1.5.14. For these fuels, in Table 1.5.15 are reported the values of the liquid–gas equilibrium pressure p_v, of the molar flow exergy difference $\Delta\psi_{\text{gas}}$ between the gas at (T_B, p_v) and the gas at (T_B, p_B)), of the molar flow exergy difference $\Delta\psi_{\text{liquid}}$ between the liquid at (T_B, p_v) and the gas at (T_B, p_B). The tables presented in this paper allow a simple and precise evaluation of the molar exergy or flow exergy of a chemical fuel, with reference to the real states of the fuel and of the environment. Sometimes, the difference between the real molar exergy and the standard molar exergy may be remarkable. Consider, for instance, the molar exergy of gaseous methane contained in a pressurized vessel, with p = 180 bar, in thermal equilibrium with an environment in the state T_B = 268.15 K, p_B =1.01325 bar, φ_B = 0.4. The exact molar exergy value, obtained by means of Tables 1.5.2 and 1.5.7, is 854.57 kJ/mol, while the standard molar exergy, for φ_B = 0.65 [5], is 832.35 kJ/mol. Therefore, the use of the standard value yields an underestimation of the molar exergy of the fuel equal to 22.22 kJ/mol, i.e., to 2.6% of the real value.

Table 1.5.6 – Values of ξ (T_B, p) - ξ (T_B, p_B) in kJ/mol for chemical fuels which do not change phase, as a function of pressure, for p = 2, 4, 6, 8, 10 MPa

Fuel	Temperature	p= 2 MPa	p= 4 MPa	p= 6 MPa	p= 8 MPa	p= 10 MPa
Methane	- 5 °C	4.5329	6.0211	6.9034	7.5270	7.9982
	10 °C	4.7853	6.3556	7.2860	7.9427	8.4435
	25 °C	5.0397	6.6931	7.6714	8.3636	8.8929
	40 °C	5.2929	7.0292	8.0562	8.7842	9.3424
Hydrogen	- 5 °C	4.5317	6.0204	6.9051	7.5363	8.0269
	10 °C	4.7855	6.3575	7.2918	7.9584	8.4769
	25 °C	5.0405	6.6957	7.6793	8.3817	8.9277
	40 °C	5.2946	7.0331	8.0665	8.8042	9.3780
Carbon Monoxide	- 5 °C	3.7273	6.0154	6.8920	7.5118	7.9879
	10 °C	4.7859	6.3531	7.2800	7.9363	8.4417
	25 °C	5.0374	6.6883	7.6653	8.3581	8.8925
	40 °C	5.2937	7.0285	8.0554	8.7844	9.3477
n-Hexane	- 5 °C	0.0001	0.0011	0.0036	0.0054	0.0079
	10 °C	-0.0002	0.0012	0.0036	0.0050	0.0088
	25 °C	0.0005	0.0017	0.0039	0.0067	0.0101
	40 °C	0.0006	0.0019	0.0044	0.0076	0.0115
n-Heptane	- 5 °C	0.0004	0.0011	0.0031	0.0048	0.0072
	10 °C	-0.0002	0.0011	0.0026	0.0054	0.0076
	25 °C	0.0005	0.0016	0.0043	0.0070	0.0098
	40 °C	0.0006	0.0014	0.0036	0.0074	0.0106
n-Octane	- 5 °C	0.0015	0.0016	0.0047	0.0062	0.0070
	10 °C	0.0002	0.0011	0.0034	0.0059	0.0090
	25 °C	0.0008	0.0019	0.0039	0.0061	0.0105
	40 °C	0.0001	0.0017	0.0038	0.0073	0.0107
n-Nonane	- 5 °C	-0.0002	0.0003	0.0018	0.0063	0.0091
	10 °C	0.0009	0.0006	0.0024	0.0043	0.0072
	25 °C	0.0003	0.0025	0.0038	0.0050	0.0093
	40 °C	0.0005	0.0017	0.0040	0.0068	0.0108
n-Decane	- 5 °C	0.0002	0.0017	0.0016	0.0045	0.0066
	10 °C	-0.0004	0.0008	0.0022	0.0056	0.0081
	25 °C	-0.0008	0.0014	0.0027	0.0059	0.0101
	40 °C	0.0003	0.0018	0.0022	0.0065	0.0097

Table 1.5.7 – Values of ξ (T_B, p) - ξ (T_B, p_B) in kJ/mol for chemical fuels which do not change phase, as a function of pressure, for p = 12, 14, 16, 18, 20 MPa

Fuel	*Temperature*	*p= 12* MPa	*p= 14* MPa	*p= 16* MPa	*p= 18* MPa	*p= 20* MPa
Methane	- 5 °C	8.363	8.647	8.868	9.040	9.178
	10 °C	8.839	9.154	9.409	9.615	9.785
	25 °C	9.314	9.657	9.939	10.174	10.371
	40 °C	9.790	10.156	10.463	10.722	10.941
Hydrogen	- 5 °C	8.429	8.768	9.062	9.322	9.554
	10 °C	8.901	9.260	9.571	9.845	10.091
	25 °C	9.375	9.753	10.080	10.370	10.628
	40 °C	9.848	10.245	10.590	10.893	11.165
Carbon Monoxide	- 5 °C	8.371	8.690	8.959	9.192	9.394
	10 °C	8.850	9.190	9.480	9.731	9.951
	25 °C	9.325	9.687	9.996	10.265	10.502
	40 °C	9.805	10.187	10.516	10.802	11.054
n-Hexane	- 5 °C	0.011	0.015	0.019	0.023	0.028
	10 °C	0.013	0.016	0.021	0.026	0.032
	25 °C	0.014	0.019	0.024	0.030	0.037
	40 °C	0.016	0.022	0.028	0.035	0.042
n-Heptane	- 5 °C	0.010	0.014	0.018	0.022	0.028
	10 °C	0.011	0.016	0.021	0.025	0.030
	25 °C	0.014	0.018	0.023	0.029	0.035
	40 °C	0.016	0.021	0.027	0.032	0.040
n-Octane	- 5 °C	0.012	0.015	0.020	0.025	0.030
	10 °C	0.012	0.017	0.022	0.027	0.032
	25 °C	0.014	0.019	0.024	0.030	0.036
	40 °C	0.016	0.021	0.027	0.033	0.041
n-Nonane	- 5 °C	0.011	0.014	0.020	0.024	0.029
	10 °C	0.010	0.015	0.021	0.025	0.032
	25 °C	0.013	0.018	0.023	0.030	0.036
	40 °C	0.016	0.020	0.026	0.033	0.039
n-Decane	- 5 °C	0.010	0.015	0.020	0.023	0.030
	10 °C	0.014	0.017	0.020	0.028	0.031
	25 °C	0.012	0.018	0.025	0.031	0.036
	40 °C	0.016	0.019	0.028	0.032	0.042

Table 1.5.8 – Values of ξ (T_B, p) - ξ (T_B, p_B) in kJ/mol for chemical fuels which change phase, as a function of pressure, for p = 2, 4, 6, 8, 10 MPa

Fuel	Temperature	*p*= 2 MPa	*p*= 4 MPa	*p*= 6 MPa	*p*= 8 MPa	*p*= 10 MPa
Ethane	- 5 °C	4.6064	6.1027	6.1088	6.1162	6.1246
	10 °C	4.8277	7.0631	7.0761	7.0890	7.1023
	25 °C	5.0670	6.9449	7.9802	8.0097	8.0339
	40 °C	5.3097	7.1421	8.6867	8.8440	8.9008
Propane	- 5 °C	2.9130	2.9147	2.9170	2.9202	2.9240
	10 °C	4.0312	4.0332	4.0365	4.0405	4.0452
	25 °C	5.1155	5.1184	5.1222	5.1278	5.1346
	40 °C	6.1672	6.1716	6.1779	6.1851	6.1935
n-Butane	- 5 °C	0.0007	0.0020	0.0032	0.0057	0.0083
	10 °C	0.8541	0.8560	0.8575	0.8606	0.8642
	25 °C	2.0505	2.0517	2.0542	2.0574	2.0618
	40 °C	3.2168	3.2182	3.2214	3.2256	3.2316
n-Pentane	- 5 °C	0.0002	0.0014	0.0029	0.0050	0.0076
	10 °C	0.0003	0.0012	0.0031	0.0057	0.0086
	25 °C	0.0005	0.0018	0.0038	0.0068	0.0103
	40 °C	0.3285	0.3300	0.3326	0.3360	0.3402

Table 1.5.9 – Values of ξ (T_B, p) - ξ (T_B, p_B) in kJ/mol for chemical fuels which change phase, as a function of pressure, for p = 12, 14, 16, 18, 20 MPa

Fuel	Temperature	*p*= 12 MPa	*p*= 14 MPa	*p*= 16 MPa	*p*= 18 MPa	*p*= 20 MPa
Ethane	- 5 °C	6.1333	6.1426	6.1523	6.1522	6.1724
	10 °C	7.1156	7.1289	7.1427	7.1560	7.1696
	25 °C	8.0558	8.0763	8.0958	8.1149	8.1336
	40 °C	8.9410	8.9749	9.0049	9.0325	9.0585
Propane	- 5 °C	2.9283	2.9332	2.9385	2.9443	2.9509
	10 °C	4.0508	4.0570	4.0637	4.0707	4.0784
	25 °C	5.1411	5.1495	5.1574	5.1663	5.1760
	40 °C	6.2027	6.2125	6.2234	6.2345	6.2459
n-Butane	- 5 °C	0.0117	0.0166	0.0203	0.0247	0.0304
	10 °C	0.8680	0.8724	0.8776	0.8836	0.8898
	25 °C	2.0667	2.0725	2.0781	2.0853	2.0918
	40 °C	3.2375	3.2434	3.2515	3.2591	3.2674
n-Pentane	- 5 °C	1.3101	1.5282	1.7458	1.9632	2.1795
	10 °C	1.3376	1.5599	1.7816	2.0028	2.2233
	25 °C	1.3669	1.5939	1.8201	2.0457	2.2705
	40 °C	1.7264	1.9581	2.1890	2.4191	2.6483

Table 1.5.10 – Values of the liquid-gas equilibrium pressure p_v and of $\Delta\xi = \xi\ (T_B, p) - \xi\ (T_B, p_B)$ for the gas state, $\Delta\xi_{gas}$ and for the liquid state $\Delta\xi_{liquid}$.

Fuel	Temperature [°C]	p_v [MPa]	$\Delta\xi_{gas}$ [kJ/mol]	$\Delta\xi_{liquid}$ [kJ/mol]
Ethane	- 5 °C	2.1115	4.7358	6.0980
	10 °C	3.0181	5.8823	7.0565
	25 °C	4.1901	7.1513	7.9300
	40 °C	–	–	–
Propane	- 5 °C	0.4061	1.4293	2.9127
	10 °C	0.6367	2.3618	4.0288
	25 °C	0.9522	3.3696	5.1146
	40 °C	1.3697	4.4323	6.1660
n-Butane	- 5 °C			
	10 °C	0.1485	0.1523	0.8545
	25 °C	0.2433	0.7275	2.0498
	40 °C	0.3785	1.5335	3.2157
n-Pentane	- 5 °C	–	–	–
	10 °C	–	–	–
	25 °C	–	–	–
	40 °C	0.1157	0.3293	0.3296

Table 1.5.11 – Values of ψ (T_B, p) - ψ (T_B, p_B) in kJ/mol for chemical fuels which change phase, as a function of pressure, for p = 2, 4, 6, 8, 10 MPa

Fuel	Temperature	p= 2 MPa	p= 4 MPa	p= 6 MPa	p= 8 MPa	p= 10 MPa
Methane	- 5 °C	6.5430	7.9759	8.7682	9.3002	9.6912
	10 °C	6.9279	8.4627	9.3223	9.9063	10.3425
	25 °C	7.3128	8.9478	9.8709	10.5051	10.9826
	40 °C	7.6949	9.4277	10.4126	11.0948	11.6119
Hydrogen	- 5 °C	6.6748	8.2482	9.1804	9.8502	10.3762
	10 °C	7.0476	8.7081	9.6916	10.3978	10.9524
	25 °C	7.4216	9.1690	10.2034	10.9463	11.5291
	40 °C	7.7946	9.6290	10.7146	11.4937	12.1049
Carbon Monoxide	- 5 °C	5.8163	8.1386	9.0188	9.6398	10.1207
	10 °C	7.0005	8.6125	9.5508	10.2148	10.7301
	25 °C	7.3770	9.0822	10.0774	10.7836	11.3325
	40 °C	7.7574	9.5552	10.6065	11.3539	11.9360
n-Hexane	- 5 °C	0.2394	0.4913	0.7433	0.9935	1.2432
	10 °C	0.2439	0.5009	0.7575	1.0117	1.2670
	25 °C	0.2496	0.5114	0.7726	1.0328	1.2921
	40 °C	0.2550	0.5222	0.7887	1.0541	1.3185
n-Heptane	- 5 °C	0.2698	0.5531	0.8364	1.1183	1.3998
	10 °C	0.2740	0.5627	0.8502	1.1379	1.4235
	25 °C	0.2797	0.5733	0.8669	1.1590	1.4499
	40 °C	0.2850	0.5836	0.8818	1.1799	1.4757
n-Octane	- 5 °C	0.3011	0.6156	0.9319	1.2453	1.5568
	10 °C	0.3049	0.6252	0.9455	1.2647	1.5832
	25 °C	0.3106	0.6364	0.9615	1.2853	1.6098
	40 °C	0.3153	0.6471	0.9775	1.3076	1.6360
n-Nonane	- 5 °C	0.3293	0.6757	1.0217	1.3696	1.7145
	10 °C	0.3357	0.6866	1.0382	1.3886	1.7386
	25 °C	0.3405	0.6996	1.0560	1.4110	1.7675
	40 °C	0.3464	0.7101	1.0733	1.4352	1.7965
n-Decane	- 5 °C	0.3598	0.7389	1.1150	1.4928	1.8688
	10 °C	0.3648	0.7494	1.1326	1.5164	1.8981
	25 °C	0.3703	0.7617	1.1505	1.5397	1.9285
	40 °C	0.3774	0.7741	1.1679	1.5640	1.9572

Table 1.5.12 – Values of ψ (T$_B$, p) - ψ (T$_B$, p$_B$) in kJ/mol for chemical fuels which change phase, as a function of pressure, for p = 12, 14,1 6, 18, 20 MPa

Fuel	*Temperature*	*p= 12* MPa	*p= 14* MPa	*p= 16* MPa	*p= 18* MPa	*p= 20* MPa
Methane	- 5 °C	9.997	10.248	10.462	10.652	10.825
	10 °C	10.688	10.972	11.216	11.430	11.623
	25 °C	11.363	11.680	11.950	12.189	12.403
	40 °C	12.026	12.372	12.669	12.931	13.165
Hydrogen	- 5 °C	10.812	11.184	11.511	11.804	12.068
	10 °C	11.411	11.804	12.148	12.455	12.733
	25 °C	12.011	12.423	12.784	13.107	13.398
	40 °C	12.610	13.042	13.420	13.757	14.062
Carbon Monoxide	- 5 °C	10.514	10.848	11.139	11.399	11.635
	10 °C	11.152	11.511	11.825	12.105	12.358
	25 °C	11.783	12.166	12.502	12.800	13.070
	40 °C	12.414	12.821	13.177	13.494	13.782
n-Hexane	- 5 °C	1.492	1.741	1.990	2.237	2.484
	10 °C	1.521	1.774	2.026	2.278	2.530
	25 °C	1.551	1.809	2.066	2.322	2.578
	40 °C	1.582	1.845	2.107	2.368	2.629
n-Heptane	- 5 °C	1.681	1.962	2.242	2.520	2.800
	10 °C	1.709	1.995	2.280	2.563	2.846
	25 °C	1.740	2.030	2.319	2.608	2.895
	40 °C	1.772	2.066	2.361	2.653	2.946
n-Octane	- 5 °C	1.872	2.182	2.496	2.807	3.117
	10 °C	1.901	2.218	2.534	2.850	3.165
	25 °C	1.932	2.254	2.575	2.896	3.215
	40 °C	1.965	2.292	2.617	2.943	3.268
n-Nonane	- 5 °C	2.058	2.401	2.745	3.087	3.429
	10 °C	2.087	2.437	2.787	3.132	3.481
	25 °C	2.122	2.476	2.830	3.183	3.535
	40 °C	2.157	2.516	2.875	3.233	3.589
n-Decane	- 5 °C	2.245	2.621	2.996	3.369	3.744
	10 °C	2.281	2.662	3.040	3.422	3.798
	25 °C	2.314	2.701	3.088	3.473	3.856
	40 °C	2.352	2.742	3.136	3.524	3.916

Table 1.5.13 – Values of ψ (T_B, p) - ψ(T_B, p_B) in kJ/mol for chemical fuels which change phase, as a function of pressure, for p = 2, 4, 6, 8, 10 MPa

Fuel	Temperature	*p*= 2 MPa	*p*= 4 MPa	*p*= 6 MPa	*p*= 8 MPa	*p*= 10 MPa
Ethane	- 5 °C	6.1578	6.3811	6.5224	6.6616	6.7988
	10 °C	6.5944	7.3689	7.5230	7.6724	7.8187
	25 °C	7.0187	8.2613	8.4822	8.6476	8.8062
	40 °C	7.4307	8.8388	9.3751	9.5756	9.7542
Propane	- 5 °C	3.0685	3.2321	3.3943	3.5557	3.7162
	10 °C	4.1928	4.3623	4.5308	4.6977	4.8635
	25 °C	5.2844	5.4614	5.6360	5.8097	5.9820
	40 °C	6.3453	6.5314	6.7149	6.8956	7.0744
n-Butane	- 5 °C	0.1821	0.3730	0.5624	0.7518	0.9401
	10 °C	1.0404	1.2367	1.4310	1.6253	1.8186
	25 °C	2.2421	2.4430	2.6431	2.8421	3.0405
	40 °C	3.4145	3.6213	3.8274	4.0323	4.2367
n-Pentane	- 5 °C	0.2105	0.4319	0.6523	0.8722	1.0915
	10 °C	0.2151	0.4409	0.6662	0.8907	1.1144
	25 °C	0.2202	0.4522	0.6814	0.9108	1.1393
	40 °C	0.5536	0.7902	1.0257	1.2602	1.4938

Table 1.5.14 – Values of ψ (T_B, p) - ψ(T_B, p_B) in kJ/mol for chemical fuels which change phase, as a function of pressure, for p = 12, 14,1 6, 18, 20 MPa

Fuel	Temperature	*p*= 12 MPa	*p*= 14 MPa	*p*= 16 MPa	*p*= 18 MPa	*p*= 20 MPa
Ethane	- 5 °C	6.9342	7.0681	7.2006	7.3218	7.4618
	10 °C	7.9622	8.1033	8.2429	8.3802	8.5162
	25 °C	8.9602	9.1105	9.2579	9.4029	9.5459
	40 °C	9.9223	10.0847	10.2423	10.3963	10.5472
Propane	- 5 °C	3.8758	4.0347	4.1927	4.3501	4.5071
	10 °C	5.0283	5.1922	5.3551	5.5169	5.6783
	25 °C	6.1521	6.3219	6.4897	6.6568	6.8232
	40 °C	7.2514	7.4266	7.6009	7.7736	7.9448
n-Butane	- 5 °C	1.1281	1.3164	1.5025	1.6883	1.8745
	10 °C	2.0107	2.2023	2.3934	2.5841	2.7740
	25 °C	3.2378	3.4345	3.6296	3.8250	4.0184
	40 °C	4.4393	4.6399	4.8413	5.0406	5.2392
n-Pentane	- 5 °C	1.3101	1.5282	1.7458	1.9632	2.1795
	10 °C	1.3376	1.5599	1.7816	2.0028	2.2233
	25 °C	1.3669	1.5939	1.8201	2.0457	2.2705
	40 °C	1.7264	1.9581	2.1890	2.4191	2.6483

Table 1.5.15 – Values of the liquid-gas equilibrium pressure p_v and of $\Delta\psi = \psi(T_B, p) - \psi(T_B, p_B)$ for the gas state, $\Delta\psi_{gas}$ and for the liquid state $\Delta\psi_{liquid}$.

Fuel	Temperature [°C]	p_v [MPa]	$\Delta\psi_{gas}$ [kJ/mol]	$\Delta\psi_{liquid}$ [kJ/mol]
Ethane	- 5 °C	2.1115	6.2444	6.2447
	10 °C	3.0181	7.2916	7.2909
	25 °C	4.1901	8.3210	8.3207
	40 °C	–	–	–
Propane	- 5 °C	0.4061	2.9383	2.9378
	10 °C	0.6367	4.0752	4.0747
	25 °C	0.9522	5.1896	5.1908
	40 °C	1.3697	6.2864	6.2857
n-Butane	- 5 °C	–	–	–
	10 °C	0.1485	0.8594	0.8591
	25 °C	0.2433	2.0644	2.0642
	40 °C	0.3785	3.2441	3.2448
n-Pentane	- 5 °C	–	–	–
	10 °C	–	–	–
	25 °C	–	–	–
	40 °C	0.1157	0.3293	0.3296

1.6 THERMODYNAMIC EFFICIENCY OF HEAT PUMPS AND BOILERS

A heat pump is a cyclic device that transfers energy from a cold reservoir *B* at constant temperature T_B into a hot reservoir *R* at constant temperature T_R by receiving work, *W* (see Fig. 1.6.1)

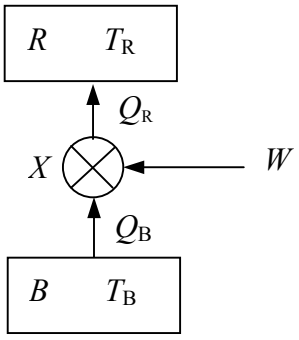

Figure 1.6.1 – Scheme for a cyclic device X that operates as a heat pump between the cold reservoir B and the hot reservoir R.

The hot reservoir can be considered, during winter functioning, as an ideal representation of the hot tank in an actual heat pump plant, and the cold reservoir can be considered as an ideal representation of the external environment, for air to water heat pumps, or of the cold tank for water to water heat pumps or ground coupled heat pumps.

The energy and entropy balances for the cyclic device yields

$$W = Q_R - Q_B \quad , \tag{1.6.1}$$

and

$$S_R - S_B + S_{irr} = 0 \tag{1.6.2}$$

in which Q_R and S_R are the energy and entropy received by reservoir R, respectively, Q_B and S_B are the energy and entropy transferred from reservoir B, respectively, and S_{irr} is the entropy generated by irreversibility in the cyclic device. By employing the definition of entropy, given in Section 1.2, one obtains:

$$Q_R = T_R S_R \qquad \text{and} \qquad Q_B = T_B S_B \quad . \tag{1.6.3}$$

From Eqs. (1.6.1 – 3) one finds

$$W = \frac{T_R - T_B}{T_R} Q_R + T_B S_{irr} \quad . \tag{1.6.4}$$

Solving Eq. (1.6.4) for Q_R, one has

$$Q_R = \frac{T_R}{T_R - T_B} W - \frac{T_R T_B}{T_R - T_B} S_{irr} \quad . \tag{1.6.5}$$

Eq. (1.6.5) shows that, for a given amount of work W, the largest amount of energy transferred to the hot reservoir B, $(Q_R)_{max}$, occurs when the process is reversible, that is, $S_{irr} = 0$. Hence, one obtains

$$\left(Q_R\right)_{max} = \frac{T_R}{T_R - T_B} W \quad . \tag{1.6.6}$$

We define the *Coefficient Of Performance* of a heat pump, COP, the ratio of the energy transferred to the hot reservoir, Q_R, to the work done on the cyclic device, W. The largest value of the coefficient of performance, COP_{max} is obtained when the cyclic process of the heat pump is reversible. By employing the definition of COP, from Eq. (1.6.6), one has

$$\text{COP}_{\max} = \frac{\left(Q_R\right)_{max}}{W} = \frac{T_R}{T_R - T_B} \quad . \tag{1.6.7}$$

We define the *thermodynamic efficiency of a heat pump*, denoted by η_T, for any given work, W, done on the cyclic device, the ratio of the energy transferred to the hot reservoir, Q_R, by an actual heat pump, to the largest amount of energy transferred to the hot reservoir, $(Q_R)_{max}$, achieved by a reversible heat pump. Both heat pumps operate between the same reservoirs. Hence, one has

$$\eta_T = \frac{Q_R}{\left(Q_R\right)_{max}} \quad . \tag{1.6.8}$$

For an actual heat pump, the values of COP as a function of the temperatures T_B and T_R are usually given by the heat pump manufacturer. As an example, Fig. (1.6.2) shows the COP values of a 73 kW water-to-water heat pump as a function of the cold tank temperature, T_B, for three different values of the hot tank temperature, namely, T_R = 35 °C (line D), T_R = 45 °C (line E), and T_R = 65 °C (line F).

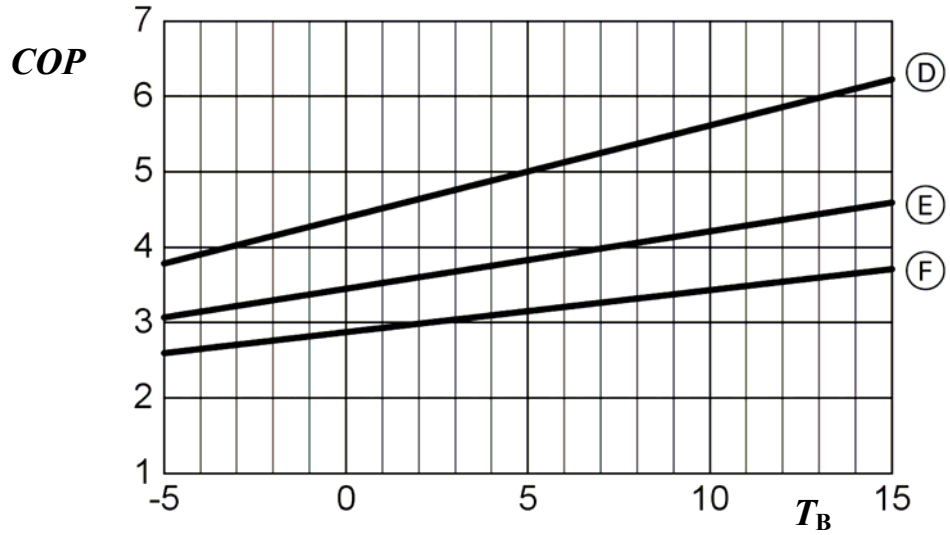

Figure 1.6.2 – COP values as a function of the cold tank temperature, T_B, and the hot tank temperature T_R=35°C (line D), T_R=45°C (line E), and T_R=65°C (line F), for a 73 kW water-to-water heat pump (from Viessmann WW 254 technical datasheet).

Eq. (1.6.7) and Fig. (1.6.2) show, in an ideal case and in a real one respectively, that the smaller the temperature difference between the reservoirs, the higher the COP of a heat pump. Therefore, for a given hot reservoir temperature, which is usually imposed by the heating plant design, the higher the cold reservoir temperature, the higher the COP of the heat pump.

On account of COP definition for an actual heat pump, one has

$$Q_R = W\ COP \quad , \tag{1.6.9}$$

therefore, by substituting Eqs. (1.6.9) and (1.6.6) into Eq. (1.6.8), for work, W, done on the cyclic device, one obtains

$$\eta_T = \frac{Q_R}{(Q_R)_{max}} = \frac{W\ COP}{W\dfrac{T_R}{T_R - T_B}} = COP\frac{T_R - T_B}{T_R} \quad . \tag{1.6.10}$$

Eq. (1.6.10) gives the thermodynamic efficiency of an actual heat pump as a function of its COP and of the temperatures of the hot and cold reservoirs.

Eq. (1.6.10) can also be written as

$$\eta_T = \frac{COP}{(COP)_{\max}} \quad , \tag{1.6.11}$$

in which $(COP)_{max}$ is the Carnot coefficient of performance, i.e.:

$$(COP)_{\max} = \frac{T_R}{T_R - T_B} \quad . \tag{1.6.12}$$

With reference to the COP values showed in Fig. 1.6.2, considering a cold reservoir temperature of 5 °C and a hot reservoir temperature of 35 °C (line D), one obtains

$$\mathrm{COP} = 5 \quad . \tag{1.6.13}$$

Hence, by employing Eq. (1.6.10), one determines

$$\eta_T = 5 \cdot \frac{30}{308.15} = 0.487 \quad . \tag{1.6.14}$$

By considering the COP values given in Fig. (1.6.2) for T_R = 35 °C and by employing Eq. (1.6.10), the thermodynamic efficiency as a function of the cold reservoir temperature, is reported in Fig. (1.6.3). The figure shows that the thermodynamic efficiency reaches a maximum value when the cold reservoir temperature, T_B, is around 0° C.

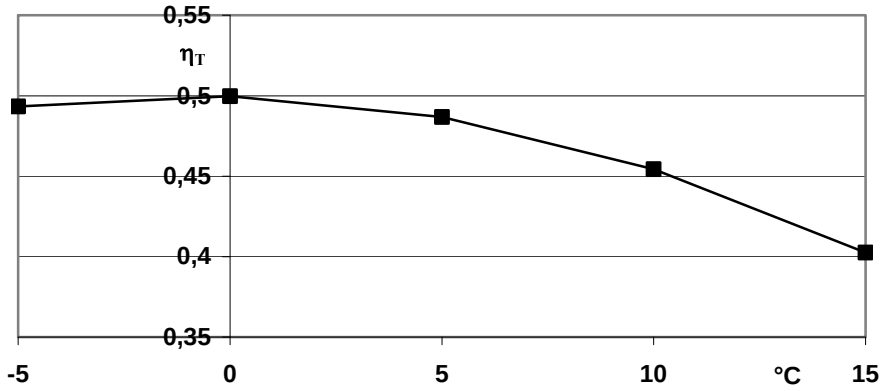

Figure 1.6.3 – Thermodynamic efficiency as a function of the cold reservoir temperature, with hot reservoir temperature T_R= 35 °C.

Boilers

A boiler is a device that is intended to transfer the most part of the maximum useful work of a fuel, that is, the fuel exergy, ξ_F, into a fluid vector, usually water, by exchanging heat between the fuel combustion products and the fluid vector.

Following the scheme proposed for the evaluation of the thermodynamic efficiency of heat pumps, let us consider two reservoirs: the hot reservoir *R* at temperature T_R, that is, an ideal representation of a hot tank in a heating plant, and the cold reservoir *B* at temperature T_B, that is an ideal representation of the atmosphere. For each mole of fuel, with exergy ξ_F, the heat delivered by the boiler to *R* is Q_R. The exergy loss, due to the expulsion of combustion products to stack and mantle loss, is ξ_L (see Fig. 1.6.4a). Alternatively, we can deliver the same amount of heat, Q_R, by means of a cyclic device *X* which operates as a heat pump between *B* and *R* (see Fig. 1.6.4b). The

thermodynamic efficiency of a boiler, denoted η_T, for a given amount of energy, Q_R, transferred to the hot reservoir R, is defined as the ratio of the minimum work done on the cyclic device when the process is reversible to the maximum work obtainable by the fuel, namely the fuel exergy. From Eq. (1.6.4), with $S_{irr} = 0$, one obtains

$$(W)_{\min} = \frac{T_R - T_B}{T_R} Q_R \quad . \tag{1.6.15}$$

Hence, the thermodynamic efficiency of a boiler is

$$\eta_T = \frac{(W)_{\min}}{\xi_F} = \frac{\frac{T_R - T_B}{T_R} Q_R}{\xi_F} = \frac{Q_R}{\xi_F} \frac{T_R - T_B}{T_R} \quad . \tag{1.6.16}$$

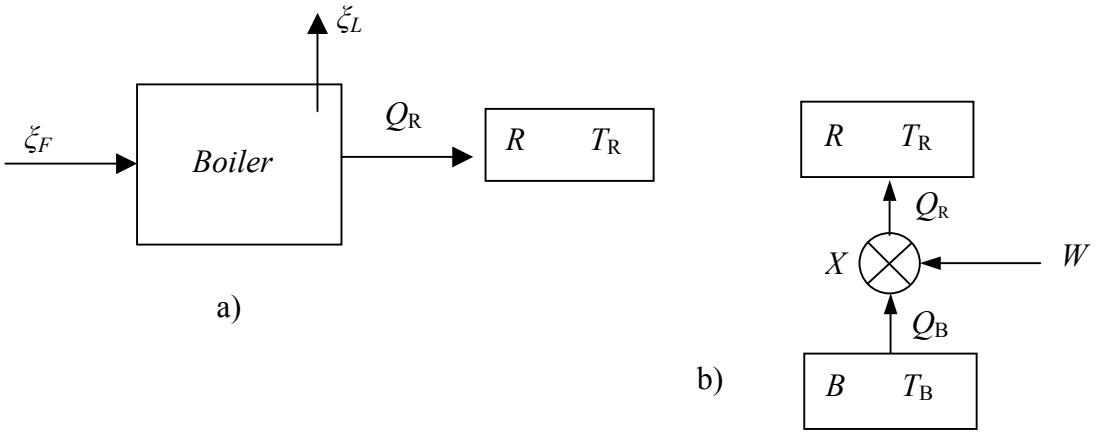

Figure 1.6.4 – Scheme for a boiler (a) and for a cyclic device X, which operates as a heat pump between the cold reservoir B and the hot reservoir R (b).

The efficiency of a boiler, η, is usually given by boiler manufacturers as the ratio of the heat, Q_R, delivered to the fluid vector, to the Low Heating Value (LHV) of the fuel, that is,

$$\eta = \frac{Q_R}{LHV} \quad . \tag{1.6.17}$$

This definition of the boiler efficiency allows values greater than 1 when a condensing boiler is employed. Indeed, a condensing boiler also exploits the latent heat of combustion products which is not included in the fuel LHV. The use of the fuel exergy value as reference to evaluate the boiler efficiency allows a better assessment of the capability of the system to exploit the maximum useful work of the fuel.

Let us explore a methane condensing boiler with an efficiency, η, equal to 1.0. By solving Eq. (1.6.17) for Q_R, and by considering LHV = 802.34 kJ/mol, one obtains for each mole of fuel

$$Q_R = \eta \, LHV = 802.34 \text{ kJ/mol} \quad , \tag{1.6.18}$$

Let us then consider that the fuel is delivered to the boiler at temperature T_B and at pressure p_B (e.g. external ambient temperature and pressure), such as ξ_F (T_B, p_B)= ψ_F(T_B, p_B), and that the relative humidity φ_B is constant and equal to 0.6. Finally, by employing Eq. (1.6.16), with ξ_F (T_B, p_B) evaluated by linear interpolation of the values reported in Table (1.5.4), the thermodynamic efficiency of the boiler as a function of the cold reservoir temperature is reported in Fig. (1.6.5) in the range –5 °C ≤ T_B ≤ 15 °C, for T_R = 35 °C and T_R = 60 °C.

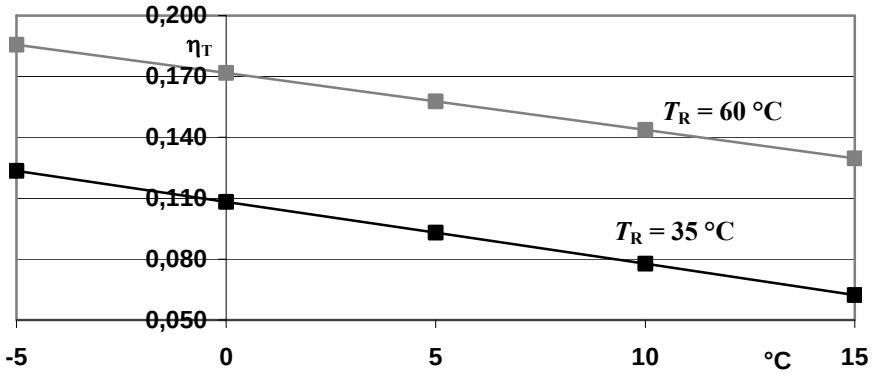

Figure 1.6.5 – The thermodynamic efficiency of the boiler as a function of the cold reservoir temperature, with the hot reservoir temperature T_R= 35 °C (black line) and T_R= 60 °C (grey line).

Fig. (1.6.5) shows that, in the temperature range considered, the thermodynamic efficiency of the boiler is, as expected, lower than that of the heat pump (see Fig. (1.6.3)) and that it increases for higher values of the hot reservoir temperature. Indeed, the values of $(W)_{min,}$ evaluated by means of Eq. (1.6.15), increase for higher values of T_R, while ξ_F decreases slightly.

1.7 CONCLUSIONS

Rigorous definitions of temperature, entropy and internal energy for both closed and open systems have been presented, together with elements of chemical thermodynamics. This theoretical basis has been employed to outline a thorough procedure for the evaluation of the molar exergy and of the molar flow exergy of a pure chemical fuel, for non-standard conditions of the environment. It has been shown that the molar exergy and the molar flow exergy coincide when the temperature and the pressure of the fuel are equal to the temperature T_B and to the pressure p_B of the environment, and a general relation between exergy and flow exergy has been proved. For hydrogen, carbon dioxide and several hydrocarbons, tables of the molar exergy have been provided, for values of T_B in the range 268.15 K $\leq T_B \leq$ 313.15 K and of the relative humidity φ_B of the environment in the range $0.1 \leq \varphi_B \leq 1$, with reference to standard atmospheric pressure. The results show, in agreement with Ertesvag [9], that the molar exergy of hydrocarbons and of hydrogen is a strictly decreasing function of both T_B and φ_B, and that the molar exergy changes owing to different conditions of the environment may be significant. Additional tables have been provided to evaluate the difference between the molar exergy or flow exergy of the fuel in a given initial state and the molar exergy of the fuel at $T = T_B$ and $p = p_B$. In these tables, it is assumed that the fuel and the environment have the same temperature and that the fuel pressure varies in the range $1.01325 \leq p \leq 200$ bar. The tables reported in this chapter allow the determination of accurate values of the molar exergy and of the molar flow exergy of a chemical fuel in thermal equilibrium with its environment, with any pressure between 1.01325 and 200 bar, with reference to the true stable equilibrium state of the fuel, either gas or liquid.

Finally, a rigorous procedure for the evaluation of the thermodynamic efficiency both for heat pumps and boilers has been presented. Furthermore, with reference to an actual heat pump and a gas condensing boiler, values of the thermodynamic efficiency as a function of the cold reservoir temperature (i.e. the cold tank for the heat pump and the external ambient for the gas boiler) have been calculated. As expected, the thermodynamic efficiency of the heat pump is higher than that of the gas boiler. For the cases considered, the results also show that, whereas the thermodynamic efficiency of the gas boiler is a linear decreasing function of the external air temperature, the thermodynamic efficiency of the heat pump, as a function of the cold tank temperature, reaches a maximum at approximately 0 °C and then decreases. This is due to the fact that the COP of an ideal heat pump increases much faster than the COP of an actual heat pump when the difference between hot and cold reservoir temperatures decreases. Note, however, that the maximization of the thermodynamic efficiency is a good target only when the operative conditions (in this case, the

temperatures of the cold and of the hot tank) are fixed. Clearly, for a heat pump system, the smaller the temperature difference between the two reservoirs, the higher the system energy performance. Indeed, this is the case of heat pumps that use soil instead of external air as the heat source or sink, which will be further discussed in the next chapters.

References

[1] Smith MA, Few PC. Second law analysis of an experimental domestic scale co-generation plant incorporatingaheatpump.ApplThermEng2001;21:93–110.

[2] Delsman ER, Uju CU, de Croon, Schouten JC, Ptasinski KJ. Exergy analysis of an integrated fuel processor and fuel cell (FP–FC) system. Energy 2006;31: 3300–9.

[3] Ertesvag IS, Kvamsdal IS, Bolland O. Exergy analysis of a gas-turbine combined-cycle power plant with precombustion CO2 capture. Energy 2005;30:5–39.

[4] Brzustowski TA, Golem PJ. Second-law analysis of energy processes, part I: exergy – an introduction. Trans CSME 1976–1977;4:209–18. [5] Brzustowski TA, Brena A. Second-law analysis of energy processes, part IV: the exergy of hydrocarbon fuels. Trans CSME 1986;10:121–8.

[6] Morris DR, Szargut J. Standard chemical exergy of some elements and compounds on the planet Earth. Energy 1986;11:733–55.

[7] Szargut J. International progress in second law analysis. Energy 1980;6: 709–18.

[8] Kotas TJ. Exergy concepts for thermal plant. Int J Heat Fluid Flow 1980;2: 105–14.

[9] Ertesvag IS. Sensitivity of chemical exergy for atmospheric gases and gaseous fuels to variations in ambient conditions. Energy Convers Manage 2007;48:1983–95.

[10] Hatsopoulos GN, Keenan JH. Principles of general thermodynamics. New York: Krieger; 1981.

[11] Gyftopoulos EP, Beretta GP. Thermodynamics: foundations and applications. Mineola: Dover; 2005.

[12] Denbigh K. The principles of chemical equilibrium. Cambridge: Cambridge University Press; 1984.

[13] Perry's Chemical Engineers' Handbook. 7th ed. New York: McGraw-Hill; 1997.

[14] NIST chemistry webbook, thermophysical properties of fluid systems, http://webbook.nist.gov/chemistry/fluid/.

[15] U.S. Standard Atmosphere, 1976-NOAA – NASA – USAF,Washington D.C.; 1976.

[16] Tans P. NOAA/ESRL, www.esrl.noaa.gov/gmd/ccgg/trends/.

Chapter 2

BOREHOLE HEAT EXCHANGER

Nomenclature			
c_p	heat capacity at constant pressure, [J/(kg K)]	Greek symbols	
F	Fourier number	α	thermal diffusivity, [m^2/s]
G	G - factor	γ	Euler constant
k	thermal conductivity, [W/(mK)]	ρ	density, [kg/m^3]
L	length [m]	τ	time, [s]
$\dot{m}$	mass flow rate, [kg/s]	Subscripts	
Nu	Nusselt number	a	annual
Pr	Prandtl number	b	borehole
q	heat transfer rate per unit length, [W/m]	c	cooling
$\overline{q}$	heat transfer rate per unit volume, [W/m^3]	cal	calorimetric
$\dot{Q}$	heat transfer rate, [W]	el	electric
r	radius, [m]	g	ground
R	linear thermal resistance, [(mK)/W]	h	heating
Re	Reynolds number	in	inlet
t	temperature, [°C]	l	length
T	temperature. [K]	m	mean
U	global heat transfer coefficient, [W/K]	out	outlet
		r	reservoir
		t	total

Heat pumps are devices that transfer heat from a low temperature heat source, to a high temperature heat sink, through mechanical work. As discussed in the previous chapter, the lower the temperature difference between the heat source and the heat sink, the lower the mechanical work needed. Heat pumps are widely employed for buildings space heating and cooling. In the heating mode a heat pump removes heat from a low-temperature source, usually air, and supplies heat to a higher-temperature sink, such as the building interior. In the cooling mode the process is reversed and the heat is extracted from the cooler inside air and rejected to the warmer outside air. Heat pumps that use external air as the heat sink or source are quite common, especially in mild climates, and they are usually called air-to-air heat pumps. Air-source heat pumps have the disadvantage that the greatest requirement for heating or cooling of buildings is necessarily coincident with the times of the year when the outdoor air is least effective as a heat source or sink. For this reason air-source heat pumps are essentially unfeasible in cold climates. Alternatively, heat pumps that use the ground as a heat source or sink can be employed. Indeed, as a result of the low thermal conductivity and high thermal capacity of the ground, the soil temperature, after the first few meters of depth, is almost equal to the annual mean temperature of the air above the ground. Figure (2.1) shows a typical soil temperature profile as function of depth. Hence, the temperature difference between the conditioned space and the heat source (heating mode) or the heat sink (cooling mode) decreases and

therefore the efficiency of the heat pump increases. As well as energy saving, a further benefit of ground-source heat pumps is that they require less maintenance than their air-source counterparts owing to the absence of any exposed outdoor equipment and more-stable operating temperature/pressure of the heat pump compressor. ASHRAE estimates the life expectancy of a ground-source heat pump (19 years) to be more than 25% longer than its air-source counterpart (15 years).

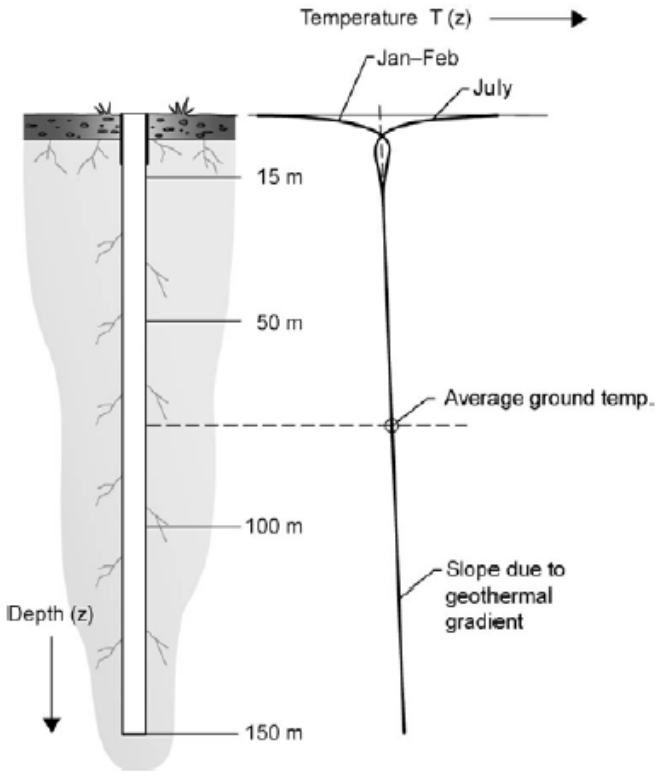

Figure 2.1 – Typical soil temperature profile [1]

In order to couple heat pumps with the ground, borehole heat exchangers are employed. These are buried closed piping loops through which a heat carrier fluid circulates. To design the proper length of borehole heat exchangers, a knowledge of the thermal properties of the ground is essential. Thermal Response Tests (TRTs) are a useful tool to determine the thermal conductivity and heat capacity of the ground. TRTs are discussed further in Section 2.3, and the design and assembly of a TRT apparatus is presented.

In Section 2.1, a description of different type of borehole heat exchangers available on the market is reported. Several design methods present in the literature are critically analysed. Finally, a numerical method for the evaluation of TRTs is presented and two case studies are illustrated.

2.1 GEOTHERMAL HEAT PUMP: AN OVERVIEW

2.1.1 Terminology and Distribution

Ground source heat pump (GSHP), often referred to as geothermal heat pump (GHP), is an all-inclusive term for a variety of systems that use the ground, groundwater, and surface water as a heat source and sink. GSHP systems can be subdivided into two basic configurations: ground-coupled (closed loop) and groundwater (open loop) heat pump systems. Trivial sketches of the two configurations are reported in Fig. (2.1.1a) for ground-coupled heat pump (GCHP) systems and Fig. (2.1.1b) for groundwater heat pump (GWHP) systems.

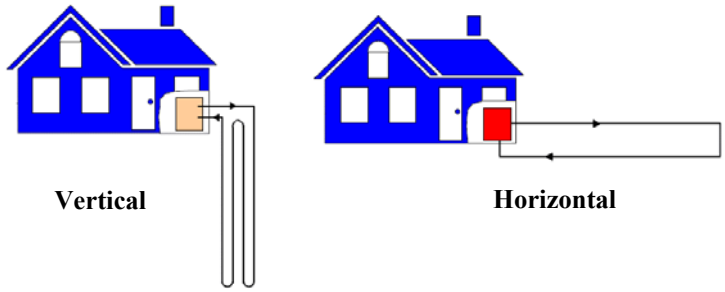

Figure 2.1.1a – Ground-coupled heat pump systems.

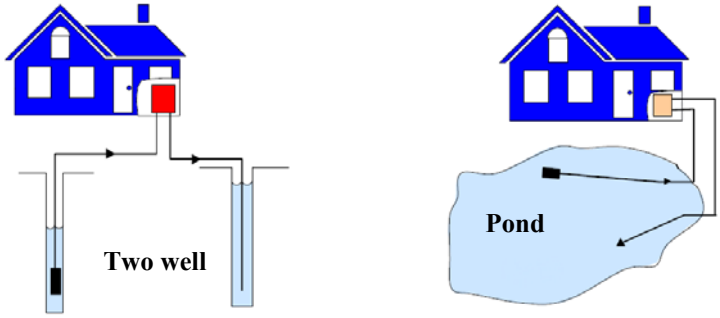

Figure 2.1.1b – Groundwater heat pump systems.

Although heat pump technology is not a new finding, since Lord Kelvin developed the concept in 1852, Robert Webber built the first direct-exchange ground source heat pump only in the 1940s, and commercial popularity was finally achieved only in the 1960s and 1970s especially in the U.S.A., Sweden and Switzerland. During 2008,110000 new units were installed in the EU 27 reaching a total of more than 780000 units. This represents an installed capacity of about 8920 MW. Sweden and Germany today show the largest absolute number of installed units: 320000 for Sweden and 150000 for Germany, corresponding to capacities of 3000 MW and 1650 MW respectively. France follows with about 122000 units representing a capacity of 1340 MW. During 2008 the geothermal heat-pump market exceeded the benchmark of 100000 units being sold

annually for the third year in a row. In terms of number of GSHP unit per capita, Sweden leads by far with almost 35 installations per 1000 habitants. Austria follows with 8 and Finland with 6 units per 1000 habitants. The highest areal density of GSHP can be found in Switzerland with 1.2 installations per square kilometre.

Italy, despite the favourable underground and climatic conditions, still has still very few installations. In 2008, there were 7500 installations, accounting a total capacity of 150 MW (which corresponds to one twentieth of Sweden's total installed capacity). Nonetheless the number of installed units per year is growing fast. This is mainly due to recently approved State financial aid for substituting the older inefficient heating systems with a GSHP system and stricter constrains on the primary energy use for new buildings.

With regard to the Italian situation, the closed loop technology is most commonly applied, even though open loop heat pump systems can reach higher overall efficiency for space heating and cooling. The reason lies in the difficulties encountered by designers and installers in obtaining the necessary installation permits and, of course, the need to have water at disposal, such as underground water (see fig. 2.1.1b, left side) or surface water (see Fig. 2.1.1b, right side). Therefore, in the following section, only ground-coupled heat pump systems are considered.

2.1.2 Horizontal and Vertical BHEs

GCHPs are systems composed of a heat pump linked to the ground by means of borehole heat exchangers (BHEs), *i.e.* a polyethylene-piping network buried in the soil. Figure (2.1.2) shows, during winter functioning, a general schematic of a heat pump (within the green rectangle) whose evaporator exchanges heat with a cold tank, which is coupled to the ground by means of BHEs, while the condenser is linked to a hot tank through which the building heat load demand is delivered.

During winter, BHEs extract heat from the soil which is therefore cooled down, while during summer, when the heat pump works in cooling mode, the soil is used as a heat sink.

GCHPs can be subdivided according to borehole heat exchanger design: horizontal or vertical [1].

Horizontal BHEs

In horizontal BHEs the coupling with the ground is obtained by means of a piping network buried in narrow trenches with a depth ranging between 1.2 m to 2 m. Different configurations can be employed: single pipe, two pipes per trench, or multiple pipe trench (see Fig. (2.1.3)).

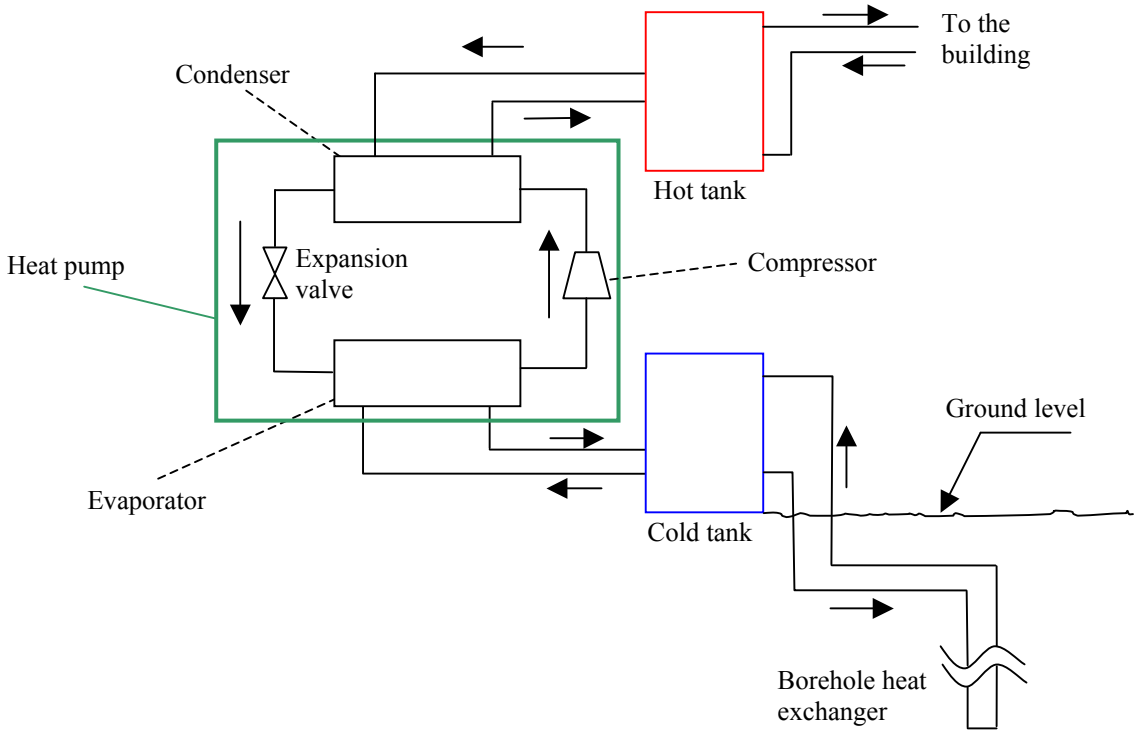

Figure 2.1.2 – Schematic representation of a ground-coupled heat pump system with a vertical borehole heat exchanger for the heating period.

In order to reduce the land area needed for horizontal loop applications, multiple pipes configurations can be employed. The most common configuration has four pipes per trench. Indeed, a higher pipe density in a single trench, although space saving, would provide a lower overall GCHP performance owing to the fact that thermal interference between multiple pipes reduces the heat transfer effectiveness of each pipe.

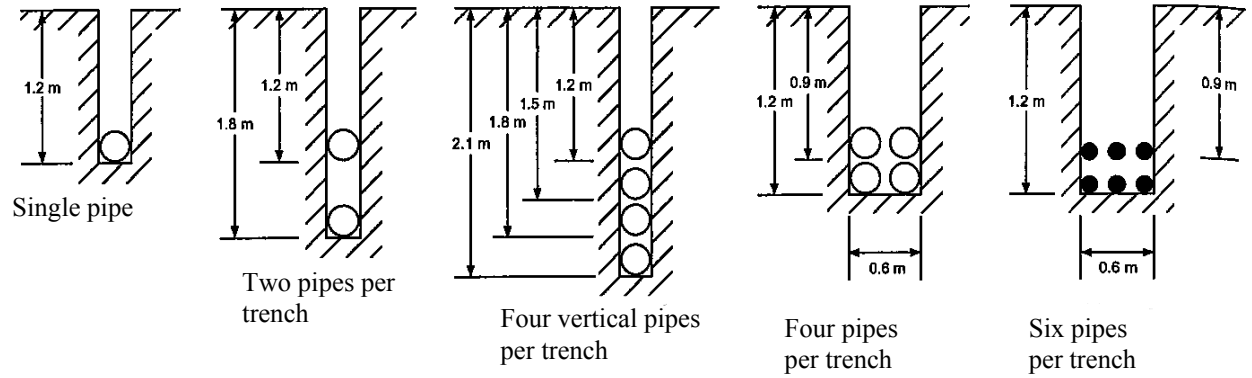

Figure 2.1.3 – Horizontal ground-loop configurations [1]

An overlapping spiral configuration has also been used in some applications [2]. The coil can be placed in vertical trenches (see Fig. (2.1.4)) as well as laying flat on the bottom of a large pit excavated with a bulldozer. The latter configuration generally performs better [1,2].

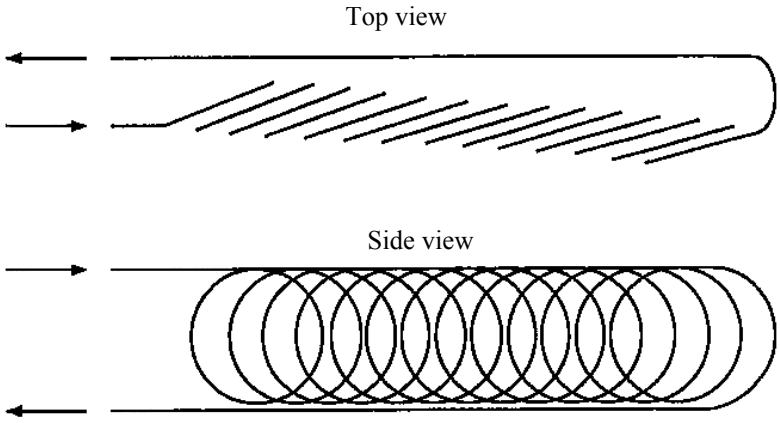

Figure 2.1.4 – General layout of a spiral earth coil [1]

The thermal properties of the soil are an important concern for any ground-loop design. With horizontal loops, the soil type can be easily determined. Ref [3] lists recommended trench lengths for various types of horizontal BHEs with reference to the thermal properties of the ground and loop configurations (single or multiple pipes per trench, spiral, etc). Plant design guidelines, minimum distance between trenches and minimum distance between pipes in a multiple pipe trench configuration are reported in ref. [4]

The advantage of GCHPs with horizontal BHEs is that they are typically less expensive than those with vertical BHEs since appropriate installation equipment and trained equipment operators are more widely available. In addition to requiring more land area, disadvantages include greater adverse variations in performance essentially due to higher ground temperature fluctuations, slightly higher pumping energy requirements, and lower overall system efficiencies [4].

Vertical BHEs

Vertical BHEs generally consist of two high density polyethylene (HDPE) tubes that are placed in a vertical borehole filled with a solid medium, called grout, which is usually a mixture of bentonite and concrete. The tubes are thermally fused at the bottom of the bore hole to form a closed return U-bend. Very often a double U-tube configuration is adopted within a single borehole. The nominal diameter of vertical tubes ranges from 19 mm to 38 mm [1], and the usual depth of the bore hole ranges from 20 m to 150 m (data refers to Italian standard applications). A sketch of a cross section of a double U-tube BHE is shown in Fig. (2.1.5).

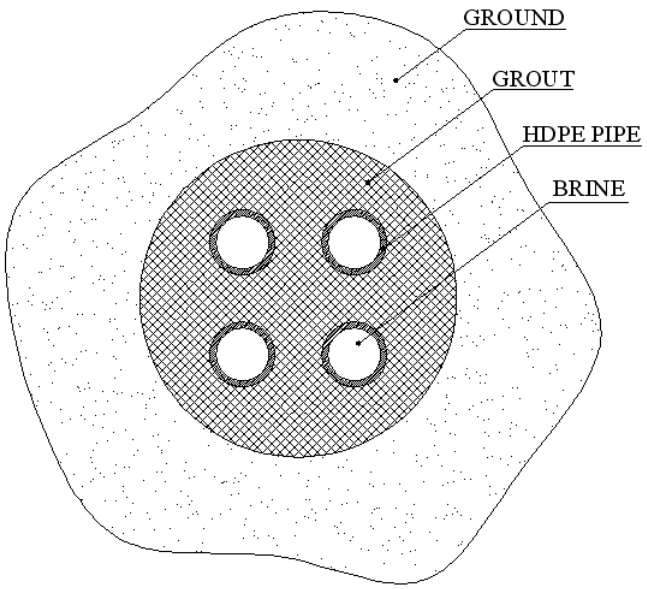

Figure 2.1.5 – Sketch of a double U-tube BHE cross-section

Double U-tube BHEs are the most common, yet coaxial borehole heat exchangers (CBHEs) are also employed. CBHEs are composed of an external tube, generally made of steel, and an inner coaxial tube, generally made of polyethylene. The fluid inlet is placed at the top of the external annular passage, while the fluid outlet is placed at the top of the internal circular tube. Indeed, this flow direction is more efficient than the opposite one [5]. CBHEs can be either inserted in a borehole which is then grouted or directly driven into the soil without drilling. For coaxial heat exchangers driven directly into the soil, the length does not exceed 20 m and the external diameter is about 50 mm. In order to install longer and thicker coaxial heat exchangers, traditional methods based on drilling and grouting must be employed.

BHEs are grouted with impermeable materials in order to prevent surface water from contaminating ground water aquifers and to prevent cross-contaminations of aquifers. Specific guidelines for grouting have not yet been published in Italy and, as a conservative practice, the borehole is generally completely grouted. Unfortunately, the thermal conductivity of the materials normally used for grouting is lower than that of most soil formations. Thus grouting tends to act as an insulator and hinders the heat transfer between the ground and the heat-carrier fluid. To solve this problem, grout with higher thermal conductivity has been developed. The thermal properties of four types of cement grout enhanced with additives have been studied, and results show that a thermal conductivity three or four times as large as that of conventional bentonite grout can be obtained [6]. The thermal properties of several kinds of soils and rocks are reported in Tab. (2.1.1), and typical grouting materials and their thermal conductivity are reported in Tab. (2.1.2) [4].

Table 2.1.1 – Thermal properties of selected soils with different water content and rocks.

	Dry density [kg/m^3]	Conductivity [W/(mK)]	Diffusivity [m^2/day]
Soils			
heavy clay, 15 % water	1925	1.4 to 1.9	0.042 to 0.061
heavy clay, 5 % water	1925	1.0 to 1.4	0.047 to 0.061
light clay, 15 % water	1285	0.7 to 1.0	0.055 to 0.047
light clay, 5 % water	1285	0.5 to 0.9	0.056 to 0.046
heavy sand, 15 % water	1925	2.8 to3.8	0.084 to 0.11
heavy sand, 5 % water	1925	2.1 to 2.3	0.093 to 0.14
light sand, 15 % water	1285	1.0 to 2.1	0.047 to 0.093
light sand, 5 % water	1285	0.9 to 1.9	0.055 to 0.12
Rocks			
granite	2650	2.3 to 3.7	0.084 to 0.13
limestone	2400 to 2800	2.4 to 3.8	0.084 to 0.13
sandstone	2570 to 2730	2.1 to 3.5	0.65 to 0.11
shale, wet		1.4 to2.4	0.065 to 0.084
shale, dry		1.0 to 2.1	0.065 to 0.074

Table 2.1.2 – Thermal properties of typical grouting materials

Grout	Conductivity [W/(mK)]
bentonite	0.73 to 0.75
neat cement	0.69 to 0.78
20 % bentonite – 80 % SiO_2 sand	1.47 to 1.64
15 % bentonite – 85 % SiO_2 sand	1.00 to 1.10
10 % bentonite – 90 % SiO_2 sand	2.08 to 2.42

At higher values of grout conductivity, the thermal interference between tubes within a single borehole, also called thermal short-circuiting, increases, with a negative effect on the overall heat transfer between the heat carrier fluid and the ground. Thermal short-circuiting effects are more relevant for deep BHEs, in which the difference between the inlet and outlet fluid temperature is high and for low fluid flow rate. Yet, they can be reduced by replacing the typical polyethylene tubes with tubes with lower thermal conductivity. In Ref. [7] the effects of thermal short-circuiting are studied with regard to coaxial borehole heat exchangers.

Installations in cold climates require that the heat carrier fluid that flows within the buried tubes, usually water, is replaced with brine or a mixture of water and antifreeze, in order to prevent the freezing of the fluid during winter functioning. Some antifreezes usually employed are: ethylene glycol, propylene glycol, methanol and ethanol. Several factors must be considered when selecting an antifreeze, such as the effect on life-cycle cost of the system, corrosivity, environmental risks, and health risks. Methanol and ethanol have good viscosity characteristics at low temperatures and therefore require lower-than average pumping power. However, they both pose a significant fire hazard and methanol is also toxic. Propylene glycol has no major concerns except slightly higher-

than-average installation and energy costs. A detailed analysis of several antifreezes is reported in Ref. [8].

The advantages of the vertical BHEs, over horizontal ones, are that they require relatively small plots of ground and that they are in contact with soil that is hardly influenced by the external air temperature and therefore can yield the most efficient GCHP system performance.

2.2 BOREHOLE HEAT EXCHANGER DESIGN METHODS

An integrated design approach for building enclosures and plants has to be pursued in order to reach the high energy performance levels required by EU regulations for new buildings, and the high thermal comfort levels requested by the construction market both for dwellings and commercial buildings. Having said that, the purpose of this section is to report an overview of the procedures typically adopted to design GCHP systems with particular reference to determing BHE length.

To size BHEs, many aspects have to be taken into account, besides technical and economic feasability:

a) Heat load and energy demand for heating, cooling and domestic hot water supply;
b) Underground water flow;
c) Thermo-physical properties of the ground and undisturbed ground temperature;
d) Thermo-physical properties of the grout and borehole thermal resistance;
e) Pumping energy requirements;
f) Plot of ground available.

a) Heat load and energy demand for heating, cooling and domestic hot water supply

The first step is to determine the building heat load and its energy demand for heating and cooling. The maximum heat load is evaluated by considering the outside design temperature of the building location, that is, the coldest outside temperature expected for a normal heating season. Traditional heating systems, *e.g.* gas boilers, are designed to match this temperature. This is not the case for heat pump systems used for heating purposes, which usually are sized to meet a lower heat load. Indeed the number of hours, in a heating season, during which the outside temperature is close to the outside design temperature is very low. This means that a heat pump system sized to meet the maximum heat load would work at full load only few hours per year. Since the initial cost for heat pumps is higher than that for boilers, it is not cost-effective to size a heat pump system to cover the maximum heat load. Hence, heat-pump systems are usually designed to deliver around 90% of the energy demand for space heating and are coupled with auxiliary boilers in order to match high

winter peak load. In contrast heat-pump systems used manly for space cooling, are sized to meet the total cooling heat load.

Once the size of the heat-pump system has been determined, one has to evaluate the energy demand for heating and cooling the building. In Northern Europe, where GCHP systems are often employed, the energy demand for winter heating prevails, and the soil is mostly used as the heat source. On the other hand, in mild climates and especially for commercial buildings, cooling demand is predominant, and hence the ground is mostly used as a heat sink. An unbalanced energy demand along the year, could lead to a long-term effect of the mean temperature of the soil drifting towards lower values (ground as heat source) or higher values (ground as heat sink), with a negative effect on the long-term performance of GCHP systems. Therefore, a correct BHE sizing should aim to limit the change in mean soil temperature to a maximum of 1 to 2 °C in 25 – 30 years of plant functioning. This could be achieved as follows: by increasing the total length of the boreholes; by increasing the distance between boreholes or, if necessary, by reducing the energy demand met by the GCHP system through auxiliary plants (such as boilers or thermal solar collectors).

Few studies on the long-term performances of GCHP systems can be found in the literature, and also direct experience is lacking, owing to the fairly recent use of this technology. Rybach et al. [9] studied the long-term performances of a coaxial BHE, used only in heating mode for the requirements of a single-family house. They showed that, during the considered working period of 30 years, the temperature of the ground around the BHE decreased, especially during the first few years. After the shut-down of heat extraction, regeneration of the ground started: the ground temperature increased steeply in the beginning and then tended asymptotically to the undisturbed initial value over 30 years. Signorelli et al. [10] simulated the long-term thermal behaviour of an array of six double U-tube BHEs considering an operation period of 30 years working only in heating mode. They concluded that in a BHE array the recovery time (70 years) is longer than for a single BHE. To limit the ground heat depletion which decreases the system performances after several years of operation, some authors suggest the combined use of GCHPs both for heating during wintertime and for cooling during summertime [11, 12]. Trillat-Berdal et al. [12] proposed the coupling of thermal solar collectors with the BHEs to enhance the natural ground recovery and to maintain a stable temperature in the ground. Priarone et al. [13] studied double U-tube BHEs with reference to some typical time-periodic working conditions and to three different BHE fields: a single BHE surrounded by infinite ground; a square field of 4 BHEs surrounded by infinite ground; the limiting case of a square field of infinite BHEs. The results showed that for the single BHE no compensation between summer and winter loads is necessary, for the square field of 4 BHEs a

partial compensation of the winter load and a minimum distance between BHEs is required, while for a large field only an almost complete compensation is possible.

b) Underground water flow

The models adopted in the papers mentioned so far, do not consider the positive effects of underground water flow in reducing the soil temperature depletion. Field observations indicate that groundwater influences borehole performance by increasing the heat transfer significantly [14-17]. Some theoretical studies have been published on the subject. References [16], [18], and [19] and present models for the influence of regional groundwater flow based on the assumption that the natural groundwater movement is reasonably homogeneously spread over the ground volume.

As shown, the effect of underground water flow on GCHP systems performance is a topic under discussion. The major difficulties encountered by researchers and GCHP system installation companies are due to the following aspects:

- lack of precise data on soil layers and their thermo-physical characteristics along the 100- or 150-m-deep boreholes;
- lack of data on groundwater flow direction and velocity;
- as this is a 3D convection heat transfer problem in a porous media, therefore simple analytical approximations cannot be reliably employed and numerical approaches lead to high computational complexity;
- availability of few experimental data for numerical model calibration.

c) Thermo-physical properties of the ground and undisturbed ground temperature

Knowledge of the thermo-physical properties of the ground and the undisturbed ground temperature is paramount. For BHE designers there are essentially two possibilities to obtain thermo-physical properties of the ground. 1) One can refer to tabled values for different types of soil (see Tab. 2.1.1) once the layer composition is known. This method is only suitable for small plant, that is, below 30 kW, for which designers can always conservatively overestimate the boreholes length by 10 – 15 % with only a small cost increasing. 2) With regard to GCHP systems for commercial buildings or building complexes, more precise data are needed. Therefore in-situ Thermal Response Tests (TRTs) are usually performed. This approach was first proposed by Mogensen [20] and consists of heating up a fluid, which circulates through a ready-to-operate BHE, by means of electric resistances that deliver constant heat load. By evaluating the inlet fluid temperature and outlet fluid temperature over time, an estimation of the average thermal conductivity of the ground is obtained. TRTs will be further discussed in Section 2.3.

The mean value of the undisturbed ground temperature along the borehole, T_g, can be estimated as the average annual temperature of the air above the ground. As for the thermal properties of the ground, T_g can be evaluated more precisely by employing the same apparatus used for TRTs without activating the electric resistances and monitoring the outlet temperature during the first minutes of functioning. A more detailed description is reported in Section 2.3.

d) Thermo-physical properties of the grout and borehole thermal resistance

Thermo-physical properties of the grout must also be taken into account for BHEs sizing. Several kinds of grout and their thermal conductivity are reported in Tab. (2.1.2). Grouting has a thermal resistance effect between the heat carrier fluid and the ground and therefore the lower the thermal conductivity, the higher the temperature difference between fluid and ground. The effects of grout low conductivity of grout have been demonstrated [21,22]. Spilker [21] showed that thermally enhanced grout reduces loop lengths by 15 to 35 %, compared to conventional grout. Kavanaugh-Allan [6] suggested the following options (their suggestion are indicated in *italic typeface*):

- G*routing only where grout is needed rather than grouting the entire bore*. This option assumes a knowledge of the soil layers and the underground water-flow distribution along the entire bore. These data, as already highlighted, are difficult to be obtained.
- *Grouting the entire bore and oversize the BHE to compensate. This would lead to significant additional cost*. Yet, when no data are available on soil layers and water content distribution, this is the only feasible solution.
- *Reduce grout quantity with smaller bore diameters, with increased grouting difficulty;*
- *Mix thermal additives into bentonite grouts. This would lead to additional cost and requires special grout pumps;*
- *Deny the problem and blame the contractor for the poor performance.* Option strongly not recommended.

Furthermore, the thermal conductivity of grout, once it is laid in the borehole can be different from that measured in laboratories. This is mainly due to problems related to installation procedures, which might cause a variation in the water content of the grout mixture and water infiltration along the borehole. In Section 2.3, an innovative method to determine the thermal conductivity and heat capacity of grout in a ready-to-operate borehole is presented.

An important reference value considered by many GCHP system design methods is the thermal resistance between the heat-carrier fluid and the borehole wall, which is commonly called borehole thermal resistance, R_b. This value depends on the arrangement of the flow channels, the convective heat transfer in the ducts, and the thermal properties of the materials involved in the thermal process

(*i.e.* grout and pipe material). Considering a simplified model of BHE, R_b allows the following relationship between the average fluid temperature, T_m, and the borehole wall temperature, T_b

$$T_b - T_m = qR_b \quad , \tag{2.2.1}$$

where q is the heat transfer rate per unit length of the borehole.

e) Pumping energy requirements

Pumping costs are a very important aspect especially for large GCHP systems. Studies have shown that, without careful attention to the design, the electric energy consumed by the circulating pumps can equal the amount of electric energy consumed by the heat pumps themselves. Reference [23] is a recommended guideline for designers; optimal flow rates, antifreeze content information, head loss data, pump motor features and layout design alternatives are there reported and exemplified.

f) Plot of ground available

The size and location of the plot of ground available for the BHEs installation, can also be important constraints that a designer must carefully consider. For instance, a small plot of ground can dictate the choice of a vertical instead of a horizontal BHE, and, in a city, the presence of underground service must be checked.

Many models have been proposed for BHE design and heat transfer analysis, but only the most sophisticated ones take into account all the aspects mentioned above. Fig. (2.2.1) shows a scheme of different design approaches as function of the plant size.

Simplified models

For small GCHP systems, simplified models are available for designers to size the BHE total length. These models can be divided into two categories: tabular methods and simplified analytical models.

Tabular methods give the heat load per unit length of BHEs as a function of the thermal properties of the ground, by means of tables. One of the most used and detailed set of tables is provided by the German regulation VDI 4640 [24]. Such tables, only for winter heat loads, can be employed under the following constraints:

- plant with installed power lower than 30 kW;
- borehole depth ranging between 40 and 100 m;
- minimum distance between boreholes of 5 m for 40- to 50-m borehole depth, and 6 m for 50 to 100 borehole depth;

- double U-tube with the following diameters: 19, 25, or 32 mm, single U-tube or coaxial boreholes with minimum diameter of 60 mm.

For applications that do not fulfil the above constraints, this simplified method is no longer valid.

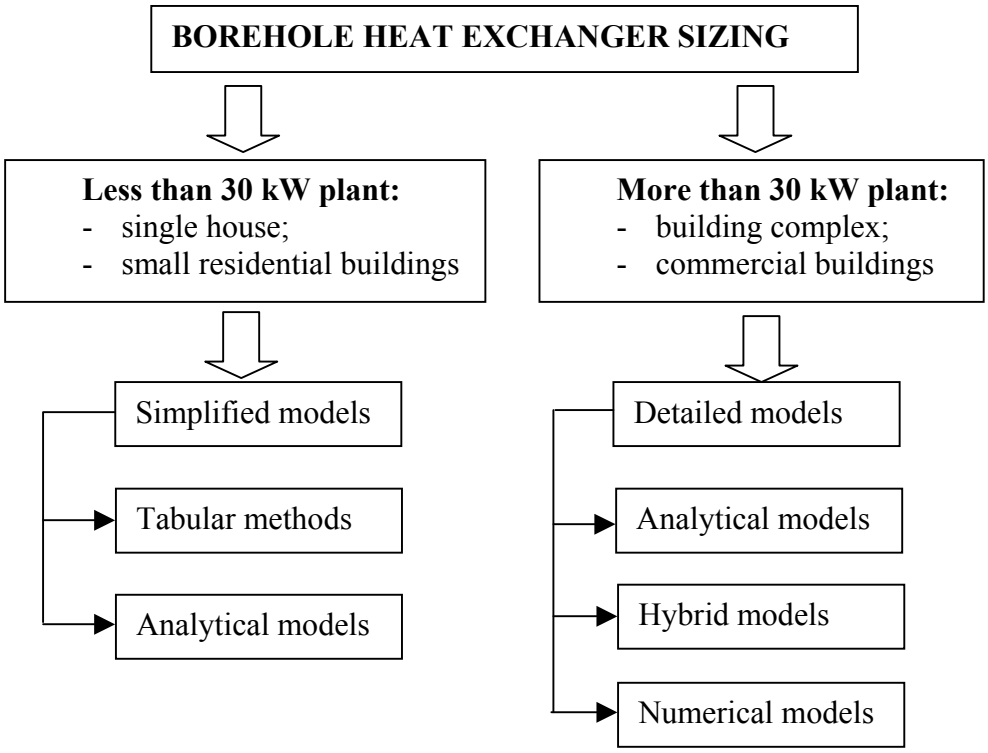

Figure 2.2.1 – Borehole heat exchanger design models

An example of a simplified analytical model was developed by Ingersoll and described by Lund [25]. This method uses a simple steady-state heat transfer equation:

$$\dot{Q} = \frac{L\left(T_g - T_m\right)}{R} \quad . \tag{2.2.2}$$

The equation is rearranged to solve for L, which is the required vertical bore length, for a constant heat transfer $\dot{Q}$. T_{m} is the mean fluid temperature, T_{g} is the undisturbed ground temperature.

Detailed models

Detailed models are applied to large GCHP systems for which TRTs are usually performed in order to determine the thermal properties of the ground. The simplest method for the evaluation of a TRT is the well-known analytical *line heat source* method, described, for instance in Refs [26, 27]. It considers the BHE as a linear power source within an infinite solid medium, which supplies a constant power per unit length, q, to the medium. By employing an approximate form of the analytical solution of the temperature field $T(r,\tau)$, one obtains:

$$T_m(\tau) - T_g = \frac{q}{4\pi k_g} \ln \tau + C \quad , \tag{2.2.3}$$

where τ is time, starting from the beginning of the heating process, T_m is the mean fluid temperature, T_g is the undisturbed ground temperature, k_g is the thermal conductivity of the ground and C is a constant given by

$$C = q \left\{ R_b + \frac{1}{4\pi k_g} \left[\ln\left(\frac{4\alpha_g}{a^2} \right) - \gamma \right] \right\} \quad . \tag{2.2.4}$$

In Eq. (2.2.3), a is the borehole radius, α_g is the thermal diffusivity of the ground, and $\gamma \approx 0.5772$ is the Euler constant

Since the *line heat source* method does not take into account the heat capacity of the materials that form the BHE, Eqs. (2.2.3) and (2.2.4) are valid only if the time elapsed from the beginning of the heating process is greater than 15 hours. By means of a linear interpolation of the experimental values of $T_m(\tau) - T_g$ versus ln τ, one determines k_g and C. Then, one fixes a plausible value of α_g and determines R_b through Eq. (2.2.4). Clearly, the method contains heavy approximations; nevertheless, if correctly applied to sufficiently long TRTs, it yields acceptable values of k_g. The approximation of R_b is worse, also because it is affected by the uncertainty of the value assumed for α_g.

Another well-known method is the *cylindrical heat source* method, given by Carslaw and Jaeger [28]. This method is also referred in the literature as the G-function method, and approximates a BHE as an infinite cylindrical surface with radius *a*, within a infinite medium at initial temperature T_g, which supplies to the external medium a constant heat flux per unit area. Values of the thermal conductivity and diffusivity of the ground are obtained by minimizing the difference between the measured value and the calculated value of $T_m(\tau)$. The cylindrical heat source method tends to overestimate the value of the thermal conductivity, so that the line heat source method is both simpler and more reliable [14].

From these two methods, many other methods have been developed: the Ingersoll method [29, 30] and Hart and Couvillion method [31] both applying the line heat source model, and the most used ASHRAE method, developed by Kavanaugh and Rafferty [4] and is based on the cylindrical heat source model. In the next chapter, the latter will be adopted as a reference for the results obtained with a design method that we propose. In the ASHRAE method, the steady-state equation proposed by Ingersoll (2.2.3) is transformed to represent the variable heat rate of a borehole heat

exchanger by using a series of constant heat rate pulses. The thermal resistance of the ground per unit length is calculated as a function of time, which corresponds to the time in which a particular heat pulse occurs. A term is also included to account for the thermal resistance of the pipe wall and interferences between the pipe fluid and the pipe and the ground. The resulting equation has the following form for cooling

$$Lc = \frac{q_a R_{ga} + \left(q_{lc} - W_c\right)\left(R_b + PLF_m R_{gm} + R_{gd} F_{sc}\right)}{t_g - \frac{t_{in} + t_{out}}{2} - t_p} \quad , \tag{2.2.5}$$

whereas for heating

$$L_h = \frac{q_a R_{ga} + \left(q_{lh} - W_h\right)\left(R_b + PLF_m R_{gm} + R_{gd} F_{sc}\right)}{t_g - \frac{t_{in} + t_{out}}{2} - t_p} \quad , \tag{2.2.6}$$

in which

F_{sc} short circuiting heat loss factor

L_c required bore length for cooling, [m]

L_h required bore length for heating, [m]

PLF_m part load factor during design month

q_a net annual average heat transfer to the ground, [kW]

q_{lc} building design cooling block load, [kW]

q_{lh} building design heating block load, [kW]

R_{ga} effective thermal resistance of ground (annual pulse), [(mK)/kW]

R_{gd} effective thermal resistance of the ground (daily pulse), [(mK)/kW]

R_{gm} effective thermal resistance of the ground (monthly pulse), [(mK)/kW]

R_b borehole thermal resistance, [(mK)/kW]

t_g undisturbed ground temperature, [°C]

t_p temperature penalty for interference of adjacent bores, [°C]

t_{in} inlet borehole water temperature, [°C]

t_{out} outlet borehole water temperature, [°C]

W_c power input at design cooling load, [kW]

W_h power input at design heating load, [kW]

Note: heat transfer rate, building loads, and temperature penalties are positive for heating and negative for cooling.

Equations (2.2.5) and (2.2.6) consider three different pulses of heat to account for long-term imbalances, q_a, average monthly heat rates during the design month, and maximum heat rates for

short-term periods during a design day. This period could be as short as 1 h, but a 4-h block is recommended.

The required bore length is the larger of the two lengths L_c and L_h found from Eqs. (2.2.5) and (2.2.6). If L_c is larger than L_h, an oversized borehole length could be beneficial during the heating season. On the contrary, if L_h is larger than L_c, then the bore length that should be chosen by the designer is L_h, and during the cooling mode the efficiency benefits of an oversized ground coil could be used to compensate for the higher installation cost. In order to evaluate the equivalent thermal resistances of the ground, R_{ga}, R_{gd}, and R_{gm}, the ASHRAE method proposes the following procedure. First one has to determine the dimensionless Fourier number (F_0), introduced by Carslaw and Jaeger [28]: the solutions of their cylindrical heat source method require that the time of operation, τ, outside borehole radius, r_b, and thermal diffusivity of the ground, α_g, be related as follows:

$$F_0 = \frac{4\alpha_g \tau}{r_b^2} \quad . \tag{2.2.7}$$

The method suggests that a system can be modelled by three heat pulses: a 10-year (3650-day) pulse of q_a, a 1-month (30-day) pulse of q_m, and a 6-h (0.25-day) pulse of q_d. Therefore, three times are defined as: $\tau_1 = 3650$ days; $\tau_2 = 3650 + 30 = 3680$ days; $\tau_f = 3650 + 30 + 0.25 = 3680.25$ days.

The Fourier number is then computed with the following values:

$$F_{0f} = \frac{4\alpha_g \tau_f}{r_b^2} \quad , \tag{2.2.8a}$$

$$F_{01} = \frac{4\alpha_g \left(\tau_f - \tau_1\right)}{r_b^2} \quad , \tag{2.2.8b}$$

$$F_{02} = \frac{4\alpha_g \left(\tau_f - \tau_2\right)}{r_b^2} \quad , \tag{2.2.8c}.$$

A further step consists, for each Fourier number F_{0f}, F_{01}, F_{02}, in evaluating a G-factor by means of the graph and table reported in Fig. (2.2.2) [4]. Finally, the equivalent thermal resistances can be computed, as follows:

$$R_{ga} = \frac{\left(G_f - G_1\right)}{k_g} \quad , \tag{2.2.9a}$$

$$R_{gm} = \frac{\left(G_1 - G_2\right)}{k_g} \quad , \tag{2.2.9b}$$

$$R_{ga} = \frac{G_2}{k_g} \quad , \tag{2.2.9c}$$

in which G_f, G_1 and G_2 are the G-factors corresponding to F_{0f}, F_{01} and F_{02}, respectively.

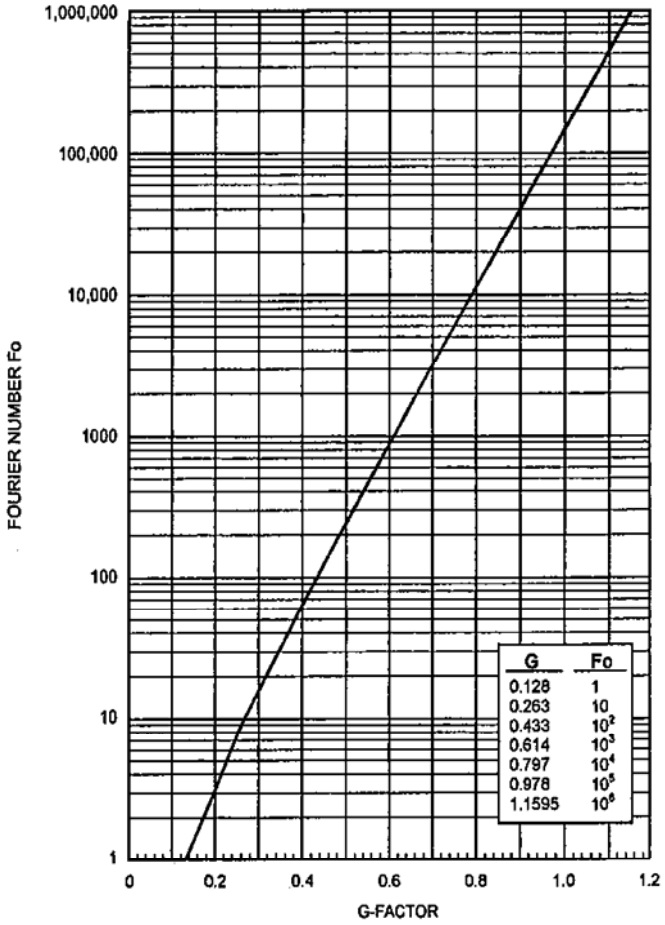

Figure 2.2.2 – Fourier number as function of G-factor [4]

Negative effects due to thermal short circuiting between pipes within a single borehole, are accounted for by introducing the short-circuiting loss factor in Eqs. (2.2.5) and (2.2.6), F_{sc}. Values of F_{sc} can vary in a range between 1.04 and 1.06 for U-tubes BHE pipes in parallel to the supply and return headers. Occasionally, when borehole depths are shallow, two or three loops can be piped in series, in these cases F_{sc} values are smaller and can varies in a range between 1.01 and 1.03.

A temperature penalty t_p is introduced in the method, in order to account for thermal interferences between adjacent borehole heat exchangers. The method suggests t_p values as function of distance between boreholes, ratio between equivalent full load hours for heating and cooling, and the type of grid patterns. These values represent a worst-case scenario since the temperature change is usually mitigated by groundwater movement. Hence the ASHRAE method tends to give slightly overestimated borehole lengths.

A well-known numerical model, that will also be employed in the next chapter to design the borehole length of a GCHP system, is the so called DST model (Duct STorage model), proposed by Hellstrom [30] and subsequently implemented in the software package TRNSYS. The soil around the BHEs is considered as a ground heat storage system, which is, by definition, a system in which heat is stored directly in the ground. The storage volume has the shape of a cylinder with a vertical symmetry axis, and the ground within the storage volume is assumed to have homogeneous thermal properties. The BHEs are assumed to be uniformly placed within the storage volume. Convective heat transfer in the ducts and conductive heat transfer in the soil are considered. The temperature at a given point of the storage is evaluated by the model as a superimposition of three parts: *a global solution, a local radial solution, and a steady-flux solution* around the nearest pipe. The global and the local problem are solved by using a finite difference method, whereas the steady-flux part is given by an analytical solution. *The global problem* covers the large-scale thermal processes, such as the interaction between the storage and the surrounding ground, between different parts within the storage, the influence of the conditions at the ground surface, etc. The numerical model uses a finite difference method dividing the storage volume into a 2D mesh. The *local problem* concerns the thermal process around the individual ducts due to short-time variations, and it is modelled using a one-dimensional radial mesh. The storage region is divided into N subregions and the local problem is assumed to be the same around each pipe in a given subregion. The solution of the *steady-flux problem*, obtained analytically by employing the cylindrical heat source model, gives the temperature field around a pipe for a constant injection/extraction rate. It is used for pulses that vary slowly in time, namely the redistribution of heat within the storage due to the circulation of the fluid. The fundamental importance of the steady-flux regime is due to the fact that any time-varying injection/extraction rate may be considered as a superposition of step-pulses of the considered type.

The DST model has been used extensively both for the evaluation of field projects and for dimensioning of BHEs. Although it gives good results for long-time evaluation, modelling the borehole by a simple borehole thermal resistance, thus neglecting the heat capacity of grout, pipe and water, gives incorrect results for short-time evaluation. Many solutions have been proposed for this problem: Yavuzturk and Spitler [31] by means of the short-time g-function method introduced by Eskilson [18], Sutton et al [32] by using the classical cylindrical heat source solution but with the material properties of the grout and replacing the U-tube arrangement with an equivalent cylinder with radius r_{eq}. The value of the equivalent radius was initially proposed by Bose [33]

$$r_{eq} = \sqrt{2} r_b \quad , \tag{2.2.10}$$

then by Kavanaugh [34]

$$r_{eq} = \sqrt{2} r_b - x \quad , \tag{2.2.11}$$

whereas the value proposed by Sutton et al. is

$$\frac{\ln\left(\frac{r_b}{r_{eq}}\right)}{2\pi k_g} = R_b \quad , \tag{2.2.12}$$

in which r_b is the actual BHE radius and x the shank spacing between the U-tube pipes.

Several other numerical models for the evaluation of TRTs and BHE sizing, with different complexities, have been proposed: 1-D finite difference models [36], 2-D finite volume models [37, 38], and 3D finite element models [27]. Even with 3-D models, it is difficult to reproduce with high accuracy the results of the first hour of a TRT, so that the comparison between experimental and numerical results is often reported starting from some hours after the initial instant. One of the difficulties is to account for the thermal inertia of the water contained in the circuit. In the next section, the key features and the results of a 2D finite-element method for the numerical simulation of thermal response tests are presented [39]. The model has been developed by means of the software package COMSOL Multiphysics 3.4. Simulation results are compared with the experimental data of TRTs that are carried out on U-pipe BHEs at different depths, placed in northern Italy. The method allows an accurate simulation even in the first hour of the heating process, and allows a reliable evaluation of the thermal properties of both the soil and grout.

2.3 FINITE-ELEMENT EVALUATION OF THERMAL RESPONSE TESTS

In order to design GCHP systems, precise information on the thermal properties of the ground are essential, as we have already discussed in the previous section. One of the most used and reliable method to determine such properties is a Thermal Response Test (TRT) in one of the BHEs that is part of the plant borehole field to be designed. The TRT consists of delivering a constant heat load, by means of electric resistances, to the heat carrier fluid, namely water, which flows in the pipes. The water inlet and outlet temperatures, T_{in} and T_{out}, with mean value T_m, as well as the mass flow rate $\dot{m}$ and the electric power $\dot{Q}_{el}$, are measured and recorded at regular time intervals.

The values of T_{in}, T_{out} and $\dot{m}$ allow the determination of the calorimetric power, that is, the power measured by flow calorimetry,

$$\dot{Q}_{cal} = \dot{m} c_p \left(T_{in} - T_{out}\right) \quad , \tag{2.3.1}$$

which, when steady state conditions are approached, is nearly equal to the thermal power exchanged between the BHE and the ground. In Eq. (2.3.1), c_p is the specific heat capacity at constant pressure of water at temperature T_m. Powers $\dot{Q}_{el}$ and $\dot{Q}_{cal}$ are functions of time determined

experimentally; while $\dot{Q}_{el}$ is almost constant, $\dot{Q}_{cal}$ becomes almost constant only after several hours.

As shown in the previous section, to determine the total length of the BHE necessary for a plant, one needs to find the values of the effective thermal conductivity k and of the effective thermal diffusivity α of the ground. Several methods, both numerical and analytical, have already been illustrated. In this section a new 2D finite element method will be presented and applied to two TRTs that we carried out on U-tube BHEs at depths of 100 m and 120 m. First, the two TRTs are described in terms of apparatus features, procedures employed, and data monitoring. The undisturbed ground temperature was evaluated. The 2D finite element method is then illustrated, and a comparison between the experimental data and simulation results is reported and exemplified.

2.3.1 Thermal Response Tests

The TRTs considered have been performed on two U-tube BHEs, each composed of four polyethylene pipes, with an inner radius of 13 mm and a thickness of 3 mm, grouted with a mixture of cement (80%) and bentonite (20%). The first BHE considered is located in Fiesso D'Artico (VE), the second is located in Cesena (FC), both in the Padana Plain (North Italy). The TRTs have been carried out by implementing the apparatus, and following the procedures recommended by ASHRAE [1]. A scheme of the apparatus employed for the TRTs is illustrated in Figure (2.3.1).

ASHRAE recommended test specifications are as follows:

- TRT should be performed for at least 36 h;
- heat rate should be 50 to 80 W per metre of bore;
- standard deviation of input power should be less than 1.5% of the average, or resulting temperature variations should be less than ± 0.3 K from a straight trend line of a log (time) versus average temperature plot;
- accuracy of the temperature measurement and recording devices should be ± 2% of the reading;
- flow rates should be sufficient to provide a differential loop temperature of 3.7 to 7.0 K;
- a waiting period of five days is suggested for low-conductivity soils [k<1.7 W/(m K)] after the ground loop has been installed and grouted before the TRT is initiated. A delay of three days is recommended for higher-conductivity soils;
- the undisturbed ground temperature measurement should be made at the end of the waiting period by direct insertion of a probe inside a liquid-filled ground heat exchanger at three locations, representing the average, or by temperature measurement as the liquid exits the loop during the period immediately after start-up;

- data collection should be at least once every 10 minutes;
- all above ground-piping should be insulated with a minimum of 13 mm closed-cell insulation or equivalent. Tests rigs should be enclosed in a sealed cabinet with a minimum of 25 mm fibreglass insulation or equivalent.

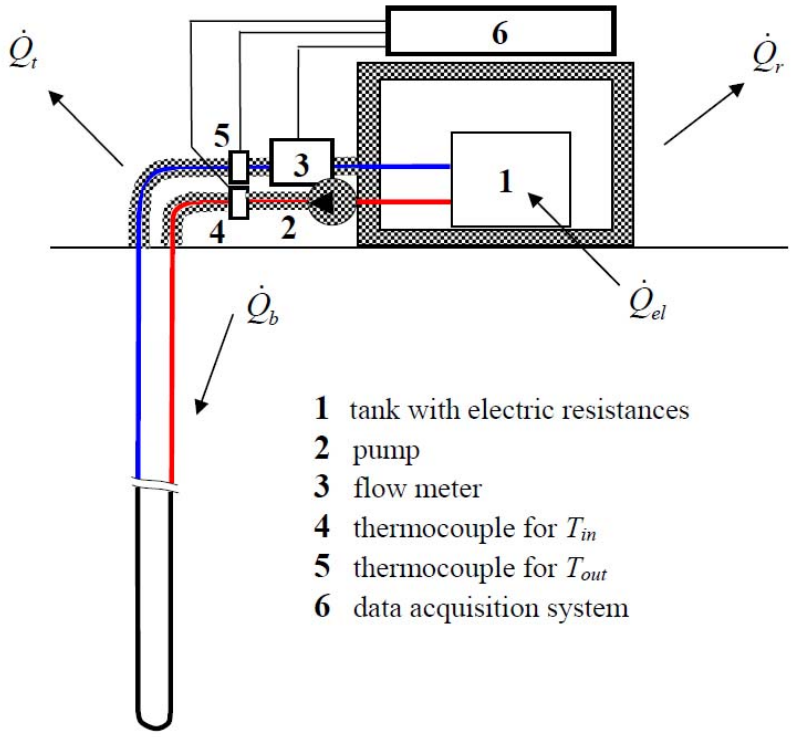

Figure 2.3.1 – Scheme of the TRT apparatus and of the energy balance

The apparatus employed for the TRTs has the following features. Three 2 kW electric resistances and one 1 kW electric resistance are located inside a 100 litre tank. A 200 ÷ 400 W centrifuge pump circulates the heat-carrier fluid through the borehole. The water flow rate is measured by means of a G.P.I. device, G2A series, with range 0.228 ÷ 2.280 m^3/h. Two type T thermocouples are positioned near the inlet and the outlet of the water tank (Figure 2.3.1) and two in the air. The acquisition system is composed of a digital millimetre AG-ILENT 34970A, with LABVIEW software, and of a device Fluke 1735 Power Logger to measure and record the electric power. The estimated error in water flow rate measurements and in electric power measurements is less than 1.5%. The estimated error in temperature measurements (verified by an high precision calibration system) is 0.2 °C in temperature values and 0.05 °C in temperature differences.

The first TRT (Fiesso D'Artico) has been carried out for more than 111 hours, the second (Cesena) for more than 86 hours. The two BHEs have the same cross section and they are made with the same materials. The BHE section is illustrated in Figure (2.3.2). The same figure shows the stationary temperature field that one obtains when the inner wall of the pipe is at 30 °C and the

external grout surface is at 20 °C, for the Fiesso D'Artico BHE. The isothermal lines have been evaluated by means of the software package COMSOL Multiphysics 3.4. The most relevant geometrical data of the two BHEs are reported in Table (2.3.1).

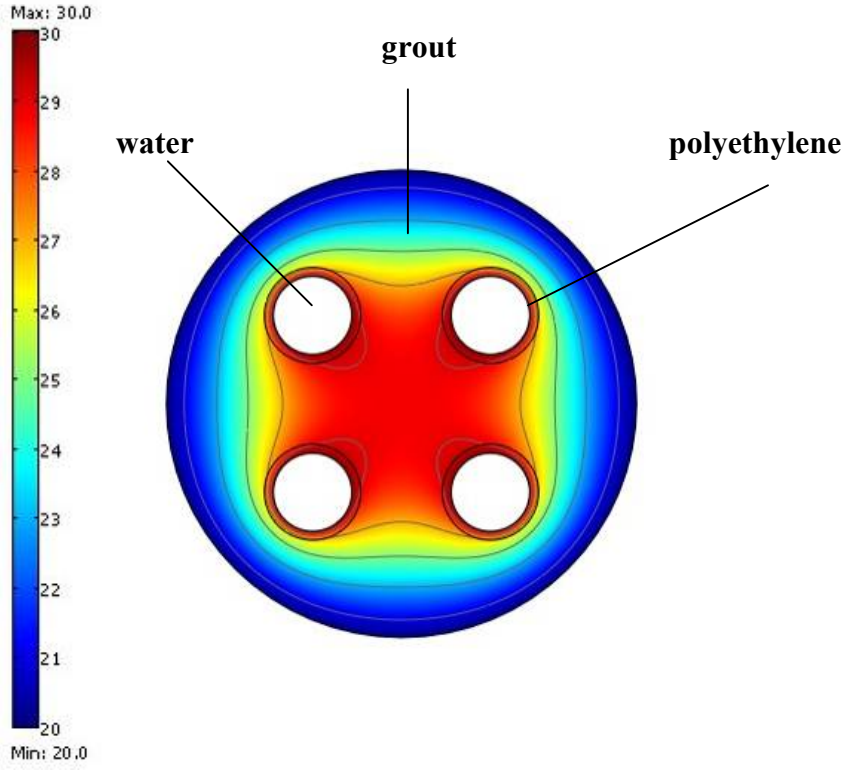

Figure 2.3.2 – Cross section of the BHEs and isothermal lines for the Fiesso D'Artico BHE

The convective heat transfer coefficient between water and the inner wall of the pipe has been calculated by means of the Dittus-Boelter correlation for circular tubes, with cooling down fluid [40],

$$Nu = 0.023\,\mathrm{Re}_D^{0.8}\,\mathrm{Pr}^{0.3} \quad , \qquad (2.3.2)$$

where Re_D is the Reynolds number for the inner diameter of the pipe. In the numerical simulation, the convective thermal resistance has been taken into account by considering an effective (lower) thermal conductivity of the polyethylene. The values of the thermal properties of water, at the mean water temperature, have been taken from [41]. Plots of the temperatures T_{in} and T_{out} recorded at Fiesso D'Artico and Cesena are reported in Figures (2.3.3a) and (2.3.3b) respectively. In the Fiesso D'Artico TRT, the mean value of the electric power during the whole test was 7679 W, with small fluctuations within 200 W. In the numerical simulations, the electric power has been considered constant. In the Cesena TRT, the mean electric power was 8200 W, with important fluctuations especially during the initial part of the test. In the numerical simulations the electric power data have been interpolated by means of a sinusoidal curve between 0 and 129000 s and by a constant value between 129000 s and the end of the test (310000 s).

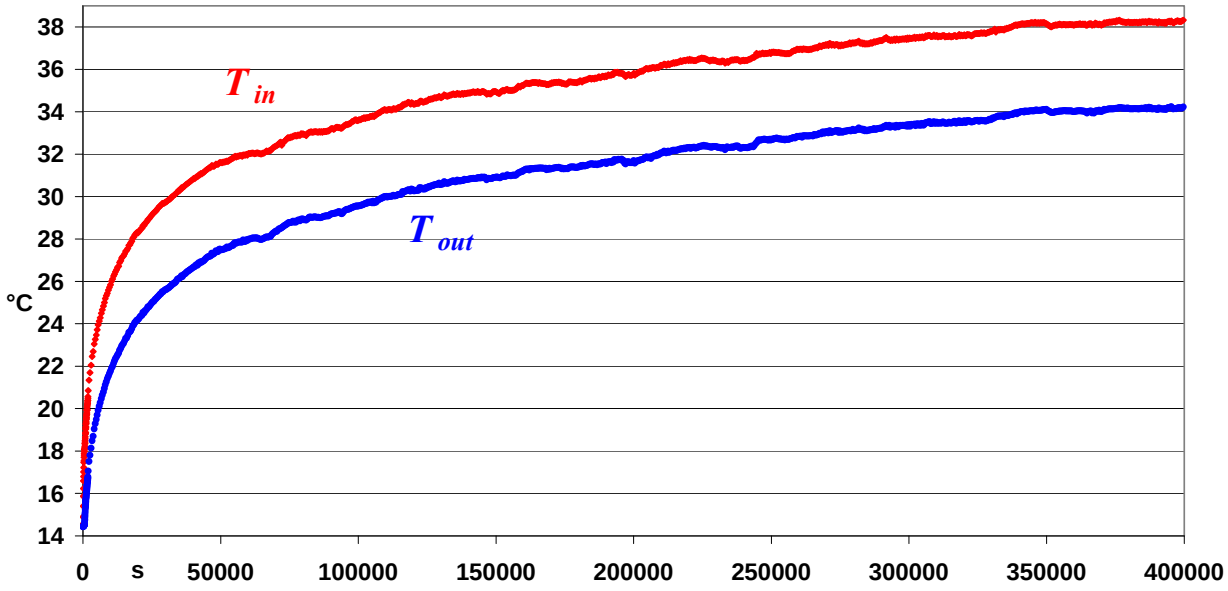

Figure. 2.3.3a – Plots of T_{in} and T_{out} versus time, Fiesso D'Artico (time in seconds)

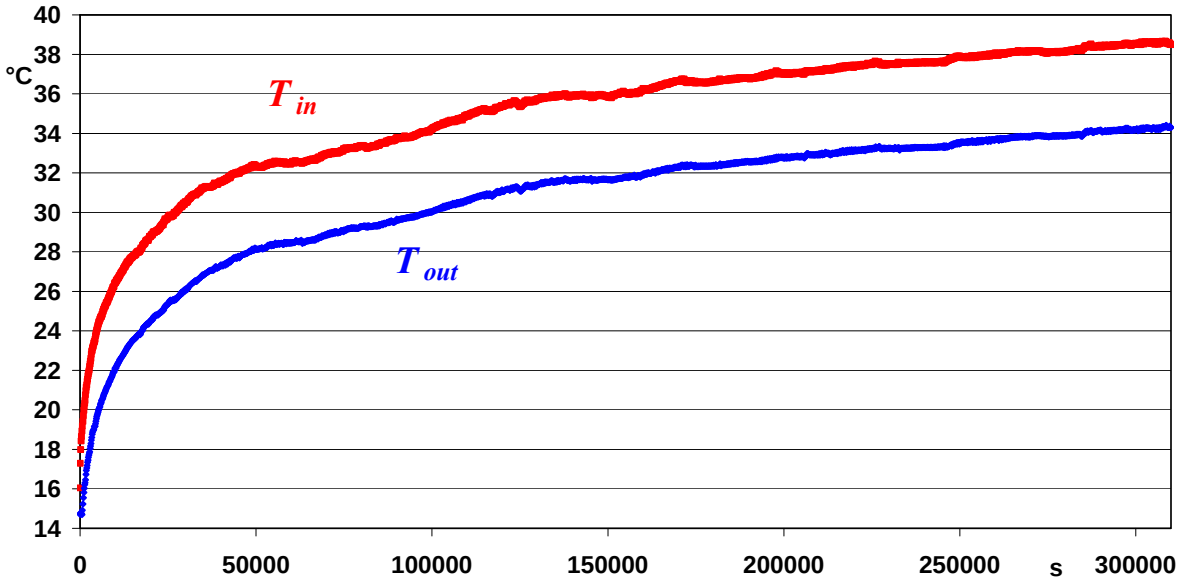

Figure 2.3.3a – Plots of T_{in} and T_{out} versus time, Cesena (time in seconds)

The simulations are based on the power $\dot{Q}_b$ received by the water which flows in the BHE. As illustrated in Fig. (2.3.1), one can write the energy balance equation

$$\dot{Q}_b = \dot{Q}_{el} - \dot{Q}_r - \dot{Q}_t \quad , \tag{2.3.3}$$

where $\dot{Q}_{el}$ is the electric power delivered by the electric resistances, $\dot{Q}_r$ is the heat loss per unit time from the tank and $\dot{Q}_t$ is the heat loss per unit time from the external tubes.

Table 2.3.1 – Main geometrical data and test conditions

	Fiesso D'Artico	Cesena
Inner tube diameter, [m]	0.026	0.026
External tube diameter, [m]	0.032	0.032
Cross section pipe area, [dm^2]	0.5309	0.5309
Borehole diameter, [m]	0.156	0.156
Borehole depth, [m]	100	120
External pipe length, [m]	10	2
Borehole water volume, [m^3]	0.2124	0.2548
Tubes water volume, [m^3]	0.0212	0.0042
Tank water volume, [m^3]	0.098	0.098
Total water volume, [m^3]	0.3316	0.3570
Volume flow rate, [l/min]	26.51	26.99
Water mean velocity, [m/s]	0.4161	0.4236
Water mean temperature, [°C]	32.32	32.89
Reynolds number	14089	14516
Nusselt number	78.28	79.85
Thermal convection coefficient, [W/(m^2K)]	1864	1905
k polyethylene, [W/(m K)]	0.4	0.4
ρ polyethylene, [kg/m^3]	940	940
c_p polyethylene, [J/(kg K)]	2300	2300
Polyethylene effective k, [W/(m K)]	0.371	0.371

In the Cesena TRT, as usual, the power $\dot{Q}_t$ was negligible because the linking pipes between the tank and the borehole were short and well insulated (less than 2 m long). In the Fiesso D'Artico TRT, on the contrary, the four pipes linking the tank to the borehole were 10 m long each and they would have been damaged by placing thermocouples. Therefore, in this case, the power $\dot{Q}_t$ was calculated by determining the global heat transfer coefficient between the pipes and the external environment. The pipes, identical to those inside the BHE, were insulated with a 19 mm thick insulation with a thermal conductivity of 0.04 W/(mK). The global heat-transfer coefficient was estimated as

$$U_t = 12.1 \text{ W/K} \quad . \tag{2.3.4}$$

The difference between the mean temperature of the water flowing in the pipes and the external temperature was 29.57 °C so that the mean thermal loss per unit time was

$$\dot{Q}_t = 358 \text{ W} \quad . \tag{2.3.5}$$

The power $\dot{Q}_r$ is small and difficult to calculate. In order to estimate $\dot{Q}_r$ and to take into account the measurements of the calorimetric power $\dot{Q}_{cal}$, the following method was adopted. In the steady-state regime one has

$$\dot{Q}_r = \left(\dot{Q}_{el} - \dot{Q}_{cal}\right)_{st} \quad , \tag{2.3.6}$$

where the subscript *st* means *steady state*. In all the TRTs carried out with the apparatus described above, the difference between $\dot{Q}_{el}$ and $\dot{Q}_c$ after 50000 s was positive and less than 2.7 % of $\dot{Q}_{el}$, but higher than the estimated value of $\dot{Q}_r$. This result confirms the reliability of measurements, but suggests that a small systematic error affects the measurements of $\dot{Q}_{cal}$. Therefore, 2/3 of the measured difference between $\dot{Q}_{el}$ and $\dot{Q}_{cal}$ under quasi-steady conditions was considered as a systematic error and $\dot{Q}_r$ was evaluated by the equation

$$\dot{Q}_r = \frac{\left(\dot{Q}_{el} - \dot{Q}_c\right)_{st}}{3} \quad . \tag{2.3.7}$$

In the Fiesso D'Artico TRT: $\dot{Q}_{el}$ = 7679 W, $\left(\dot{Q}_{el} - \dot{Q}_c\right)_{st}$ = 162 W, $\dot{Q}_t$ =358 W. From Eq. (2.3.7) and (2.3.3) one has

$$\dot{Q}_b = 7267 \text{ W} \quad . \tag{2.3.8}$$

Thus, the mean heat-transfer rate per unit length of the borehole was 72.67 W/m, which satisfies the ASHRAE recommended test specifications.

In the Cesena TRT the power data were approximated with the following equation

$$\dot{Q}_{el} = 8250 + \{300\sin[0.000075\times(t-12000)]-163\}\times U(129500-t) \quad , \tag{2.3.9}$$

where U is Heaviside's unit step function, $\left(\dot{Q}_{el} - \dot{Q}_c\right)_{st}$ =216 W, $\dot{Q}_t \cong 0$, thus

$$\dot{Q}_b = 8178 + \{300\sin[0.000075\times(t-12000)]-163\}\times U(129500-t) \quad . \tag{2.3.10}$$

The mean value of $\dot{Q}_b$ was 8200 W, hence the mean heat-transfer rate per unit length of the BHE was 68.33 W/m. This value satisfies the ASHRAE recommended test specifications.

2.3.2 Evaluation of the Undisturbed Ground Temperature

For the evaluation of the undisturbed ground temperature, T_g, the following method is recommended [42]. The BHE is filled with water some days before the test and reaches thermal equilibrium with the ground. Then, water flow through the apparatus is produced by the pump, with electric resistances switched off; the water-flow rate and the temperatures T_{in} and T_{out} are measured and recorded. The undisturbed ground temperature T_g is calculated by averaging T_{out} until all the fluid initially contained within the borehole has passed through. If the difference between the external temperature and the undisturbed ground temperature is large, the external condition can alter the results [42]. This phenomenon took place in the Fiesso D'Artico TRT, where the external temperature was much lower than the undisturbed ground temperature. In order to estimate and reduce this error, in both TRTs considered the experimental determination of T_g has been matched

with a numerical simulation of the measurement procedure, carried out by the method described in Section 2.3.3.

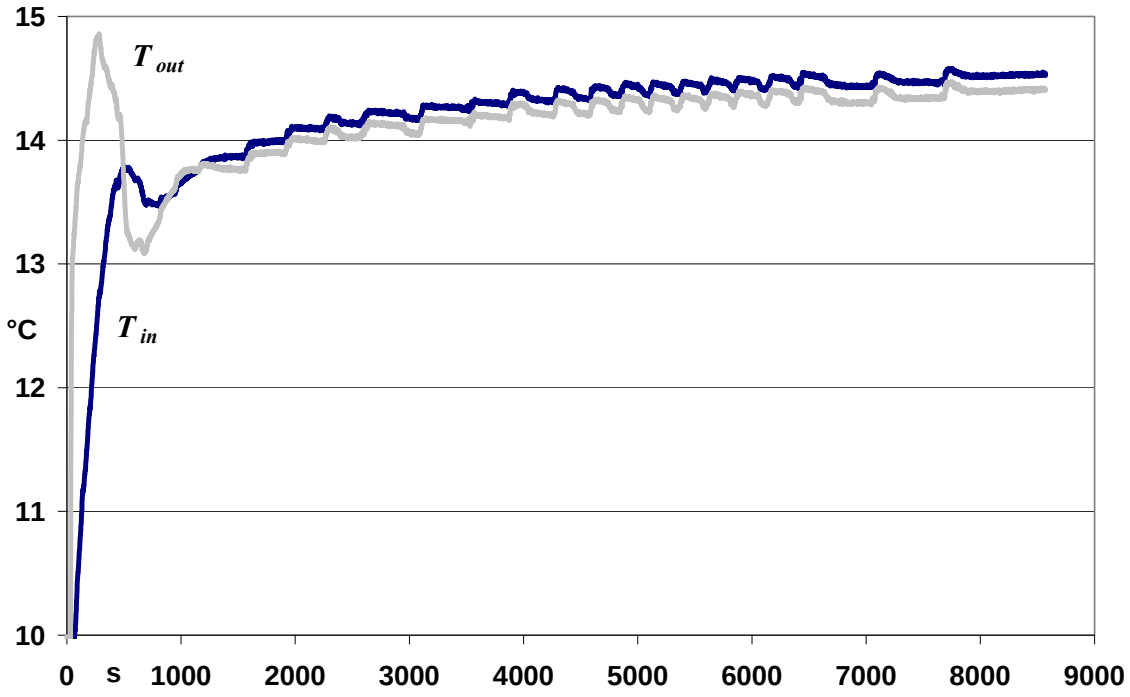

Figure 2.3.4 – Plots of T_{in} and T_{out} versus time, during the measurement of the undisturbed ground temperature, Fiesso D'Artico

The injection into the borehole of water at a lower temperature, coming from the tank, has been simulated by a power subtraction during a time period which has been deduced by the plots of T_{in} and T_{out}; the electric power delivered by the pump has been also considered. At the end of the simulation, the mean fluid temperature T_m must coincide with the measured value. In the Fiesso D'Artico TRT, this procedure determined a + 0.2 °C correction of the value obtained experimentally. Figure (2.3.4) illustrates the time evolution of T_{in} and T_{out} during the measurement of T_g at Fiesso D'Artico. One can observe the temperature fluctuations due to the injection of colder water, for about 900 s, followed by a progressive rising of the mean water temperature due to the heat injected by the pump. The undisturbed ground temperature measured experimentally was 14.1 °C. The simulation by means of COMSOL Multiphysics 3.4 revealed that the effective undisturbed ground temperature was about 14.3 °C. Therefore we assumed for the Fiesso D'Artico TRT

$$T_g = 14.3\ °C \quad . \tag{2.3.11}$$

For the Cesena TRT, the measured value of the undisturbed ground temperature was 14.6 °C, which was in perfect agreement with the numerical simulation. Therefore we assumed

$$T_g = 14.6\ °C \quad . \tag{2.3.12}$$

The numerical simulation of the measurement of the undisturbed ground temperature allowed us to determine the temperature distribution over the BHE and the ground around it. This temperature

distribution has been adopted as the initial condition for the simulation of the heating part of the test.

2.3.3 Simulation Method and Results

In U-tube BHEs, the mean fluid temperature is almost independent of the vertical coordinate. Moreover, for BHEs deeper than 100 m, the effects of the vertical changes in the ground temperature close to the surface are negligible. Therefore the problem has been considered as two-dimensional. The cross section of the BHEs is represented in its true geometry. The convective thermal resistance between the water and the pipes has been taken into account by considering an effective thermal conductivity of the polyethylene. Water has been simulated as a solid with very high thermal conductivity (k = 1000 W/(mK)) in which uniform heat generation takes place. The heat generation per unit volume, $\overline{q}_g$, has been calculated by dividing the power $\dot{Q}_b$ by the water volume within the borehole. Hence, by means of Eqs. (2.3.8) and (2.3.10), using data from Table (2.3.1), lead to the following values of $\overline{q}_g$:

$$\overline{q}_g = 34218 \text{ W/m}^3 \quad , \tag{2.3.13}$$

for the Fiesso D'Artico BHE and

$$\overline{q}_g = 32090 + \{1177 \sin[0.000075 \times (t - 12000)] - 640\} \times U(129500 - t) \tag{2.3.14}$$

for the Cesena BHE.

In order to simulate the thermal inertia of the water within the circuit, an effective water density has been considered. During the very initial part of the heating test, T_{out} does not change and the derivative with respect to time of $T_m = (T_{in} + T_{out})/2$ is equal to one half of the derivative of T_{in}; moreover, the time derivative of T_{in} is driven by the thermal inertia of the water in the tank. Therefore, the initial water volume to be considered in simulations is twice the tank volume.

By comparing the time derivative of T_{in} with the time derivative of $T_{out,}$ the time interval after which they become almost identical has been evaluated (see Fig. 2.3.5). After this time interval, it is reasonable to take into account the heat capacity of all the water within the circuit. Thus, the effective density of water has been calculated at the beginning and at the end of this interval by the equation

$$\rho_{eff} = \rho \frac{V_{eff}}{V_b} \quad , \tag{2.3.15}$$

in which ρ is the water density, V_{eff} is the effective volume of water, evaluated as described above, V_b is the water volume within the borehole. To evaluate the thermal properties of water, the mean

water temperature between 0 and 50000 s has been considered. By this method, the data reported in Table (2.3.2) have been obtained.

Table 2.3.2 – Evaluation of the effective density of water

	Fiesso D'Artico	Cesena
T_m between 0 and 50000 s, [°C]	23.82	26.62
Water c_p, [J/(kg K)]	4179	4177
Water ρ, [kg/m^3]	997.4	996.6
V_{eff} /V_b at initial time	0.923	0.769
V_{eff} /V_b at final time	1.561	1.401
Water ρ_{eff} at initial time	920	767
Water ρ_{eff} at final time	1557	1397
Final time, s	570	740

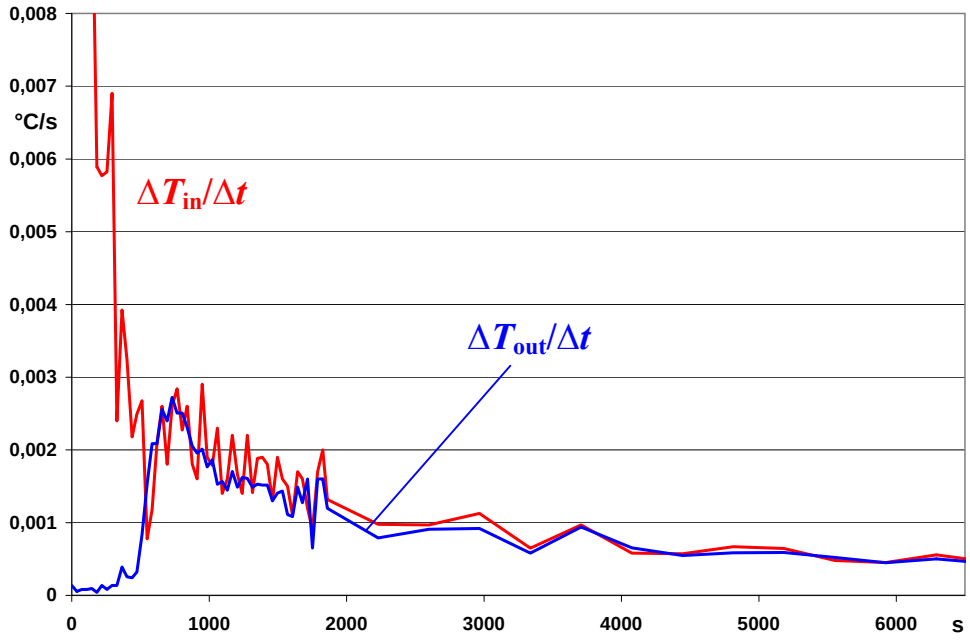

Figure 2.3.5 – Time derivative of Tin and Tout as function of time

The changes in the effective water density from the initial to the final value have been set using the "flc2hs" function of COMSOL Multiphysics, that generates a smoothed Heavyside function with continuous second derivative. The grout and soil are represented in their true situation, but the movement of groundwater has not been considered. Indeed, the target of a TRT is to find effective values of the thermal diffusivity and conductivity of the ground that reproduce the real heat flows by pure conduction. The computational domain included the ground placed between the borehole radius, r = 0.078 m, and a 5 m external radius; the latter is large enough to make the results independent of the domain extension. The values of the thermal conductivity k and of the heat capacity per unit volume $\rho\ c_p$ of both the grout and the ground have been evaluated by an iterative

procedure, by minimizing the standard deviation between measured and calculated values of T_m. Preliminary calculations have been carried out by a computational grid with 16032 triangular elements; the final calculations have been carried out by a computational grid with 64128 triangular elements. In Fig. (2.3.6) the BHE cross-section with the final computational grid is illustrated.

The simulation time has been divided into intervals of variable duration: 50 s from 0 to 2000 s; 200 s from 2000 to 10000 s; 500 s from 10000 to 40000 s; 5000 s from 40000 to the end of the simulation. The differential equation to be solved, in the considered domain, is the Fourier equation for conduction with internal heat generation,

$$\rho c_p \frac{\partial T}{\partial \tau} = k\nabla^2 T + \overline{q}_g \quad . \tag{2.3.16}$$

For the simulation of the measurement of the undisturbed ground temperature, the initial condition is a uniform temperature distribution $T = T_g$. For the simulation of the heating part of the test, the initial condition is the final temperature field of the previous simulation. Continuity conditions have been imposed at the interfaces between different materials; the isothermal boundary condition $T = T_g$ has been set at the boundary of the computational domain (5-m radius circumference). The zero-heat-flux condition on this boundary gives the same results. The standard deviation between the values of T_m obtained by the final grid and those obtained by the preliminary grid was less than 6×10^{-5} °C.

The values of the thermal properties of the grout and the soil that minimize the standard deviation between the measured and calculated values of T_m are reported in Table (2.3.3), together with the values of the BHE thermal resistance per unit length, R_b. The latter has been evaluated by the numerical simulation of steady conduction in the BHE, by considering a 10 °C difference between the internal and the external surface and the value of k for grout reported in Table (2.3.3).

Table 2.3.3 – Simulation results

	Fiesso D'Artico	Cesena
Grout k, [W/(m K)]	1.13	1.08
Grout ρcp, [MJ/(m^{3}K)]	1.8	1.3
Soil k, [W/(m K)]	1.77	1.50
Soil ρcp, [MJ/(m^{3}K)]	2.5	2.5
R_b. [mK/W]	0.0921	0.0950

The isothermal lines thus obtained for the Fiesso D'Artico BHE are shown in Figure (2.3.2). A comparison between the experimental and simulated values of T_m is shown in Figures (2.3.7) and (2.3.8). The figures reveal an excellent agreement between experimental results and simulations, even in the initial part of the heating process. The standard deviation between experimental and simulated values of T_m is 0.16 °C for the Fiesso D'Artico BHE and 0.12 °C for the Cesena BHE.

The simulation method proposed allows an accurate reproduction of the time evolution of the mean temperature of the water contained in the BHEs, even during the initial part of the TRTs. The accuracy obtained permits a reliable determination of the values of the effective thermal properties of both the ground and the grout. Moreover, the method allowed us to verify and to correct the measured values of the undisturbed ground temperature.

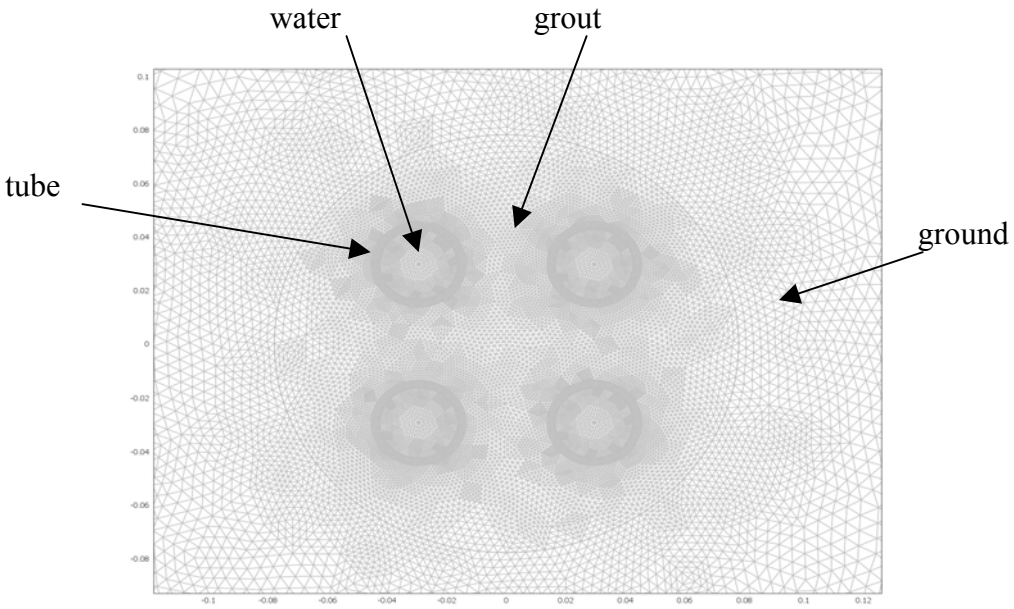

Figure 2.3.6 – Cross section of a BHE and details of the final computational grid (central part of the domain)

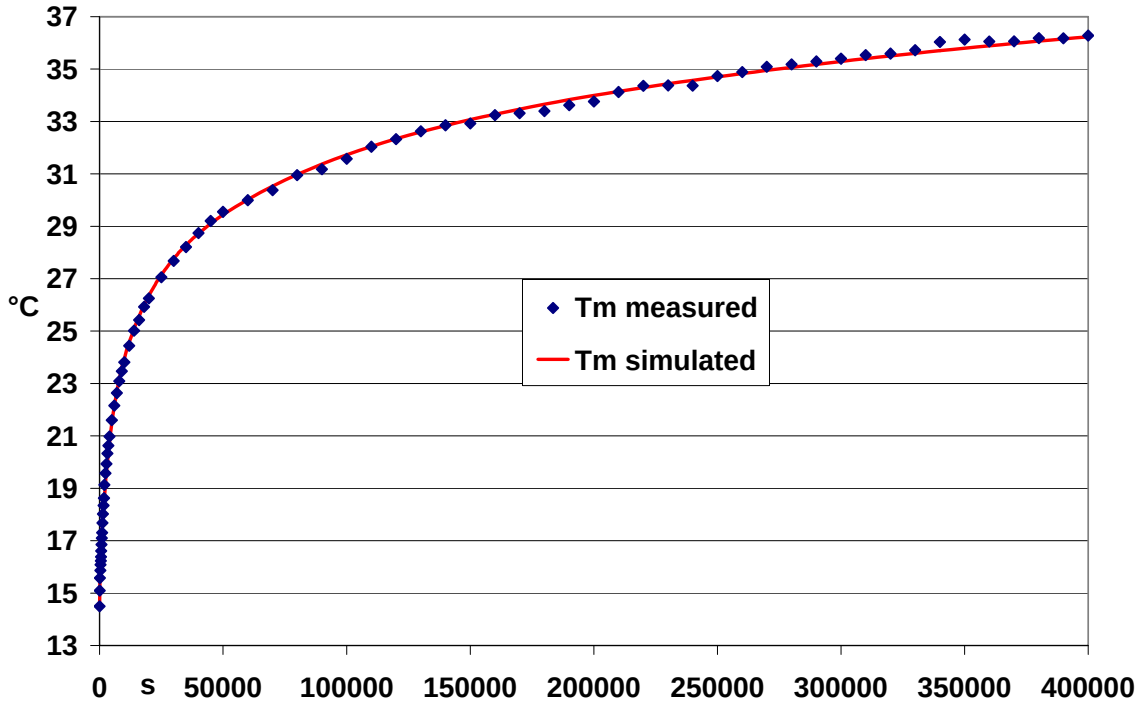

Figure 2.3.7 – Comparison between the simulated values of T_m (red line) and the measured value (blue squares) for the Fiesso D'Artico BHE.

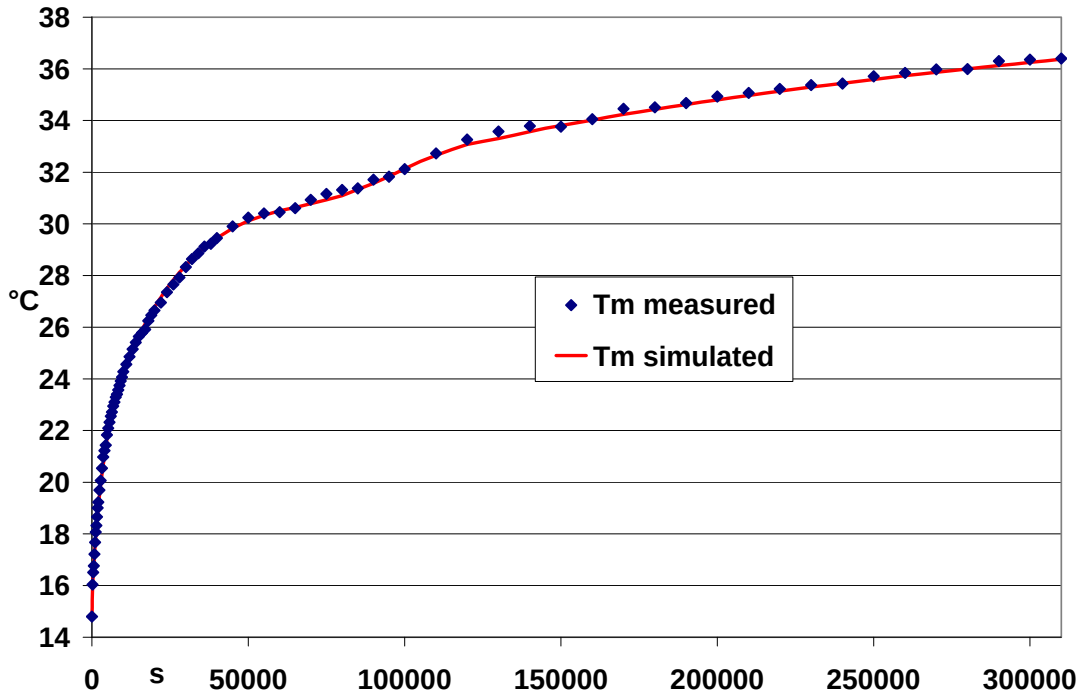

Figure 2.3.8 – Comparison between the simulated values of T_m (red line) and the measured value (blue squares) for the Cesena BHE.

2.4 CONCLUSIONS

Exploiting the ground or groundwater as the heat source or sink allows heat pumps to be more energy effective than their air-source counterparts. Yet, a correct design of all the components of a GCHP system is essential to assure both system functionality and economic feasibility. In this chapter an overview of design methods of a specific component, that is, borehole heat exchanger, has been reported and analysed. It shows that many aspects must be considered for a correct sizing of the total length of BHEs. Thermal compensation between heat extracted from the soil for winter heating and heat transferred to the soil for summer cooling has been showed as an important factor for designers. Indeed, for large borehole fields, with the absence of groundwater flow, a seasonal compensation of the thermal load has been revealed as necessary. Further studies on this issue are needed.

A precise knowledge of undisturbed ground temperature and of ground and grout thermo-physical properties are also crucial. Thermal response tests have been presented as a very common and useful method to determine such properties. Analytical and numerical models for evaluating TRT experimental data have been discussed: for large plants simplified models and analytical and numerical methods that do not take the heat capacity of the grout into account are not recommended.

A 2–D finite element method for the numerical simulation of TRTs developed by the author has been presented, which was employed to evaluate the experimental data of two TRTs performed in

northern Italy. The method allowed us to evaluate the effective thermo-physical properties of both the grout and the ground by means of an iterative procedure, which consisted in minimizing the standard deviation between measured and calculated values of the mean temperature of the water flowing in the BHEs. Results have shown that the differences between the measured and simulated values are very small, even during the first few hours of the test, during which the heat capacity of the water and the thermo-physical properties of the grout play an important role.

Although the proposed method allowed us to obtain a very good approximation of the experimental data of the TRTs, it considers only pure conduction heat transfer between boreholes and the ground. The possible presence of groundwater flow is taken into account by an increased value of the effective thermal conductivity of the soil. Hence, this method can be successfully employed only with a low groundwater flow. A further development of the method that also includes the convective heat transfer resulting from groundwater flow is now under investigation. It will allow a better understanding of long-term effects (20–30 years) on the underground mean temperature drift due to no thermal compensation between winter and summer heat load. Yet, precise values of groundwater flow velocity, meaning the Darcy-velocity that depends on soil porosity, are lacking. Methods to determine the groundwater flow velocity are available, but their reliability is not confirmed by literature. This is an important issue that requires further research.

The sizing of BHEs is part of the design process of a GCHP system. Anyhow, design choices for all the components of a GCHP system are strongly correlated with one another. A thorough design procedure of the whole system is reported in the next chapter.

References

[1] ASHRAE Handbook – HVAC Applications, Ch. 32, 2007.

[2] Phetteplace G. Geothermal heat pumps. Journal of Energy Engineering 2007; 32 – 38.

[3] Kavanaugh SP, Clavert TH. Performance of ground source heat pumps in North Alabama. Final Report, Alabama University and Tennessee Valley Authority Research Consortium. University of Alabama, Tuscaloosa, 2003.

[4] Kavanaugh SP, Rafferty K. Ground-source heat pumps – Design of geothermal systems for commercial and institutional buildings. ASHRAE, 1997

[5] Zanchini E, Lazzari S, Priarone A. Effects of flow direction and thermal short-circuiting on the performance of coaxial ground heat exchangers. International Conference on Renewable Energies and Power Quality, Valencia, 2009.

[6] Kavanaugh SP, Allan ML. Testing of thermally enhanced cement ground heat exchanger grouts, ASHRAE Transactions. Career and Technical Education pg. 446, 1997

[7] Zanchini E, Lazzari S, Priarone A. finite element simulation of coaxial borehole heat exchangers. 8th International Conference on Sustainable Energy Technologies. Aachen, Germany, 2009.

[8] Heinonen EW, Tapscott RE. Assessment of anti-freeze solutions for ground-source heat pump systems. ASHRAE Research Project RP-863, Report, 1997.

[9] Rybach L, Megel T, Eugster WJ. At what time scale are geothermal resources renewable?. Proc. of World Geothermal Congress 2000, Kyushu - Tohoku, Japan, 2000.

[10] Signorelli S, Kohl T, Rybach L. Sustainability of production from borehole heat exchanger fields, Proc. of World Geothermal Congress 2005, Antalya,Turkey, 2005.

[11] Rybach L, Mongillo M. Geothermal sustainability - A review with identified research reeds, GRC Transactions, Vol. 30, 2006.

[12] Trillat-Berdal V, Souyri B, Achard G. Numerical study of the evolution of ground-coupled heat pump system performance. Proc. of 9th Int. IBPSA Conference, Montréal, Canada, 2005.

[13] Priarone A, Lazzari S, Zanchini E. Numerical evaluation of long-term performance of borehole heat exchanger fields. Proc. of the COMSOL Conference, Milan, Italy, 2009.

[14] Gehlin S. Thermal Response Test—In situ measurements of thermal properties in hard rock. Licentiate thesis 1998:37. Div. of Water Resources Engineering. Lulea, University of Technology, 1998.

[15] Sanner B, Reuss M, Mands E. Thermal response test—experiences in Germany. Proc., 8th International Conference on Thermal Energy Storage, Stuttgart, Germany, Vol. I, pp. 177–182, 2000.

[16] Chiasson A, Rees SJ, Spitler JD. A preliminary assessment of the effects of ground-water flow on closed-loop ground-source systems. ASHRAE Transactions;106(1):380–93, 2000.

[17] Witte HJL. Geothermal Response Tests with heat-extraction and heat-injection: application in research and design of Geothermal Ground Heat Exchangers. Europa¨ischer Workshop u¨ber Geothermische response test. Ecole Polytechnique Federale de Lausanne, Lausanne 25–26 10, 2001.

[18] Eskilson P. Thermal analysis of heat extraction boreholes. PhD-thesis, Department of Technical Physics. University of Lund, Sweden, 1987.

[19] Claesson J, Hellstrom G. Analytical studies of the influence of regional groundwater flow on the performance of borehole heat exchangers. Proc. of the 8th International Conference on Thermal energy storage, Terrastock 2000, Stuttgart, Germany, 2000.

[20] Mogensen, P. Fluid to duct wall heat transfer in duct system heat storages. Proceedings of the International Conference on Subsurface Heat Storage in Theory and Practice. Swedish Council for Building Research, 1983.

[21] Spilker EH. Ground –coupled heat pump loop design using thermal conductivity testing and the effect of different backfill materials on vertical bore length, ASHRAE Transactions 104 (1B): 775-779, 1998

[22] Remund CP, The effect of grout thermal conductivity on vertical geothermal heat exchanger design and performance. Report No. TR-108529. Palo Alto, Calif: Electric Power Research Institute, 1996

[23] Kavanaugh SP. Development of Guidelines for the selection and design of the pumping/piping subsystem for ground-coupled heat pump systems", ASHRAE Research Project No. 1217-TRP Final Rep., Atlanta, 2003

[24] Thermische Nutzung des Untergrundes Erdgekoppelte Warmepumpenanlagen, Verein Ingenieure, Dusseldorf, Germany, 2001

[25] Lund JW, Geothermal heat pump – an overview, Geo-Heat Center Bullettin (GHC), March 2001

[26] Roth P et al., First in situ determination of ground and borehole thermal properties in Latin America, Renewable Energy, Vol. 29, 1947-1963 (2004)

[27] Signorelli S, et al., Numerical evaluation of thermal response tests, Geothermics, Vol. 36, 141-166 (2007)

[28] Carslaw HS, Jaeger JC, Conduction of heat in solids, Oxford University Press, Oxford, 1959

[29] Ingersoll LR, Zobek OJ, Ingersoll AC, Heat conduction with engineering, geological and other applications, New York: McGraw-Hill, 1954

[30] Hellstrom G. Ground heat storage. Thermal analysis of duct storage systems, PhD thesis, University of Lund, Department of Mathematical Physics, Sweden, 1991

[31] Yavuzturk C, Spitler JD, A short time step response factor model for vertical ground loop heat exchangers, ASHRAE Trans. 105 (2), 1999

[32] Sutton MG, Couvillion RJ, Nutter DW, Davis RK, An algorithm for approximating the performance of vertical bore heat exchangers installed in a stratified geological regime, ASHRAE Trans. 108 (2), pp 177-184, 2002

[33] Bose J, Closed loop ground-coupled heat pump design manual, Oklahoma State University, Engineering Technology Extension, 1984

[34] Kavanaugh S, Simulation and Experimental verification of vertical ground-coupled heat pump systems, Oklahoma State University, Engineering Technology Extension, 1985

[35] Lamarche L, Beauchamp B, New solutions for the short time analysis of geothermal vertical boreholes, International Journal of Heat and Mass transfer, pp 1408 – 1419, 2006

[36] Gehlin A, Hellstrom G, Comparison of four models for thermal response test evaluation, ASHRAE Transactions, vol. 109, pp. 131-142, 2003

[37] Yavuzturk C, Spitler JD and Rees SJ, A transient two-dimensional finite volume model for the simulation of vertical U-tube ground heat exchanger, ASHRAE Transactions, vol. 105, pp. 465-474, 1999

[38] Austin WA, Yavuzturk C, Spitler JD, Development and analysis procedure for measuring ground thermal properties, ASHRAE Transactions, vol. 106, pp. 365-379, 2000

[39] Zanchini E, Terlizzese T, Finite-Element Evaluation of Thermal Response Tests Performed on U-Tube Borehole Heat Exchangers, Proc. of the COMSOL Conference, Hannover, Germany, 2008

[40] Incropera FP, de Witt DP, Fundamentals of Heat and Mass Transfer, Wiley, New York, 1985

[41] Raznjevic K, Handbook of thermodynamic tables, Begell House, New York, 1995

[42] Ghelin S, Nordell B, Determining undisturbed ground temperature for thermal response tests, ASHRAE Transactions, vol. 109, pp 151-156, 2003

Chapter 3

DYNAMIC SIMULATION AND EXERGY ANALYSIS OF BUILDING-PLANT SYSTEMS

Nomenclature

c_p	heat capacity at constant pressure, [J/(kg K)]	τ	transmission factor
E	energy, [MWh]	Subscripts	
F_R	heat removal factor	aux	auxiliary
g	solar factor	b	borehole
k	thermal conductivity, [W/(mK)]	c	control
$\dot{Q}$	heat transfer rate, [W]	d	distribution
s	thickness, [m]	dhw	domestic hot water
R	linear thermal resistance, [(mK)/W]	e	emission
U_L	heat transfer coefficient, [W/(m^{2}K)]	gd	ground
Z	thermal resistance per unit area, [(m^{2}K)/W]	hp	heat pump
Greek symbols		n	need
α	absorption coefficient	s	supply
η	efficiency	st	storage
λ	thermal conductivity, [W/(mK)]		
ρ	density, [kg/m^3]		

3.1 INTRODUCTION

Since a few decades, energy saving in the heating and cooling of buildings has been considered as an important target both in industrialized and in developing countries; thus, much research activity in this field has carried out [1-8]. The present chapter analyses the feasibility of zero carbon emission plants for heating, cooling and domestic hot water (DHW) supply, for a residential building complex planned for construction in Poggio Piccolo, a small village close to Bologna in northern Italy. Two alternative plants are considered:

- Plant A: air-to-water heat pumps (AWHPs), with electric energy provided by photovoltaic (PV) collectors and DHW supplied by thermal solar collectors and a wood pellet boiler;
- Plant B: as Plant A, with Ground-Coupled Heat Pumps (GCHPs), instead of AWHPs.

In both cases, thermal solar collectors are placed on the roof of a centralized boiler room.

The complex is composed of seven four-apartment houses and five two-apartment houses. An aerial view of the building complex is reported in Figure (3.1.1). Each apartment has a heated floor area of 111.41 m^2, so that the total heated floor area of the complex (38 apartments) is about 4234 m^2. Each apartment has two floors. The ground floor is composed of an entrance hall, a living room, a bathroom and a garage (unheated). The first floor is composed of a kitchen with dining room, two bedrooms, a bathroom and a small terrace. All houses have a timber frame and wooden walls, and

are insulated with wood-derived insulating materials. A view of a house with 4 apartments and a map of the first floor are illustrated in Figures (3.1.2a) and (3.1.2b).

Figure 3.1.1 – Aerial view of the building complex

Space heating and cooling is provided by an AWHP system (Plant A) or by a GCHP system (Plant B) with electric energy provided by PV solar collectors. The DHW is produced by thermal solar collectors (70%) and by a wood pellet boiler (30%), which can also be used to meet exceptional winter load peaks. Radiant floor heating and cooling systems are employed. Fresh air is supplied by a forced ventilation circuit provided with a humidity control and heat recovery system.

The heating and cooling energy need for the building complex per hour and the total length of the borehole heat exchangers for Plant B, are determined by dynamic simulations performed through the software package TRNSYS. The financial payback time of Plant A and Plant B is determined with respect to a conventional plant, which employs a condensing gas boiler for space heating and DHW supply, and an air-to-air heat pump for each apartment for space cooling and humidity control.

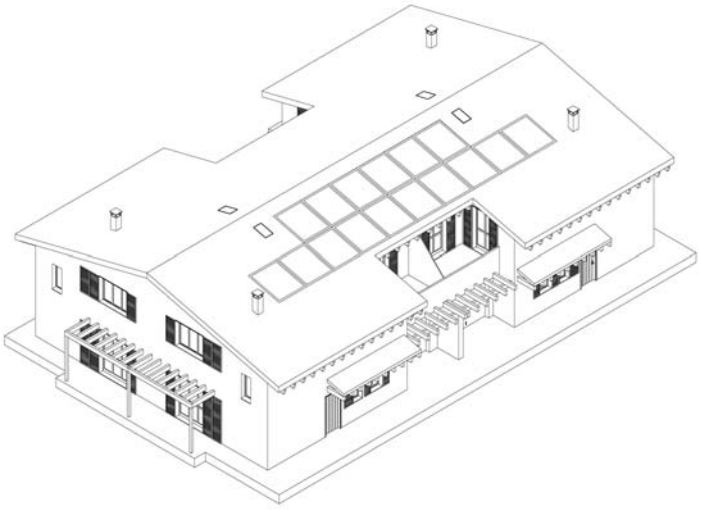

Figure 3.1.2a House with 4 apartments: view of the building

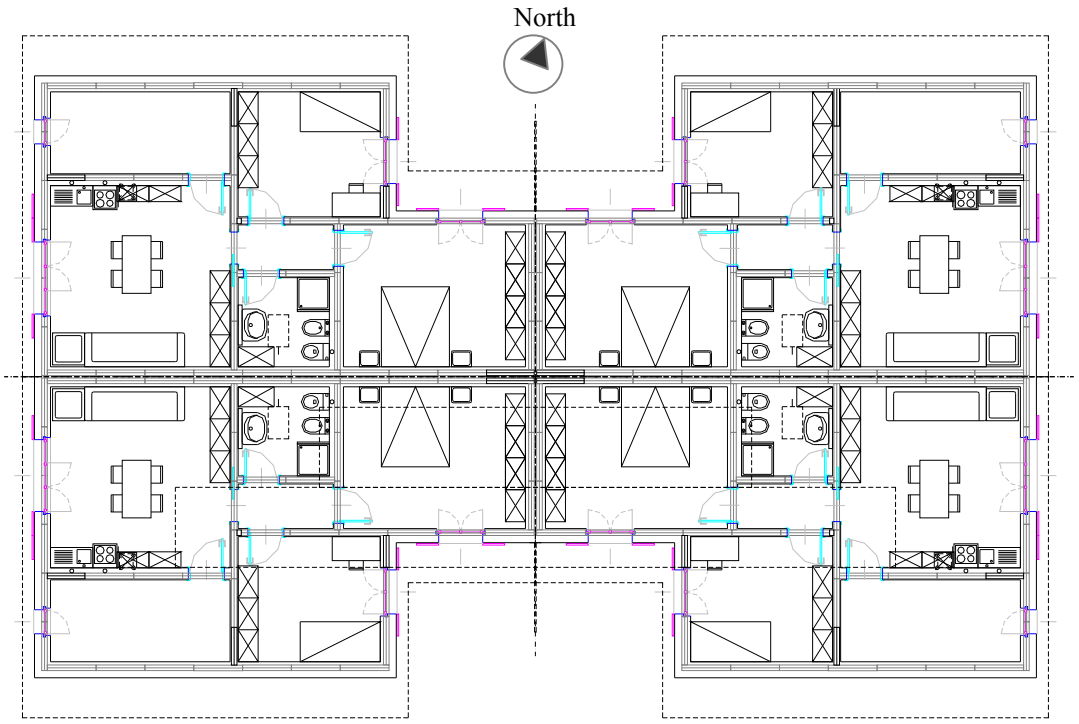

Figure 3.1.2b House with 4 apartments: map of the first floor

3.2 ENERGY DEMAND FOR HEATING, COOLING, AND DHW SUPPLY

The component materials of the external wall between the timber pillars and their thermal properties are listed in Table (3.1.1), starting from outside, where s is layer thickness, λ is thermal conductivity, and ρc is heat capacity per unit volume. Oriented Strand Board (OSB) is

manufactured from waterproof wood strands that are arranged in cross-oriented layers. For air layers, the *effective* thermal conductivity is reported in the Table, evaluated as

$$\lambda = \frac{s}{Z} \quad , \tag{3.2.1}$$

where Z is the thermal resistance per unit area of the layer. A timber frame is located, instead of the wood fibre insulation, every 0.6 m in order to ensure structural resistance to the external wall. Thus, the transmittance of the external wall, evaluated according to EN ISO 6946:2008, is 0.170 W/(m^{2}K) in correspondence of the wood fibre insulation (layers listed in Table 3.2.1) and 0.326 W/(m^{2}K) in correspondence of the timber frame. In the dynamic simulation, the external surface resistance has been evaluated as a function of the wind velocity and of the external surface temperature.

The roof has a composition similar to that of the external vertical wall. The wood beams, which are placed under the roof, provide additional thermal resistance. The roof transmittance, evaluated according to EN ISO 6946:2008, is 0.15 W/(m^{2}K) in correspondence of the timber frame and 0.21 W/(m^{2}K) elsewhere.

The heat exchange between the building and the ground has been evaluated by considering the real, time dependent, temperature distribution in the soil, determined by means of TRNSYS Type 501. The ground is composed of heavy clay with 15% water content. The following values of the ground thermal conductivity k_{gd} and heat capacity per unit volume $(\rho c_p)_{gd}$ have been considered: k_{gd} = 1.70 W/(mK); $(\rho c_p)_{gd}$ = 2.938 MJ/(m^{3}K) [9]. Double glazed windows with 4-mm-thick panes separated by a 16-mm-thick argon layer have been considered. The window transmittance, including frame, is 1.4 W/(m^{2}K); the frame area is 20% of the total window area, and the glazed surface solar factor is g = 0.589. In order to assess solar energy gains, the self-shading effects of the house have been evaluated by means of the software package Sombrero. The software allows us to define planes for which the shading should be calculated, 3-D objects, and their geographical position. The main result is the geometrical shading factor, that is, the shaded fraction of the *target* area (the planes), for every hour of the year. Sombrero outputs can be employed by TRNSYS to determine the solar radiation that hits an external surface (the Sombrero *target*) taking shadings into account.

Shadowing effects have been considered to evaluate solar energy gains. The width of the shading devices placed above the windows (see Figure 3.1.2a) has been designed to shelter completely the direct solar radiation from April 15 to September 15 for windows facing South.

The heat capacity of internal walls has been taken into account. The internal heat loads have been evaluated, for each hour, according to ISO 13790:2008. Values of the internal heat loads adopted for the kitchen and the bedrooms are reported in Table 3.2.2. The heat loss due to

ventilation has been determined by assuming an air change rate of 0.3 hours^{-1} and the employment of a heat recovery system with efficiency 0.6.

Table 3.2.1 - Materials of the external wall

Material	s	λ	ρc
1: Plaster	0.5	0.9	1.638
2: Mineralized wood fibre	5	0.083	0.840
3: Air	4	0.222	0.000
4: Vapour barrier	0.1	0.077	0.034
5: Air	4.5	0.149	0.000
6: Low *emissivity* layer	0.1	0.071	0.034
7: Mineralized wood fibre	3.5	0.083	0.756
8: OSB	1.2	0.13	1.701
9: Wood fibre	12	0.038	0.105
10: Air	2	0.111	0.000
11: Vapour barrier	0.1	0.071	0.034
12: OSB	1.2	0.13	1.701
13: Mineralized wood fibre	5	0.083	0.756
14: Cellulose – gypsum board	1.3	0.32	1.265

Table 3.2.2 – Internal heat loads per unit floor area

	Time of the day from – to	Heat load [W/m^2]
Kitchen	0 – 7	2
	7 – 17	8
	17 – 23	20
	23 – 24	2
Bedrooms during week days	0 – 7	6
	7 – 23	1
	23 – 24	6
Bedrooms during week end	0 – 7	6
	7 – 17	2
	17 – 23	4
	23 – 24	6

The weather data for Bologna have been considered, with reference to the typical meteorological year (TMY) determined in Ref. [10]. During winter, the internal air temperature is set at 20 °C during the day and at 18 °C during the night, except for bathrooms, where it is kept 2 °C higher. During summer, the internal air temperature is set at 28 °C during the day, the cooling system is turned off during the night, while the relative humidity of the internal air is kept at 50% both night and day. The heating and cooling heat load for the whole building complex, in kW, and the external air temperature during one year, in degrees Celsius, are illustrated in Fig. (3.2.1). The annual energy

need for the whole building complex is: 131.75 MWh for heating and 64.00 MWh for cooling, excluding the latent heat demand, which is 10.34 MWh.

The domestic hot water demand, determined according to ISO 13790:2008, is 165.66 litres per day, per each apartment. By assuming a temperature rise from 15 to 40 °C, one obtains a total energy need, for the whole building complex given by

$$E_{ndhw} = 66.70 \text{ MWh} \quad . \tag{3.2.2}$$

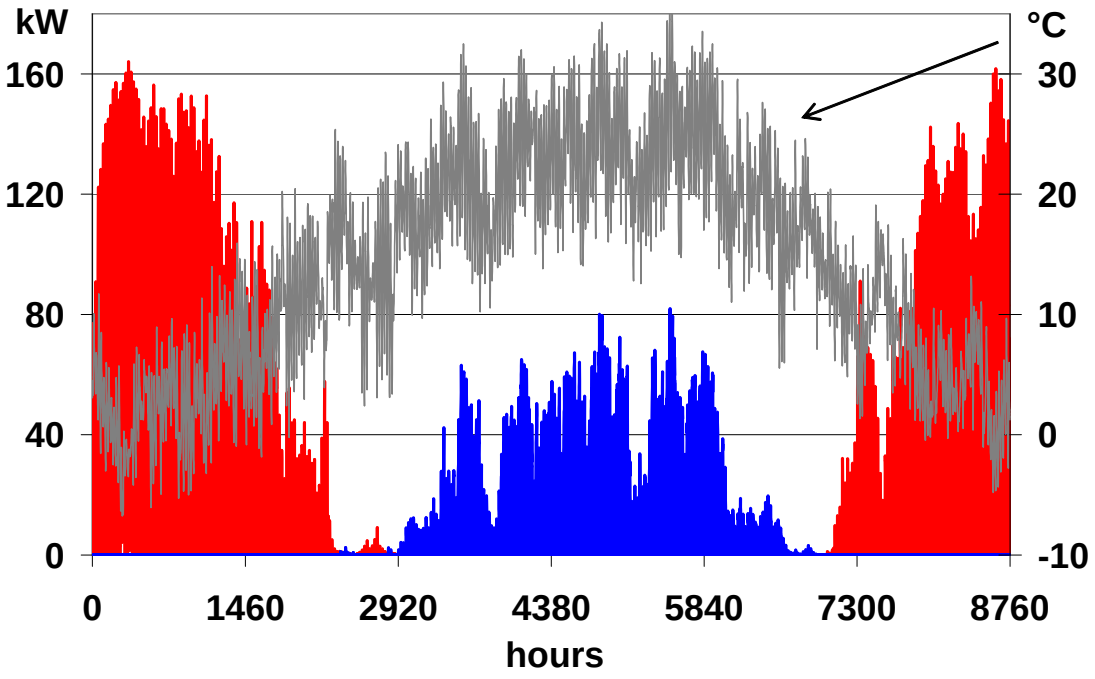

Figure 3.2.1 - Heating (red) and cooling (blue) heat load for the whole building complex and external air temperature (gray) during a typical meteorological year.

3.3 PLANT SIZING AND PRIMARY ENERGY USE

The heating and cooling energy need is matched by an AWHP system (Plant A), or a GCHP system (Plant B), which receives electric energy from PV solar collectors. The latent heat for air humidity control is supplied by air-to-air dehumidifiers, each placed in an apartment. The heat for DHW supply is provided by thermal solar collectors and by a wood pellet boiler, which also matches exceptional winter heat loads (0.08% of the heating energy use in the TMY considered). A floor radiant panel heat distribution system is adopted, for both heating and cooling. The distribution efficiency, the emission efficiency and the control efficiency have been evaluated according to ISO 13790:2008: η_d=0.97, η_e=0.99, and η_c=0.99, respectively. A schematic representation of Plant B is shown in Figures (3.3.1a) and (3.3.1b) during winter and summer functioning, respectively.

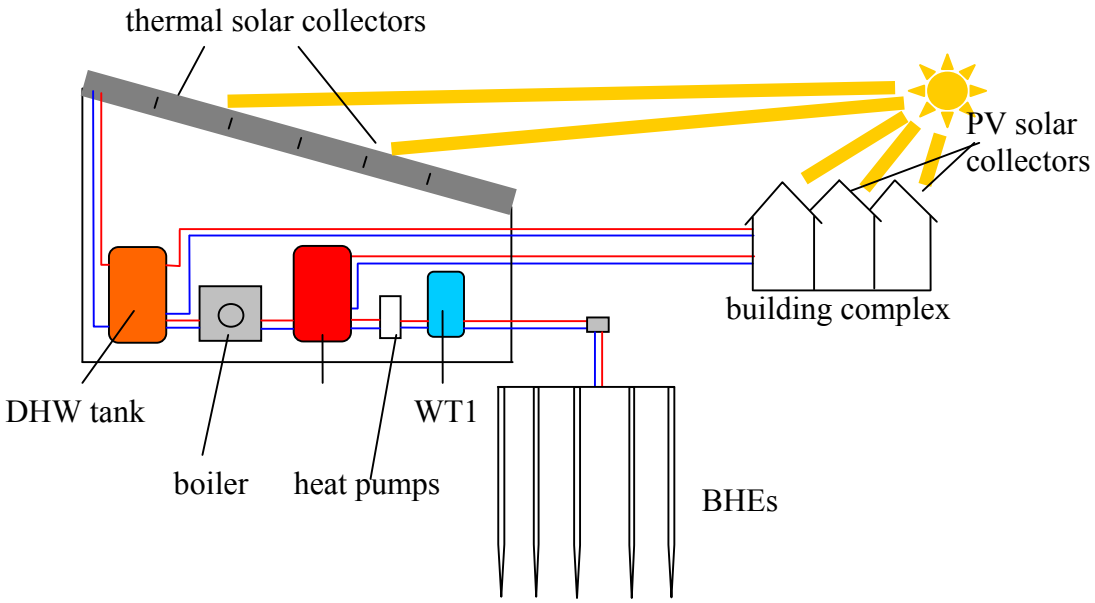

Figure 3.3.1a – Scheme for Plant B during winter functioning

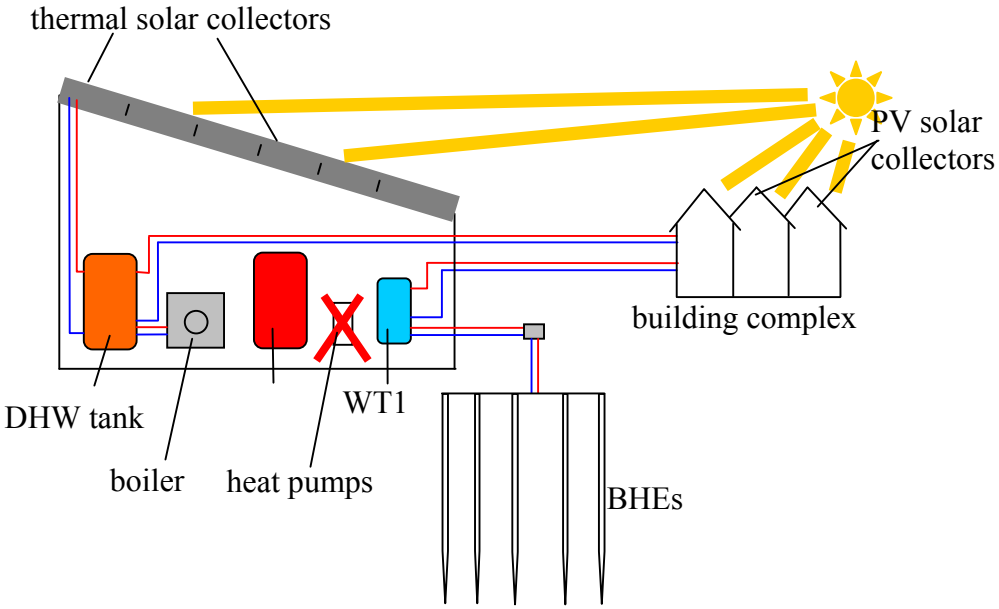

Figure 3.3.1a – Scheme for Plant B during summer functioning

For Plant B, double U–tube borehole heat exchangers (BHEs) with the following features have been considered: high density polyethylene tubes SDR 11 with external diameter 32 mm; borehole diameter 156 mm; grout thermal conductivity 1.1 W/(mK). Borehole thermal resistance, R_b = 0.095 mK/W, have been evaluated by means of the 2-D finite element model described in Chapter 2. The undisturbed ground temperature has been assumed to be 14 °C. The GCHP system has two water tanks: WT1, between the BHEs and the heat pumps; WT2 between the heat pumps and the radiant

panels. The total length of the BHEs has been designed by iterative simulations, performed through TRNSYS.

The water tank WT2 is present both in Plant A and in Plant B. For this tank, a maximum water temperature of 35 °C has been considered; the latter is sufficient to match the design heat load of 166.9 kW (external temperature – 5 °C).

Both for Plant A and for Plant B, two heat pumps, with a heating power of 79.5 kW each, have been selected, so that the maximum heating power supplied by the heat pumps is $\dot{Q}_{hp}^{\max}$ = 159 kW. For each plant, the coefficient of performance (COP) of the heat pumps has been evaluated for each hour, by considering the external air temperature (Plant A) or the water temperature in WT1 (Plant B), with a constant value of the water temperature in WT2 (35°C). For these evaluations, COP data provided by the manufacturers have been used. The seasonal weighted mean values of the COP are as follows: for Plant A, COP = 3.81 during the heating period and COP = 3.60 during the cooling period; for Plant B, COP = 5.32 during the heating period, while the heat pumps are not used for cooling (free cooling).

For each hour, the power supplied to the building is

$$\dot{Q}_s = \frac{\dot{Q}_n}{\eta_d \eta_e \eta_c} = \dot{Q}_{hp} + \dot{Q}_{aux} \quad , \tag{3.3.1}$$

where $\dot{Q}_n$ is the net thermal power required by the building, $\dot{Q}_{hp}$ is the thermal power supplied by the heat pumps and $\dot{Q}_{aux}$ is the auxiliary thermal power for heating supplied by the wood pellet boiler.

For plant B, the power extracted from the ground to meet the winter heat load is given by

$$\dot{Q}_{gd} = \dot{Q}_{hp}\left(1 - \frac{1}{COP}\right) \quad . \tag{3.3.2}$$

Simulations of the BHEs have been performed through TRNSYS Type 557, by employing the data obtained with Eq. (4). The total length of the BHEs has been determined by iterations, in order to obtain a minimum temperature of WT1 not lower than 4 °C. A total length of 4000 m has been obtained, which corresponds to 40 BHEs 100 m deep. A plot of the temperature of WT1 versus time, for a period of two years, is reported in Figure 4. The figure shows that the temperature of WT1 during summer exceeds 18 °C only exceptionally. The thermal power extracted from the building by the radiant panels, with a water inlet temperature of 18 °C and an internal air temperature of 28 °C, is 28.9 W/m^2.

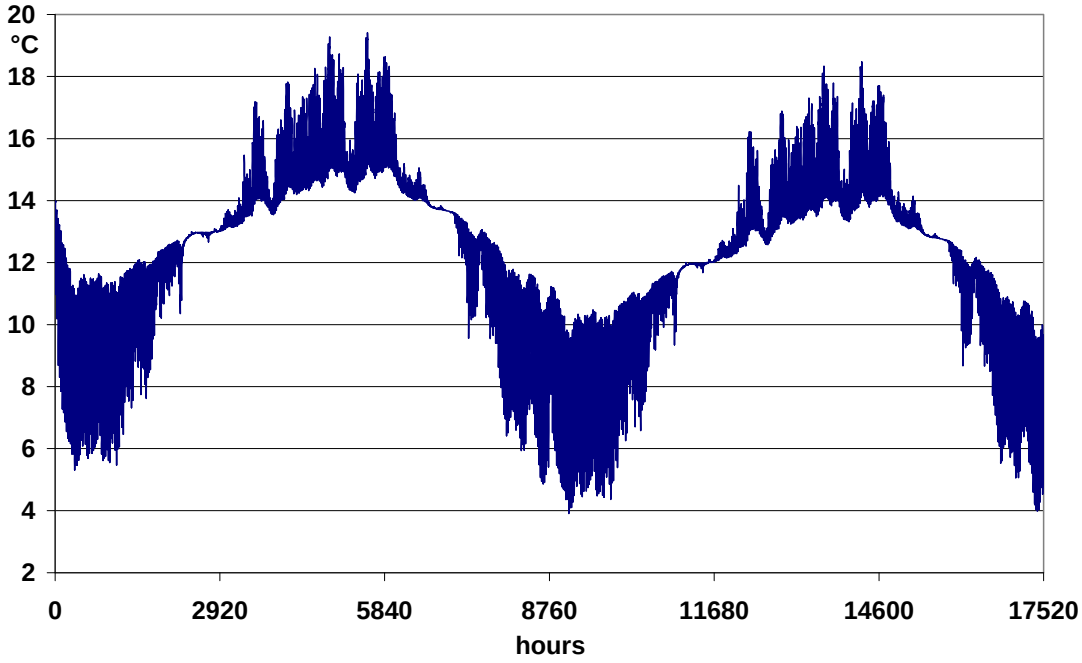

Figure 3.3.1 - Temperature of WT1 *versus time, for a period of 2 years*

Simulations of the apartments have been performed by TRNSYS under the following constraints: the maximum heating power during winter, per unit floor area, is equal to the design heating power for each room and the maximum cooling power per unit floor area during summer is equal to 28.9 W/m^2. By means of these simulations, the electric energy required by the heat pump system has been determined, for both plants. Moreover, the thermal energy supplied for heating by the wood pellet boiler during one year have been evaluated. Finally, it has been verified that, for Plant B: the internal set point temperature (28 °C) is reached in summer by free cooling, that is, sending water directly from WT1 to the radiant panels.

For both plants, during summer nights the water flow in the radiant panels is stopped; nevertheless, the internal air temperature is usually lower than 29 °C and exceeds this value only exceptionally. These temperature conditions and 50% relative humidity have been considered as satisfactory.

The electric energy consumed by the heat pumps per year, E_{hp}, has been determined as the integral, during one year of $\dot{Q}_{hp}/COP$. The results are: E_{hp} = 55.10 MWh for Plant A; E_{hp} = 26.05 MWh for Plant B. The auxiliary thermal energy for heating per year, supplied by the wood pellet boiler, is E_{aux} = 0.11 MWh for both plants.

The thermal energy supplied per year to the DHW system is

$$E_{sdhw} = \frac{E_{ndhw}}{(\eta_d \eta_{st} \eta_s)_{dhw}} \quad , \tag{3.3.3}$$

where, η_d, η_{st} and η_s are the distribution, storage and supply efficiencies for the domestic hot water system, which have been evaluated according to EN 15316-3-1:2007. Their product is 0.89; thus, from Eqs. (2) and (5) one obtains

$$E_{sdhw} = 74.94 \text{ MWh} \quad . \tag{3.3.4}$$

The total thermal energy supplied by the boiler during one year is given by

$$E_b = \frac{E_{sdhw}(1-f)+E_{aux}}{\eta_b} \quad , \tag{3.3.5}$$

where f is the fraction of E_{sdhv} supplied by the thermal solar collectors, η_b is the boiler efficiency. A wood pellet boiler with a power of 200 kW and an efficiency of 0.92 has been chosen. Thermal solar collectors have been sized to yield $f = 0.70$, so that

$$E_b = 24.56 \text{ MWh} \quad . \tag{3.3.6}$$

Since electric energy for the heat pumps and water circulation is provided by PV collectors, Eq. (3.3.6) gives the total primary energy use of the building complex for heating, cooling and DHW supply. This consumption corresponds to 5.80 kWh/(m^{2}year), with zero carbon emission.

The electric energy use for water circulation and dehumidification has been evaluated as follows. For the piping system between WT2 and the radiant panels, the total head loss and flow rate are 69.9 kPa and 8.03 litres/s, respectively. The estimated energy consumption is 5.34 MWh per year.

The electric energy use for pumping domestic hot water is estimated as 0.05 MWh per year; the electric energy use for dehumidification is estimated as 4.92 MWh per year.

For Plant B, the BHEs piping system is composed of 8 parallel loops, each with 5 BHEs piped in parallel. The water flow rate is 20 litres per minute, for each BHE. The total head loss, evaluated as suggested in Ref. [6], is 93.9 kPa, and the estimated energy consumption is 8.51 MWh per year.

Therefore, the total electric energy use per year for heating, cooling, air humidity control and domestic hot water supply is

$$E^e_{tot} = 65.41 \text{ MWh} \tag{3.3.7}$$

for Plant A, and

$$E^e_{tot} = 44.87 \text{ MWh} \tag{3.3.8}$$

for Plant B.

The PV collectors have been sized in order to supply 65.41 MWh of electric energy per year for Plant A, and 44.87 MWh of electric energy per year for Plant B; the design software available in Ref. [7] has been employed. The following PV system features have been considered: tilt angle 14°, azimuth angle – 21°, combined PV system losses 25.5%. The desired energy supply is obtained by a

PV system with 62.8 kWp (peak power) for Plant A, with 43.1 kWp for Plant B. The PV collectors are roof-integrated, in each house. For a house with four apartments, the PV collector area is about 53 m^2 for Plant A and about 36 m^2 for Plant B.

Single glazed flat plane thermal solar collectors with a selective absorbing surface have been chosen with the following plant features: tilt angle 45°; azimuth angle 0°; $F_R(\tau\alpha)_0 = 0.824$, where F_R is the heat removal factor and $(\tau\alpha)_0$ is the effective transmittance-absorptance product at normal incidence; $F_R U_L = 3.66$ W/(m^2K), where U_L is the overall heat transfer coefficient; storage volume 75 kg/m^2. The plant has been sized by the *f-chart* method [8], with the same climatic data employed for the building simulation [5]; it provides 70% of E_{sdhw} with a transparent collector area of about 87.5 m^2. Thermal collectors are placed on the roof of a detached boiler room, which contains the wood pellet boiler, the heat pumps, WT1 and WT2.

3.4 ECONOMIC ANALYSIS

The economic feasibility of the proposed plants has been analysed by comparison with a conventional heating and cooling plant. The latter, which will be called Plant C, is composed of a central heating plant, with a condensing gas boiler, and an air-to-air heat pump for each apartment, for summer cooling and air humidity control. The thermal solar collectors have been considered in all plants, unchanged.

Since a comparative economic analysis of Plants A, B and C has been performed, the costs of the *common components*, present in all plants, have not been considered. These components are: radiant panels, water-distribution system to radiant panels, tank WT2, thermal solar collector system, and DHW distribution circuit. The capital costs of Plants A, B, and C, excluding the common components, are reported in Table (3.4.1).

The operating costs have been evaluated as follows. The current rates of fuels and electricity in Bologna have been considered: 0.23 €/kg for wood pellet; 0.70 €/m^3 for natural gas; 0.25 €/kWh for electricity. The State financial support given for PV electricity production in Italy has been taken into account: only the annual difference between the electric energy consumed by the plant and the electric energy produced by the PV system is paid by the user (zero in this case); all the PV electricity produced is paid by the State at the rate 0.422 €/kWh, for roof-integrated PV Panels.

The annual operating costs/incomes for Plants A, B and C are reported in Table III. A maintenance additive cost has been considered: 2900 €/year for Plant A, and 2000 €/year for Plant B.

Table 3.4.1 – Plant costs

PLANT A	
Heat pumps	40000 €
Dehumidifiers	20500 €
PV solar collectors	301600 €
Pellet boiler	12000 €
TOTAL	374100 €
PLANT B	
BHE, loop and pump	207200€
Cold Tank	2000 €
Heat pumps	40000 €
Dehumidifiers	20500 €
PV Solar collectors	206900 €
Pellet Boiler	12000 €
TOTAL	488600 €
PLANT C	
Gas Boiler	11000 €
Air-to-air heat pumps	114000 €
TOTAL	125000 €

Table 3.4.2 – Annual cost (income) for energy use (production)

	Cost	Income
PLANT A		
Wood pellet	1200 €	
PV electricity		27600 €
Maintenance	2900 €	
Annual income		23500 €
PLANT B		
Wood pellet	1200 €	
PV electricity		18900 €
Maintenance	2000 €	
Annual income		15700 €
PLANT C		
Methane	11200 €	
Electricity	6000 €	
Annual cost	17200 €	

On account of the uncertainty in the forecast of the cost of money and of the annual increase of the unit costs of fuels and electricity, we have performed our economic analysis by assuming zero cost of money and zero annual increase in fuels and electricity costs. The total capital plus operating cost versus time is plotted in Fig. (3.4.1), for each plant, for a period of 20 years. The figure shows that Plant A is the most economical. It has a payback time, with respect to Plant C, of about 6 years; moreover it has a total cost always lower than that of Plant B.

Clearly, the results illustrated in Fig. (3.4.1) are strongly influenced by the presence PV systems with different areas and by the State incentives to PV electricity production. Therefore, it may be interesting to perform a comparative economic analysis of Plants A, B, C, in the absence of PV systems. The results of this analysis are reported in Fig. (3.4.2), and show that Plant A remains the most convenient, for a time interval of 20 years.

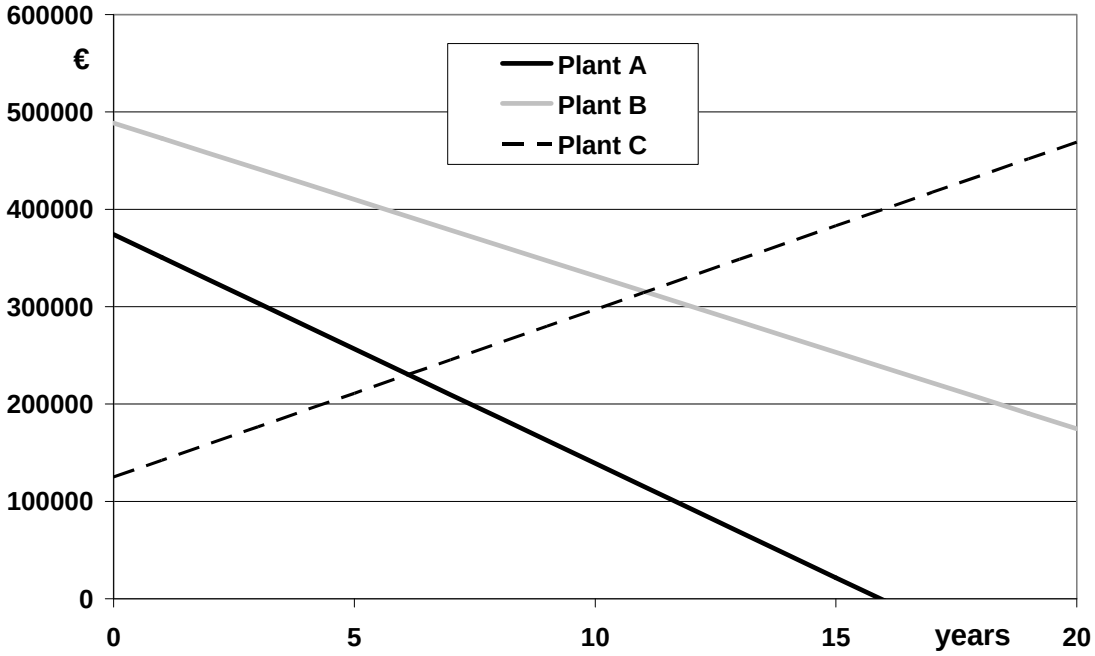

Figure 3.4.1 – Capital plus operating cost versus time, for Plants A, B, C.

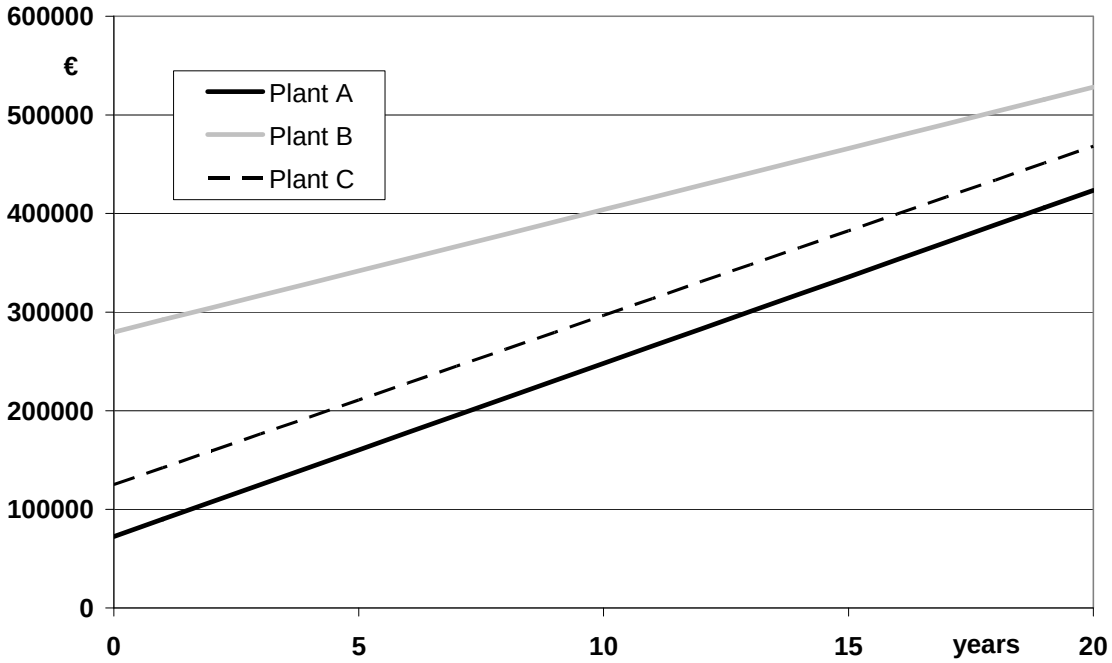

Figure 3.4.2 – Capital plus operating cost versus time, for Plants A, B, C, in the absence of PV collectors.

3.5 EXERGY ANALYSIS

A comparative energy analysis of Plants A, B, and C has been performed. As usual, we call the *embodied energy* of a plant-component the exergy loss due to the construction and the installation of the component. As in the case of the economic analysis, the embodied energy of the common components of Plants A, B, and C has not been considered.

For each plant, the embodied energy of each non-common component has been evaluated as follows. For heat pumps, boilers, dehumidifiers and tanks, the real mass has been considered, together with the mass fractions of the constituent materials given in Ref. [9], while the value of the embodied energy of each material, per unit mass, has been taken from Ref. [10]. Detailed data are reported in Table (3.5.1). For the high density polyethylene tubes of BHEs, the real mass has been considered and the value of the embodied energy per unit mass has been taken from Ref. [10], by considering the feedstock energy as no longer available. The embodied energy of PV collectors has been evaluated by assuming an embodied energy per unit peak power equal to 8.5 MWh/kWp, as reported in Ref. [11]. The exergy loss due to borehole drilling has been evaluated by considering a diesel fuel consumption of 1 litre per meter of borehole (typical consumption for the soil considered), and by approximating the diesel fuel exergy with its lower heating value, namely 10.02 kWh/litre [12, 13].

The values of the embodied energy for the non common components of Plants A, B, and C are summarized in Table (3.5.2). The table shows that the total embodied energy for Plant B is greater than that for Plant A, and that (excluding the components common to all plants) the ratio between the embodied energy of Plant B and that of Plant A is about 1.49.

For each plant, the exergy loss due to the plant operation during a typical meteorological year has been evaluated, and the total exergy loss due to the plant construction and operation has been plotted versus time, for a period of 20 years. The results, for Plants A, B and C are illustrated in Figure (3.5.1). For Plants A and B, the electricity is provided by PV collectors; therefore, the annual exergy use is due only to the wood pellet consumption, which is the same for both plants. The figure shows that the lowest exergy use after 20 years is obtained by Plant A. However, the exergy analysis illustrated in Figure (3.5.2) does not yield a direct comparison between the exergy use of an air to water heat pump system and a ground-coupled heat pump system, because Plant A and Plant B have different PV collector areas.

Table 3.5.1 – Embodied energy evaluation table for: heat pumps of plants A and B, the wood pellet boiler of plants A and B , dehumidifiers of plants A and B, the tank of plant B, the boiler of plant C and the heat pump of plant C.

Constituent material	Mass Fraction [%]	Mass [kg]	Embodied energy per unit mass [kWh/kg]	Embodied energy [MWh]
79.5 kW HEAT PUMP (total mass 520 kg)				
Steel	0.4	208	6.78	1.41
Copper	0.3	156	19.17	2.99
Aluminium	0.15	78	43.06	3.36
PVC	0.03	15.6	21.44	0.33
Polyurethane	0.03	15.6	20.03	0.31
Alloy Steel	0.09	46.8	18.89	0.88
TOTAL				**9.29**
200 kW WOOD PELLET BOILER (total mass 600 kg)				
Steel	0.6	360	6.78	2.44
Copper	0.2	120	19.17	2.30
PVC	0.03	18	21.44	0.39
Rock wool	0.03	18	4.67	0.08
Alloy steel	0.14	84	18.89	1.59
TOTAL				**6.80**
0.36 kW DEHUMIDIFIER (total mass 5.04 kg)				
Steel	0.4	2.02	6.78	0.014
Copper	0.3	1.51	19.17	0.029
Aluminium	0.15	0.76	43.06	0.033
PVC	0.03	0.15	21.44	0.003
Polyurethane	0.03	0.15	20.03	0.003
Alloy Steel	0.09	0.45	18.89	0.009
TOTAL				**0.09**
6000 litres TANK (total mass 1116 kg)				
Steel	0.95	1058	6.78	7.17
Polyurethane	0.05	58	21.60	1.25
TOTAL				**8.42**
250 kW BOILER (total mass 750 kg)				
Steel	0.6	450	6.78	3.05
Copper	0.2	150	19.17	2.88
PVC	0.03	22.5	21.44	0.48
Rock wool	0.03	22.5	4.67	0.11
Alloy steel	0.14	105	18.89	1.98
TOTAL				**8.50**
4 kW AIR-TO-AIR HEAT PUMP (total mass 56 kg)				
Steel	0.4	22,4	6.78	0.15
Copper	0.3	16,8	19.17	0.32
Aluminium	0.15	8,4	43.06	0.36
PVC	0.03	1,68	21.44	0.04
Polyurethane	0.03	1,68	20.03	0.03
Alloy Steel	0.09	5,04	18.89	0.10
TOTAL				**1.00**

Table 3.5.2 – Embodied energy of Plants A, B and C considering only non-common components

Component	Quantity	Embodied energy per item	Embodied energy [MWh]
PLANT A			
Heat pump	2 items	9.29 MWh/item	18.58
Dehumidifiers	38 items	0.09 MWh/item	3.42
Wood pellet boiler	1 item	6.80 MWh/item	6.80
PV solar collectors	62.83 kWp	8.5 MWh/kWp	534.06
TOTAL			**562.86**
PLANT B			
Heat pumps	2 items	9.29 MWh/item	18.58
Cold Tank	1 item	8.42 MWh/item	8.42
Boreholes	4000 m	10.02 x 10^{-3} MWh/m	40.08
BHE pipes	16750.8 kg	23.44 x 10^{-3} MWh/kg	392.64
Dehumidifiers	38 items	0.09 MWh/item	3.42
PV Solar collectors	43.1 kWp	8.5 MWh/kWp	366.35
Wood pellet boiler	1 item	6.80 MWh/item	6.80
TOTAL			**836.29**
PLANT C			
Gas Boiler	1 item	8.50 MWh/item	8.50
Air-to-air heat pumps	38 items	1.00 MWh/item	38 .00
TOTAL			**46.50**

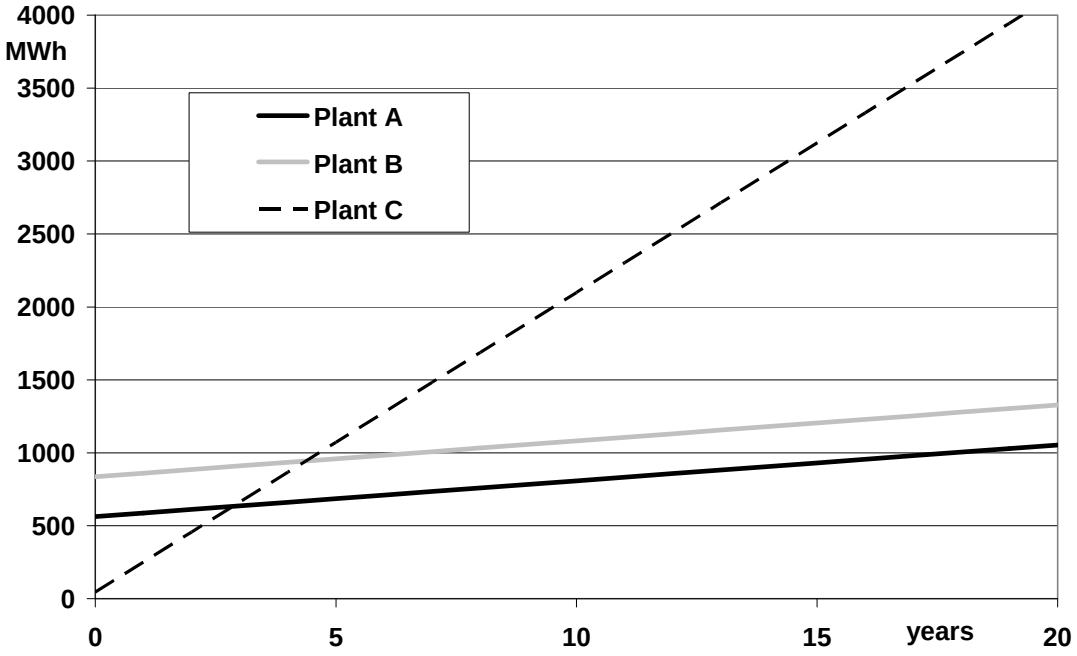

Figure 3.5.1 - Total (construction + operation) exergy use versus time, for Plants A, B, C.

To obtain a direct comparison, the exergy analysis has been repeated by excluding the embodied energy and the annual exergy production of the PV system. The results are reported in Figure (3.5.2). The figure shows that the lowest exergy use after 20 years is obtained by Plant B.

Therefore, the exergy analysis reveals that ground-coupled heat pump systems yield the lowest consumption of primary energy sources, even in ground with a rather low thermal conductivity (k_{gd} = 1.70 W/(mK)), as in the case considered here.

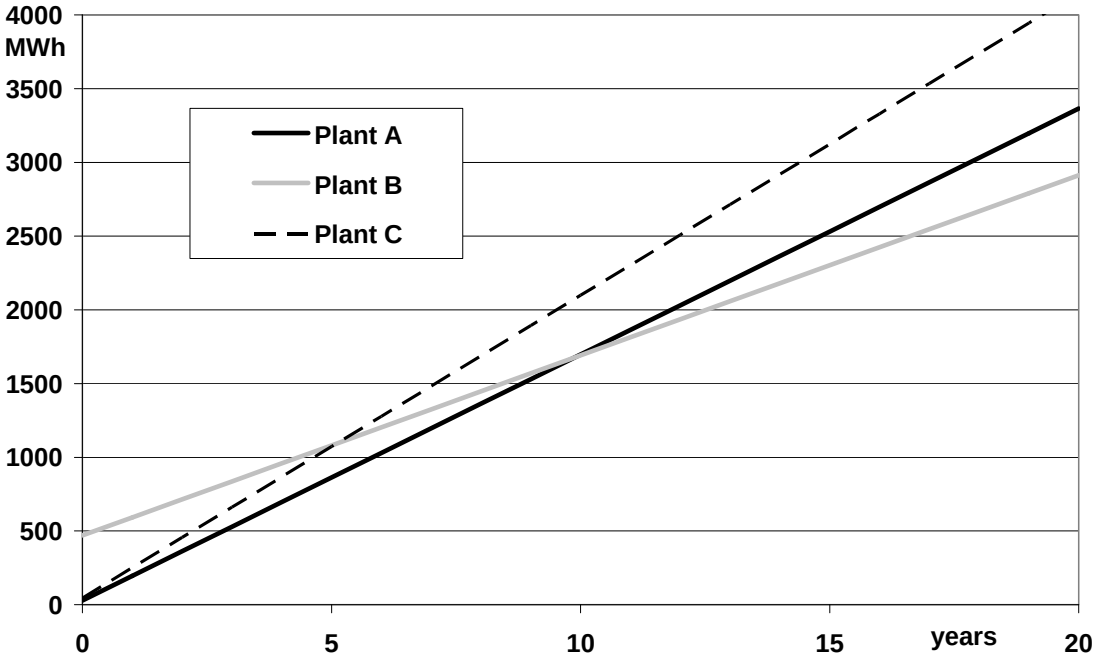

Figure 3.5.2 - Total (construction + operation) exergy use versus time, for Plants A, B, C, in the absence of PV collectors.

3.6 CONCLUSIONS

Two alternative zero carbon plants for heating, cooling, humidity control and domestic hot water supply, for a new building complex in Northern Italy, have been studied by means of the simulation code TRNSYS and compared with a conventional plant. Both plants employ heat pumps that receive electricity by PV panels and thermal solar collectors for DHW supply. Plant A employs air to water heat pumps, whereas Plant B employs ground-coupled heat pumps; they have the same, very little, primary energy use (wood pellets) and different PV collector areas.

The economic analysis has shown that both Plant A and Plant B are feasible, and that Plant A has a lower financial payback time (6 years) than Plant B (11 years). The exergy analysis has shown that Plant A yields also a lower total exergy consumption after 20 years of operation. However, this result is due to the higher PV collector area employed in Plant A. If the exergy analysis is repeated without considering the PV panels, then the lowest exergy consumption after 20 years is obtained by Plant B.

The results point out that ground-coupled heat pumps ensure a lower environmental impact than air to water heat pumps, but are economically less feasible, at least in a ground with a low or medium thermal conductivity. Therefore, financial support for the installation of ground-coupled heat pumps should be given by public administrations.

References

[1] Chan HY, Riffat SB, Zhu J, Review of passive solar heating and cooling technologies, Renewable and Sustainable Energy Reviews 14 (2010) 781–789.

[2] Rijksen DO, Wisse CJ, van Schijndel AWM, Reducing peak requirements for cooling by using thermally activated building systems, Energy and Buildings 42 (2010) 298–304.

[3] Zhao X, Yang S, Duan Z, Riffat SB, Feasibility study of a novel dew point air conditioning system for China building application, Building and Environment 44 (2009) 1990–1999.

[4] Wang L, Gwilliam J, Jones P, Case study of zero energy house design in UK, Energy and Buildings 41 (2009) 1215–1222.

[5] Hinnells M, Technologies to achieve demand reduction and microgeneration in buildings, Energy Policy 36 (2008) 4427–4433.

[6] Balaras. CA. et al. 2000. Potential for energy conservation in apartment buildings. Energy and Buildings. Vol. 31. pp 143-154.

[7] Griffith. B. et al. 2007. Assessment of the Technical Potential for Achieving Net Zero-Energy Buildings in the Commercial Sector. http://www.nrel.gov/ docs/fy08osti/41957.pdf

[8] Lang. S. 2004. Progress in energy-efficiency standards for residential buildings in China. Energy and Buildings. Vol. 36. pp.1191–1196.

[9] 2007 ASHRAE Handbook – HVAC Applications. Ch. 32.

[10] U.S. Department of Energy. Energy Efficiency and Renewable Energy. http://www.eere.energy.gov/.

[11] Kavanaugh. SP. Rafferty. K. 1997. Ground-Source Heat Pumps. Design of Geothermal Systems for Commercial and Institutional Buildings. ASHRAE.

[12] Joint Research Centre. Institute for Energy. http://re.jrc.ec.europa.eu/pvgis/apps3/pvest.php.

[13] Kelin. SA. Beckman. WA. Duffie. JA. 1976. A Design Procedure for Solar Heating Systems. Solar Energy. Vol 18. pp113-127. UK.

[14] Cammarata. G. Marletta. L. Embodied Energy versus Energy Efficiency in Building Heating Systems. Proceedings of CLIMA 2000/Napoli 2001 World Congress. Vol. 1. pp. 15-18 (Naples. 2001).

[15] Hammond. GP. Jones. CI. Embodied energy and carbon in construction materials. Proceedings of Institution of Civil Engineers: Energy. Vol. 161. n 2. pp 87-98. 2008.

[16] Kaldellis. JK. Zafirakis. D. Kondili. E. Optimum autonomous stand-alone photovoltaic system design on the basis of energy pay-back analysis. Energy. Vol. 34. pp. 1187–1198. 2009.

[17] UNI 10389-1. Heat generators. Flue gases analysis and measurement on site of combustion efficiency. September 2009.

[18] EN 590. Automotive fuels - Diesel - Requirements and test methods. October 1st 2009.

Publications

Zanchini E, Terlizzese T, *Exergy of pure chemical fuels*, Proceedings of HEFAT 2007 – 5th International Conference on Heat Transfer, Fluid Mechanics and Thermodynamics, 6 pages, Sun City, South Africa (2007).

Zanchini E, Galgaro A., Terlizzese T. e Falcioni S., *Test di Risposta termica di Sonde Geotermiche ad U con Valutazione Numerica*, XXVI Congresso Nazionale UIT on Heat Transfer (Palermo, Italy 23 – 25 Giugno 2008)

Zanchini E, Terlizzese T, *Finite-Element Evaluation of Thermal Response Tests Performed on U-Tube Borehole Heat Exchangers*, Proc. of COMSOL Conference 2008 (Hannover, Germany, 4-6 November 2008)

Zanchini E, Terlizzese T, *Molar Exergy and Flow Exergy of Pure Chemical Fuels*, Energy (2009), pp. 1246 – 1259

Zanchini E, Morini GL, Terlizzese T, *Design of a Ground Coupled Heat Pump and Solar Collector System for a Zero Carbon Residential Building Complex*, 8th International Conference on Sustainable Energy Technologies (Aachen, Germany, 31 August – 3 September 2009)

Submitted to the international journal Energy and Buildings (March 2010):

Terlizzese T, Zanchini E, *Economic and exergy analysis of alternative plants for a zero carbon building complex*